Max-Planck-Institut für Kolloid- und Grenzflächenforschung
Abteilung Theorie

Simulation of Annealed Polyelectrolytes in Poor Solvents

Dissertation
zur Erlangung des akademischen Grades
"doctor rerum naturalium"
(Dr. rer. nat.)
in der Wissenschaftsdisziplin "Theoretische Physik"

eingereicht an der
Mathematisch-Naturwissenschaftlichen Fakultät
der Universität Potsdam

von

Sahin Uyaver

Potsdam, den 12.05.2004

Acknowledgment

I would like to mention my special gratitude to all people who have helped me during this work.

I thank Prof. Dr. Reinhard Lipowsky for giving me the great opportunity to work at Max Planck Institute of Colloids and Interfaces.

I am so grateful to my supervisor Dr. Christian Seidel. He accepted me as a PhD student and introduced me to polymer physics and simulation work. He was very kind and nice to me and helped me through the work. Working with him was a great experience.

The environment in the institute was very friendly and fruitful. I mention my personal gratitude to all members of this international community, especially to the people of theory department.

My family has always supported me during this work, my wife Kadriye always motivated me, especially with her great patience with our two kids. Thank you.

In addition I would like to recognize the DFG (Deutsche Forschungsgemeinschaft) and Max Planck Society for their financial support of my PhD project.

Contents

Chapter 1

Introduction

1.1 Polyelectrolytes

Polyelectrolytes (PELs) are polymer chains containing a certain amount of ionizable monomers. When such polymers are dissolved in a polar solvent like water, the ion pairs dissociate and the polymer becomes charged. While the one type of charges is localized on the chain, the corresponding oppositely charged counterions are scattered in the solution [1]. PELs are present everywhere in our daily life. On the one hand biopolymers, including DNA and proteins, are PELs, on the other hand, many artificial water soluble polymers are charged. With these specific properties PELs acquire big importance in molecular and cell biology as well as in technology [2, 3, 4, 5]. Despite large effort during the last five decades PELs are still poorly understood compared to other materials. The complexity arises mainly from the simultaneous presence of long-ranged electrostatic interaction and local interactions, but also from the crucial role of counterions. In the 1950s many of the physical and chemical properties of a single chain have been understood by the outstanding contribution of the school of Katchalsky [6]. A second major step forward occurred when de Gennes and collaborators introduced the scaling approach and and the isotropic model for semi-dilute solutions [7]. During the last 10-15 years, new theoretical, computational and experimental approaches have been used to receive deeper insight into the behavior of PELs.

The combination of macromolecular properties and long-range electrostatic interaction results in an impressive variety of phenomena and properties, which makes these systems interesting from a fundamental as well as technological point of view. Besides fundamental questions motivated primarily by scientific interest, PELs are intensively concerned in technological questions and for numerous applications. PELs can be used, e.g., as viscosity modifiers to reduce drag in oil pipelines and to make low-fat milk products creamy. A better understanding of PELs becomes increasingly important also in biochemistry and molecular biology.

Compared to neutral polymers the theory of PELs is less understood. There are several reasons: The presence of long range interaction makes renormalization group and scaling techniques difficult to apply. Electrostatic interactions introduce into the system additional length scales. On the other hand, the complexity makes the study of PELs very interesting. In particular, this is valid for PELs in poor solvents. A poor solvent environment causes an

effective attraction between monomers. Hence, for PELs in a poor solvent, there occurs a competition between attraction and repulsion, which is responsible for the rich phase diagram of such systems.

One important parameter of PELs is the line charge density along the chain, which is related to the degree of charging f. With respect to this parameter PELs are classified into weakly charged ($f \ll 1$) and strongly charged ones ($f \approx 1$). On the other hand, with respect to different dissociation behavior one can distinguish between strong and weak PELs, the classification which is used in chemistry community, or between quenched or annealed PELs, the classification which is used in physics community [1, 8]. For strong PELs, typically represented by polysalts, the degree of dissociation is independent of the solution pH and the distribution of charged groups along the chain is only determined by the synthesis of the polymer. Therefore strong PELs are also called quenched ones. For weak PELs, i.e., polyacids and polybases, the average total charge on the polymer is not fixed, but it can be tuned by the pH of the solution. The positions of the charges along the polymer chain are also not fixed. The charges can move by recombination and redissociation. That is why weak PELs are also called annealed ones [1].

1.2 Description of the study

Over the last three decades, computer simulations became a third, independent branch of research complementary to analytical theories and experiments. Although there are limitations in the accessible time and length scales, computer simulations offer a couple of advantages such as greater freedom in and control over the preparation of the systems and their microscopic interactions, direct access to microscopic structure and dynamics, and (within the statistical error) "exact" results for well-defined model systems.

While most of theoretical and simulation work on PELs in poor solvent was focused to quenched PELs, in the study presented here the understanding of annealed PELs in poor solvent is addressed. Extensive Monte Carlo simulations have been carried out in a (semi)-grand canonical ensemble where the charges are in contact with a reservoir of constant chemical potential. For the first time it was proved that an annealed PEL in a poor solvent undergoes a first-order phase transition, as predicted by theory, from a weakly charged globular structure to a highly charged stretched configuration. Also for the first time the existence of pearl-necklace structures could be shown by computer simulations for annealed PELs. Compared to quenched PELs pearl-necklaces exist, however, only in a rather limited parameter range. Tuning the screening length of the electrostatic interaction by varying the salt concentration annealed PELs exhibit a rather unusual non-monotonic stretching behavior which can include both continuous and discontinuous transitions. The simulation results are compared with theoretical predictions and, as far as available, with related experimental work.

Chapter 2

Polymer models and theoretical predictions

A polymer is a large molecule made up of many elementary chemical units, joined together by covalent bonds. For example, polyethylene (CH_3 – $(CH_2)_N$ – CH_3) is a long chain-like molecule composed of ethylene molecules and DNA is an extremely long molecule built by (up to) 17 nucleotides.

Most artificially produced polymers are a repetitive sequence of a particular atomic group, and take the form (–A–A–A–). One unit of this sequence is called the "structural unit" or "monomer unit". The number of units in the sequence is called degree of polymerization. Usually a molecule is called polymer if the degree of polymerization exceeds 100. It is possible to have polymers containing over 10^5 units. There are even natural biological polymers with a degree of polymerization exceeding 10^9 (see, e.g., Fig. 2.1). Materials composed of this kind of macromolecules display properties which are completely different from materials composed of small molecules. Roughly speaking, polymeric materials may be very flexible (like rubber) and can be easily formed into fibres, thin films, etc. To understand the properties of polymeric materials, as usually in material science, one has to consider a large assembly of molecules. However, in the case of polymers, the molecules themselves are quite large. Correspondingly, the degrees of freedom of one molecule are very large which allows to apply statistical methods even to a single molecule. One way to investigate the properties of a single polymer is to study it in a highly dilute solution, so that interaction between the chains can be neglected. Experimentally, such dilute polymer solutions are used to determine molecular weight (degree of polymerization).

In this chapter, models and techniques used to study polymers by means of standard methods of statistical physics are discussed. The physical properties of polymers are governed by three main factors: (1) The degree of polymerization is large, $N \gg 1$. (2) Monomer units are connected along the chain; i.e., they do not have the freedom of independent motion like systems of disconnected particles as, e.g., in simple liquids. Therefore polymer systems are poor in entropy. (3) Polymer chains are generally flexible [10].

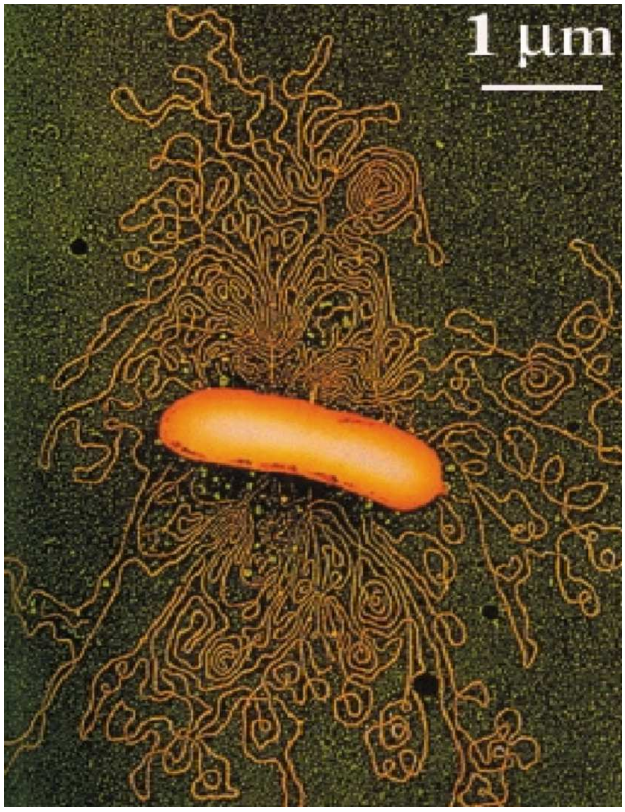

Figure 2.1: Electron microscope picture of bacterial DNA partially released from its native cell. (Picture from [9].)

2.1 Neutral polymers

Neutral polymers where all structural units are uncharged, have been extensively studied theoretically, experimentally and in simulations. They are rather well understood.

2.1.1 Ideal chains

An ideal chain consists of N freely-jointed links, each of length b and able to point in any direction independently of each other (see Fig. 2.2).

The conformation of this chain is represented by the set of $(N+1)$ position vectors $\{\mathbf{R}_n\} \equiv (\mathbf{R}_0, \ldots, \mathbf{R}_N)$ of the joints, or alternatively by the set of bond vectors $\{\mathbf{r}_n\} \equiv (\mathbf{r}_1, \ldots, \mathbf{r}_N)$ where

$$\mathbf{r}_n = \mathbf{R}_n - \mathbf{R}_{n-1}, \qquad n = 1, 2, \ldots, N. \tag{2.1}$$

Since the bond vectors $\mathbf{r}_n$ are independent of each other, the distribution function for the polymer conformation can be written as

$$\Psi(\{\mathbf{r}_n\}) = \prod_{n=1}^{N} \psi(\mathbf{r}_n) \tag{2.2}$$

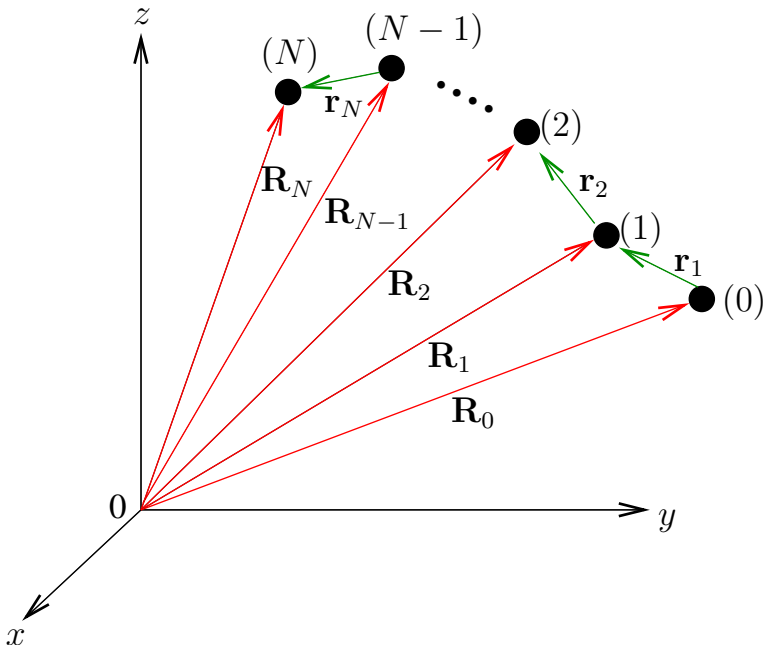

Figure 2.2: A polymer chain of $N+1$ monomers.

where $\psi(\mathbf{r})$ denotes the random distribution of a vector of constant length b:

$$\psi(\mathbf{r}) = \frac{1}{4\pi b^2}\delta(\mid \mathbf{r} \mid -b). \tag{2.3}$$

This distribution is normalized to

$$\int d\mathbf{r}\, \psi(\mathbf{r}) = 1. \tag{2.4}$$

To characterize the size of a polymer, one can consider the end-to-end vector $\mathbf{R}$ of the chain,

$$\mathbf{R} = \mathbf{R}_N - \mathbf{R}_0 = \sum_{n=1}^{N} \mathbf{r}_n. \tag{2.5}$$

Since $\langle \mathbf{r}_n \rangle = 0$, $\langle \mathbf{R} \rangle$ is zero, but $\langle \mathbf{R}^2 \rangle$ has a finite value, which can be used as a characteristic length of the chain. Let R be defined by

$$R \equiv \langle \mathbf{R}^2 \rangle^{1/2} = \langle (\mathbf{R}_N - \mathbf{R}_0)^2 \rangle^{1/2}. \tag{2.6}$$

From Eqn. 2.5 $\langle \mathbf{R}^2 \rangle$ is given by

$$\begin{aligned} \langle R \rangle^2 &= \sum_{n,m=1}^{N} \langle \mathbf{r}_n \cdot \mathbf{r}_m \rangle \\ &= \sum_{n=1}^{N} \langle \mathbf{r}_n^2 \rangle + 2 \sum_{n>m} \langle \mathbf{r}_n \cdot \mathbf{r}_m \rangle \\ &= N b^2 = R_0^2. \end{aligned} \tag{2.7}$$

Because the angle ϑ_{nm} between two bonds $\mathbf{r}_n$ and $\mathbf{r}_m$ $(n \neq m)$ has an uniform distribution between 0 and 2π, i.e.

$$\langle \mathbf{r}_n . \mathbf{r}_m \rangle = b^2 \langle \cos \vartheta_{nm} \rangle = 0.$$

Thus R is given by [11]

$$R = b\sqrt{N}. \tag{2.8}$$

The probability distribution that the end-to-end vector of a chain with N bonds is $\mathbf{R}$ can be written

$$\varphi(\mathbf{R}, N) = \int d\mathbf{r}_1 \int d\mathbf{r}_2 \cdots \int d\mathbf{r}_N \, \delta\left(\mathbf{R} - \sum_{n=1}^{N} \mathbf{r}_n\right) \Psi\left(\{\mathbf{r}_n\}\right). \tag{2.9}$$

Using Eqn.2.2, after some manipulation and a little algebra, in the limit $N \gg 1$, the distribution function can be approximated by

$$\varphi(\mathbf{R}, N) \simeq \left(\frac{3}{2\pi N b^2}\right)^{\frac{3}{2}} \exp\left(-\frac{3\mathbf{R}^2}{2Nb^2}\right). \tag{2.10}$$

The distribution of the end-to-end vector is therefore a Gaussian distribution [10, 11].

Eqn. 2.8 and Eqn. 2.10 are well-known results from the theory of random walks. Obviously the great majority of the conformations taken by the chain during its thermal motion are strongly coiled in space. Being proportional to the logarithm of the number of configurations, the entropy S of the chain can be taken as follows:

$$S(\mathbf{R}, N) \simeq k_{\mathrm{B}} \ln \varphi(\mathbf{R}, N) \tag{2.11}$$

which gives

$$S(\mathbf{R}) \sim -k_{\mathrm{B}} \frac{\mathbf{R}^2}{Nb^2}. \tag{2.12}$$

This result implies that the entropy of the chain decreases if it is stretched (for instance, considering a fully stretched chain, there remains only one conformation). The random coiled conformation corresponds to the maximum of entropy and all the conformations lie on the same equipotential surface (in the phase space).

For models that do not include long-range interactions the overall statistical properties of the chain do not depend on the details of the model if N is large. Therefore, to obtain an overall description of the chain, it is convenient to use a model with a simple mathematical formulation as possible [11, 12]. Among non-lattice models of polymer chains, the Gaussian model is mathematically the simplest. It assumes that the bond vector $\mathbf{r}$ itself possesses some variability and follows a Gaussian distribution

$$\psi(\mathbf{r}) = \left(\frac{3}{2\pi b^2}\right)^{3/2} \exp\left(-\frac{3\mathbf{r}^2}{2b^2}\right) \tag{2.13}$$

so that

$$\langle \mathbf{r}^2 \rangle = b^2. \tag{2.14}$$

The conformational distribution function of such a chain is given by

$$\begin{aligned} \Psi(\mathbf{r}) &= \prod_{n=1}^{N} \left(\frac{3}{2\pi b^2}\right)^{3/2} \exp\left(-\frac{3\mathbf{r}_n^2}{2b^2}\right) \\ &= \left(\frac{3}{2\pi b^2}\right)^{3N/2} \exp\left(-\sum_{n=1}^{N} \frac{3(\mathbf{R}_n - \mathbf{R}_{n-1})^2}{2b^2}\right). \end{aligned} \tag{2.15}$$

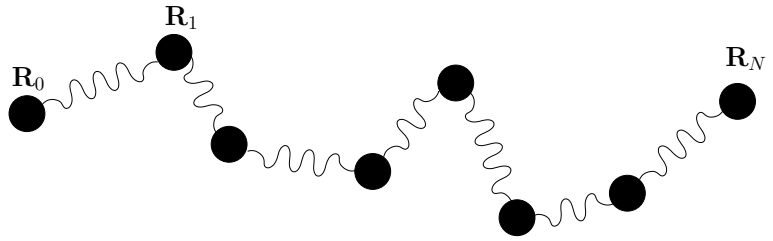

Figure 2.3: Gaussian chain.

The Gaussian chain is often represented by a mechanical model (see Fig. 2.3). $(N+1)$ 'beads' are considered to be connected by harmonic springs the potential energy of which is given by

$$U(\{\mathbf{R}_n\}) = \frac{3k_{\mathrm{B}}T}{2b^2}\sum_{n=1}^{N}(\mathbf{R}_n - \mathbf{R}_{n-1})^2. \tag{2.16}$$

At equilibrium, the Boltzmann distribution for such a model is exactly the same as Eqn. 2.15 [11].

An important property of the Gaussian chain is that the distribution of the vector $\mathbf{R}_n - \mathbf{R}_m$ between any two units n and m is Gaussian, being given by

$$\varphi(\mathbf{R}_n - \mathbf{R}_m, n-m) = \left(\frac{3}{2\pi b^2 \mid n-m \mid}\right)^{3/2} \exp\left(-\frac{3(\mathbf{R}_n - \mathbf{R}_m)^2}{2 \mid n-m \mid b^2}\right), \tag{2.17}$$

which follows from the properties of Gaussian integrals. Furthermore it holds for any n and m

$$\langle(\mathbf{R}_n - \mathbf{R}_m)^2\rangle = \mid n-m \mid b^2. \tag{2.18}$$

The suffix n of the Gaussian chain is often regarded as a continuous variable. In such cases $\mathbf{R}_n - \mathbf{R}_{n-1}$ is replaced by $\partial\mathbf{R}_n/\partial n$ and Eqn. 2.15 is written as

$$\Psi(\mathbf{R}_n) = \text{const} \times \exp\left(-\frac{3}{2b^2}\int_0^N dn \left(\frac{\partial\mathbf{R}_n}{\partial n}\right)^2\right). \tag{2.19}$$

This distribution is known as the Wiener distribution [11].

2.1.2 Structure of polymers in solution

The radius of gyration R_{g}, defined by

$$R_{\mathrm{g}}^2 = \frac{1}{N+1}\sum_{n=0}^{N}\left\langle(\mathbf{R}_n - \mathbf{R}_{\mathrm{CM}})^2\right\rangle. \tag{2.20}$$

with the center of mass vector $\mathbf{R}_{\mathrm{CM}} = \frac{1}{N+1}\sum_{n=0}^{N}\mathbf{R}_n$, is a quantity which can be directly measured in experiments such as static light, X-ray and neutron scattering. For an ideal chain, it is [11]

$$R_{\mathrm{g}}^2 = \frac{1}{6}Nb^2. \tag{2.21}$$

The shape parameter given by

$$s = \frac{R^2}{R_g^2} \tag{2.22}$$

describes the shape of the polymer chain in a relatively simple way. It is 2 for a spherical globule, 6 for an ideal chain and 12 for a rigid rod. This quantity is very useful especially in computer simulations, because it offers a quite simple way to estimate the degree of coiling.

As already mentioned above the size of polymer coils can be measured in scattering experiments on polymer in dilute solution. The scattering cross section can be written [13, 14]:

$$\frac{d^2\sigma}{d\Omega^2} \approx S_{\text{intra}}(q) S_{\text{inter}}(q). \tag{2.23}$$

Because single chain models are considered in this study, henceforth only the intrachain structure factor or form factor $S_{\text{intra}}(q) = S(q)$

$$S(\mathbf{q}) = \frac{1}{N+1} \sum_{i,j=0}^{N} \left\langle e^{i\mathbf{q}\cdot(\mathbf{R}_i - \mathbf{R}_j)} \right\rangle \tag{2.24}$$

is considered, where $\mid \mathbf{q} \mid = (4\pi/\lambda)\sin(\theta/2) = |\mathbf{q}_f - \mathbf{q}_i|$ is the difference of the wave vectors of scattered and incident beam, with λ being the wavelength and θ the scattering angle. At $N \gg 1$ the sums can be replaced by integrals, and, for the Gaussian chains

$$\begin{aligned} S(\mathbf{q}) &= 1 + \frac{1}{N+1} \sum_{i \neq j} \langle e^{\mathbf{i}\mathbf{q}\cdot(\mathbf{R}_i - \mathbf{R}_j)} \rangle \\ &\simeq 1 + \frac{1}{N} \int_0^N d\tau \int_0^N d\tau' \exp\left(-\frac{b^2 q^2}{6} |\tau - \tau'| \right) \\ &\simeq 1 + N D(q^2 R_g^2), \end{aligned} \tag{2.25}$$

where $D(q^2 R_g^2)$ is the Debye function

$$D(x) = \frac{2}{x^2} \left(e^{-x} + x - 1 \right). \tag{2.26}$$

The asymptotic behavior of $S(\mathbf{q})$ is given by

$$S(\mathbf{q}) \simeq \begin{cases} N\left(1 - \dfrac{q^2 R_g^2}{3}\right) & \text{for} \quad qR_g \ll 1 \quad \text{(Guinier region)}, \\ \\ 1 + \dfrac{2N}{q^2 R_g^2} & \text{for} \quad qR_g \gg 1 \quad \text{(Porod region)}. \end{cases} \tag{2.27}$$

If the chain is not fully flexible, the persistence length L_p is defined as the length scale over which correlations between the monomer directions are lost. It marks the crossover between rod-like behavior at length scales smaller than L_p and flexible chain behavior at length scales larger than L_p (see Fig. 2.4). For a semi-flexible chain, the energy associated with bending can be written

$$E_{\text{bend}} = \bar{\kappa} \int_0^{L=Nb} ds \left(\frac{d\mathbf{t}(s)}{ds} \right)^2, \tag{2.28}$$

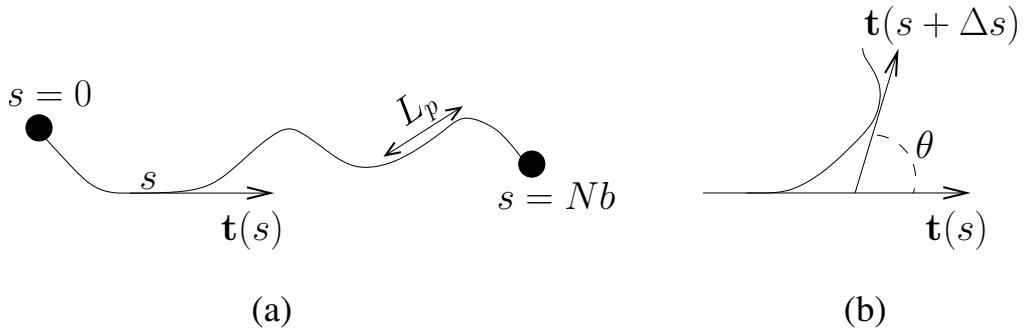

Figure 2.4: (a) Schematic view of a semi-flexible chain. The tangent to the chain contour is $\mathbf{t}(s)$ where $s \in [0, L]$. A typical persistence length L_p is indicated on the figure. (b) The deflection point θ of a short segment of length Δs.

where $\mathbf{t}(s)$ is the unit tangent vector to the contour of the chain ($\mathbf{t}(s) = d\mathbf{R}(s)/ds$) and $\bar{\kappa}$ is the bending rigidity of the chain which has units of length times energy. The coordinates of the monomers are $\mathbf{R}(s)$ where the position along the chain is denoted by s and $0 \leq s \leq L$. This model is called *worm-like chain model* or *Kratky Porod chain model* [15]. It can be shown that the orientational correlation function exhibits an exponential decay

$$\langle \mathbf{t}(s)\mathbf{t}(s')\rangle = \exp\left(-\frac{1}{L_\mathrm{p}} \mid s - s' \mid\right), \tag{2.29}$$

where the persistence length L_p is related to the bending rigidity by

$$L_\mathrm{p} = \frac{\bar{\kappa}}{k_\mathrm{B}T}. \tag{2.30}$$

2.1.3 Excluded volume effect

In the models considered so far, the interaction among the polymer segments is limited to within a few neighbors along the chain. In reality, however, segments distant along the chain do interact if they come close to each other in space. An obvious interaction is steric: since the segment has finite volume, other segments cannot occupy the same space (see Fig. 2.5). This interaction swells the polymer; the coil size of a chain with such interaction is larger than an ideal chain. Even when there are attractive forces, as long as the repulsive force dominates, the polymer will swell. This effect is called *excluded volume effect*.

It had been recognized by Kuhn [16] and Flory [17, 18] that the volume interaction changes the statistical property of the chain entirely. For example, $\langle \mathbf{R}^2 \rangle$ is no longer proportional to N but to a higher power of N

$$\langle \mathbf{R}^2 \rangle \propto N^{2\nu}. \tag{2.31}$$

The exponent ν is about 3/5, so that the excluded volume effect is very important for long chains.

In real polymers, the nature of the volume interaction is quite complicated: the interaction will include steric effects, van der Waals attraction, and also may involve other specific

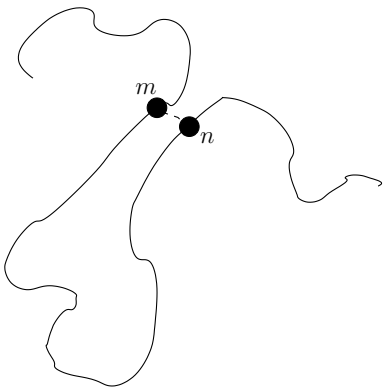

Figure 2.5: Excluded volume interaction.

interactions mediated by solvent molecules. However, as far as the property of large length scale is concerned, the detail of interaction will not matter. Thus the interaction between the polymer segments n and m can be expressed by a short range function [11]

$$v\, k_{\mathrm{B}}T\, \delta(\mathbf{R}_n - \mathbf{R}_m), \tag{2.32}$$

where v is the excluded volume and has the dimension of volume.

The total interaction energy is thus written as

$$E = \frac{1}{2} v\, k_{\mathrm{B}}T \int_0^N dn \int_0^N dm\, \delta(\mathbf{R}_n - \mathbf{R}_m). \tag{2.33}$$

Using the local concentration of the segments

$$c(\mathbf{r}) = \sum_j \delta(\mathbf{r} - \mathbf{R}_n) = \int_0^N dn\, \delta(\mathbf{r} - \mathbf{R}_n), \tag{2.34}$$

Eqn. 2.33 may be rewritten

$$E = \int d\mathbf{r}\, \frac{1}{2} v k_{\mathrm{B}}T c(\mathbf{r})^2. \tag{2.35}$$

This expression indicates that Eqn. 2.33 is the first term in a virial expansion of the free energy with respect to the local concentration $c(\mathbf{r})$. Therefore the excluded volume parameter v can be understood as the second order virial coefficient.

In principle the virial expansion can be continued to include higher order terms such as

$$E = \int d\mathbf{r}\, \left[\frac{1}{2} v k_{\mathrm{B}}T c(\mathbf{r})^2 + \frac{1}{6} w k_{\mathrm{B}}T c(\mathbf{r})^3 + \ldots \right]. \tag{2.36}$$

However, the higher order terms may be neglected since the segment density inside the polymer coil is small: the segment density is estimated as

$$\bar{c} \simeq \frac{N}{R^3} \propto N^{1-3\nu} = N^{-4/5} \qquad (\text{when} \quad \nu = 3/5) \tag{2.37}$$

which becomes very small for large N. Therefore the essential features of the excluded volume effect can be studied using the potential given by Eqn. 2.33.

For a given combination of polymer and solvent, v varies with temperature and can be zero at a certain temperature, called the Θ or Flory temperature. At the Θ temperature, the chain becomes nearly ideal [11] [1].

An appropriate expression for the temperature dependence of v may be obtained as follows. Suppose that the interaction between the segments is expressed by a potential energy $u(r)$ which depends only on their separation r. Then the second virial coefficient is evaluated by the standard formula for an imperfect gas (see, for example, chapter 11 in ref. [22])

$$v(T) = \int d\mathbf{r} \left[1 - \exp\left(-\frac{u(r)}{k_{\mathrm{B}}T}\right)\right]. \tag{2.38}$$

In the high temperature limit one has $v(T) = v^{(0)}$. As T decreases, the value of v is reduced until it reaches zero at some temperature Θ. Near the Θ point, the excluded volume can be represented as

$$v \propto -v^{(0)}\tau, \tag{2.39}$$

where

$$\tau = \frac{\Theta - T}{\Theta}. \tag{2.40}$$

2.1.4 Solvent effects

In general, three types of solvents can be distinguished: good, poor (bad) and theta. In a simple mean-field approach due to Flory [18] one can calculate the size of the polymer at different solvent quality:

(i) Good solvent: In a good solvent, the effective interaction between the monomers is repulsive and the polymer chain swells. This effective interaction results from a superposition of monomer-monomer, monomer-solvent and solvent-solvent interactions. The repulsive energy is of the form

$$E_{\mathrm{good}} = k_{\mathrm{B}}T \int d\mathbf{r}\, \frac{v}{2}c^2, \tag{2.41}$$

where c is the local monomer concentration and v is the excluded volume, as discussed above.

In mean-field approximation and neglecting numerical prefactors, the free energy of a polymer chain in a good solvent can be written as:

$$\frac{F_{\mathrm{good}}}{k_{\mathrm{B}}T} \simeq \frac{R^2}{Nb^2} + v\frac{N^2}{R^3}. \tag{2.42}$$

The first term in Eqn. 2.42 gives the Gaussian elasticity of the chain while the second term is a simple estimate of Eqn. 2.41. Minimization with respect to R, with $v \simeq v^{(0)}$, gives:

$$R_{\mathrm{good}} \simeq bN^{3/5}, \tag{2.43}$$

which yields $\nu = 3/5$ which is close to the experimental data [23, 24, 25, 26] (From renormalization group theories, ν is exactly calculated to be $\nu = 0.588\ldots$ [27].)

[1] Even at the Θ temperature the chain is not ideal since there is a three-body collision term [19, 20, 21]. However, the effect of the three-body collision is quite weak and gives only a logarithmic correction to $\langle \mathbf{R}^2 \rangle$.

(ii) Poor solvent: In a poor solvent (also called "bad") the effective monomer-monomer interaction is attractive. This is the case, for example, when the monomers have hydrophobic groups and the polymer is immersed in water. In this case the polymer chain collapses to a dense globule whose size is much less than R_0. Because the second virial coefficient is negative one has to include the third virial coefficient to ensure stability:

$$\frac{E_{\text{poor}}}{k_{\text{B}}T} = \int d\mathbf{r} \left(-\frac{1}{2} \mid v \mid c^2 + \frac{w}{6} c^3 \right) \simeq - \mid v \mid \frac{N^2}{R^3} + w \frac{N^3}{R^6} \tag{2.44}$$

The balance between these two terms, with $v \simeq b^3 \tau$ and $w \simeq b^6$, gives

$$R_{\text{poor}} \simeq \frac{b}{\tau^{1/3}} N^{1/3}, \tag{2.45}$$

which corresponds to a collapsed globule.

The form factor of a uniform hard sphere with radius R reads

$$S(\mathbf{q}) \approx \left[\frac{\sin(qR) - qR\cos(qR)}{(qR)^3} \right]^2 \tag{2.46}$$

(see Fig. 2.10). In the high q limit, it becomes

$$S(\mathbf{q}) \approx \frac{4.5}{q^4 R^4} \tag{2.47}$$

which is known as "Porod law" [28]. Below this scaling law is used as the asymptotic limit of $S(\mathbf{q})$ for globular structure.

(iii) Theta solvent: The third case is a theta solvent, i.e. the point where the second virial coefficient vanishes. In this case the leading term in the expansion is the third virial coefficient w:

$$E_\Theta = k_{\text{B}}T \int d\mathbf{r} \frac{w}{6} c^3. \tag{2.48}$$

The Flory free energy now reads:

$$\frac{F_\Theta}{k_{\text{B}}T} \simeq \frac{R^2}{Nb^2} + w \frac{N^3}{R^6}. \tag{2.49}$$

Minimizing with respect to R, with $w \simeq \left(v^{(0)}\right)^2$, leads to:

$$R_\Theta \simeq b N^{1/2}. \tag{2.50}$$

A schematic display of these three cases in shown in Fig. 2.6.

2.1.5 Blob picture

Within scaling theory approaches a very intuitive physical picture can be obtained by introducing so-called blobs. The blob size is given by a correlation length ξ that sets the distance below which a certain interaction is suppressed by thermal fluctuations. A neutral chain in

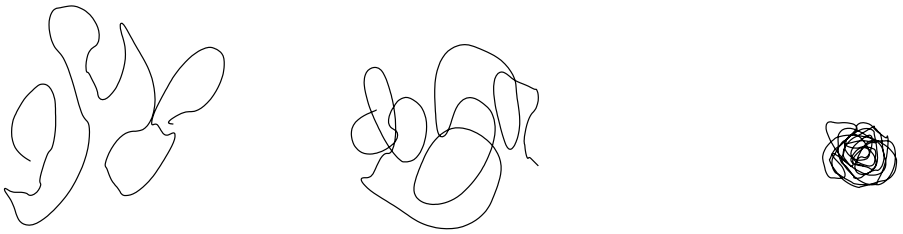

(a) Good solvent $R \propto N^{3/5}$ (b) Theta solvent $R \propto N^{1/2}$ (c) Poor solvent $R \propto N^{1/3}$

Figure 2.6: A polymer chain in different solvents: (a) in a good solvent, (b) in a Θ solvent and (c) in a poor solvent.

poor solvent forms a globule as discussed above. The monomer density ρ_g inside the globule is defined by the balance of the two-body attraction $vN\rho_g = -\tau b^3 N\rho_g$ and the three-body repulsion $b^6 N\rho_g^2$ (both interactions measured in units of $k_B T$) and one obtains

$$\rho_g \simeq \frac{\tau}{b^3}. \tag{2.51}$$

Below the thermal correlation length ξ_t the two-body attraction plays no role and the chain obeys Gaussian statistics, i.e.

$$\xi_t \cong g_t^{1/2} b, \tag{2.52}$$

where g_t is the number of monomers per blob. On the other hand, at length scales larger than ξ_t density fluctuations are suppressed and blobs are densely packed to a globule (see Fig.2.7),

$$\rho_g \simeq \frac{g_t}{\xi_t^3}. \tag{2.53}$$

Finally Eqns. 2.51-2.53 yield

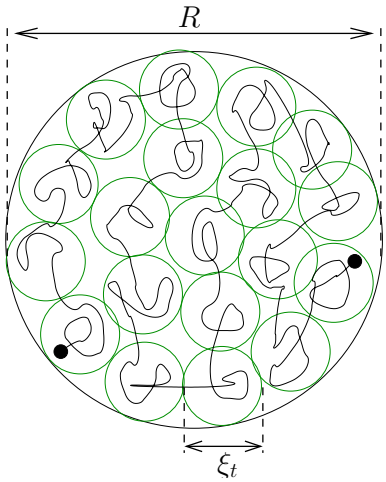

Figure 2.7: Globule consisting of thermal blobs.

$$\xi_t \simeq \frac{b}{\tau} \tag{2.54}$$

and the number of monomers g_t becomes

$$g_t \simeq \frac{1}{\tau^2}. \tag{2.55}$$

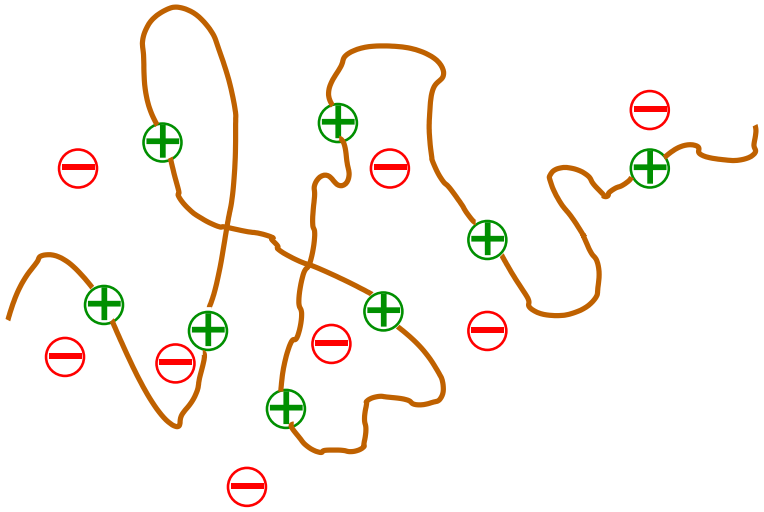

Figure 2.8: Schematic display of PEL.

Hence, the globule size obeys

$$R \simeq \xi_{\mathrm{t}} \left(\frac{N}{g_{\mathrm{t}}}\right)^{1/3} \simeq b \left(\frac{N}{\tau}\right)^{1/3} \tag{2.56}$$

The surface tension of the globule is of order of $k_{\mathrm{B}}T$ per thermal blob [7, 29]

$$\gamma \simeq \frac{k_{\mathrm{B}}T}{\xi_{\mathrm{t}}^2} \simeq k_{\mathrm{B}}T\frac{\tau^2}{b^2}. \tag{2.57}$$

2.2 Polyelectrolytes

In polar solvents such as water, polymers with ionizable groups can dissociate into charged macroions and small counterions (Fig. 2.8). Macromolecules of this type are commonly called polyelectrolytes (PELs) [1], a class which includes proteins and nucleic acids as well as synthetic polymers such as sulfonated polystyrene and polyacrylic acid. Most PELs are water soluble due to the gain of translational entropy of the dissociated counterions, an effect which probably contributes significantly to their importance in biological systems. PEL solutions are controlled by a complex interplay of short- and long-range interactions. The screening of the electrostatic interactions (i.e. the tendency of oppositely charged objects to arrange themselves in such a way that the effective interaction between charges becomes short-ranged) introduces an additional length scale into the problem. Depending on the ion strength, the screening length may be comparable to the chain size R as well as to the correlation length ξ_{t}. However, the distribution of counterions around macroions limits not only the range of their effective interaction but due to the so-called 'counterion condensation' [30] it can also cause a renormalization of the charge of macroions. Therefore, the most general case of PEL solution can be extremely complex and the general case of flexible PEL chains is not completely understood so far [31, 32, 33].

Strong or quenched PELs are completely dissociated at any accessible pH. The position of charges along the chain is fixed by chemical synthesis. On the other hand, in weak or annealed

PELs dissociation of charges depends on solution pH; therefore the degree of charging is a function of pH, i.e. $f = f(\mathrm{pH})$. Dissociation or recombination of ion pairs along the chain causes spatial and/or temporal fluctuations in the local degree of dissociation [34].

2.2.1 Quenched polyelectrolytes

In quenched PELs the charge distribution is frozen. They can be partially as well as completely charged. Partially charged ones correspond to heterogeneous copolymers with a random sequence of charged and neutral monomers. The specific sequence of each copolymer is determined during the polymerization stage and represents one possible realization of the random distribution [35]. A typical example of these quenched PELs would be a polystyrene chain with a few sulfonated monomers [36].

2.2.1.1 Electrostatics

The classical approach for treating a solution with ions dissolved in a solvent is to consider this electrolyte solution as a continuous medium. Let the charge density in solution be $\rho(\mathbf{r})$, then the electrostatic potential generated by $\rho(\mathbf{r})$ is given by the Poisson equation:

$$\triangle\varphi(\mathbf{r}) = -\frac{\rho(\mathbf{r})}{\varepsilon_0\varepsilon(\mathbf{r})}, \tag{2.58}$$

where $\varepsilon(\mathbf{r})$ is the dielectric function of the medium. Eqn. 2.58 can be easily solved in the case of a distribution of M point-like particles of charge Q in an infinite dielectric medium ($\varepsilon(\mathbf{r}) = const = \varepsilon$). The charge density of such a system is:

$$\rho(\mathbf{r}) = Q\sum_{j=1}^{M}\delta(\mathbf{r}-\mathbf{r}_j) \tag{2.59}$$

and the corresponding electrostatic potential becomes:

$$\varphi(\mathbf{r}) = \frac{Q}{4\pi\varepsilon_0\varepsilon}\sum_{j=1}^{M}\frac{1}{\mid \mathbf{r}-\mathbf{r}_j \mid}. \tag{2.60}$$

Considering a solution of j ionic species, each of valence z_j and bulk concentration c_j, within the mean-field approach, i.e. disregarding local fluctuations and taking the time average of the electrostatic potential, the local concentrations $c_j^{\mathrm{loc}}(\mathbf{r})$ obey a Boltzmann law:

$$c_j^{\mathrm{loc}}(\mathbf{r}) = c_j\exp\left(-\frac{z_j e\langle\varphi(\mathbf{r})\rangle}{k_{\mathrm{B}}T}\right). \tag{2.61}$$

The charge density inside the solution is

$$\rho(\mathbf{r}) = e\sum_j z_j c_j^{\mathrm{loc}}(\mathbf{r}) \tag{2.62}$$

and Eqn. 2.58 can be written as:

$$\triangle\langle\varphi(\mathbf{r})\rangle = -\frac{e}{\varepsilon_0\varepsilon}\sum_j z_j c_j\exp\left(-\frac{z_j e\langle\varphi(\mathbf{r})\rangle}{k_{\mathrm{B}}T}\right). \tag{2.63}$$

This is the well-known Poisson-Boltzmann (PB) equation. Explicit general solutions of this equation are not available. That is why approximations come into play. The first attempt by Debye and Hückel [37] starts from a linearized form of the PB equation. Expanding Eqn. 2.63 for weak potential ($\langle\varphi(\mathbf{r})\rangle \ll k_{\mathrm{B}}T/z_j e$) and taking into account the condition of electroneutrality $\sum_j z_j c_j = 0$, one obtains the linearized PB equation:

$$\triangle\langle\varphi(\mathbf{r})\rangle = \frac{1}{\lambda_{\mathrm{D}}^2}\langle\varphi(\mathbf{r})\rangle \tag{2.64}$$

where

$$\lambda_{\mathrm{D}} = \sqrt{\frac{\varepsilon_0\varepsilon k_{\mathrm{B}}T}{e^2\sum_j z_j^2 c_j}} \tag{2.65}$$

is the *so-called Debye (screening) length*. Assuming that the potential is spherically symmetric around a test ion, the solution of Eqn. 2.64 becomes

$$\langle\varphi(\mathbf{r})\rangle = \frac{z_j e}{4\pi\varepsilon_0\varepsilon}\frac{e^{-r/\lambda_{\mathrm{D}}}}{r}. \tag{2.66}$$

The corresponding pair interaction energy reads:

$$U_{\mathrm{DH}}(r_{ij}) = z_i z_j k_{\mathrm{B}}T\frac{\lambda_{\mathrm{B}}}{r_{ij}}e^{-r/\lambda_{\mathrm{D}}} \tag{2.67}$$

with the *Bjerrum length*

$$\lambda_{\mathrm{B}} = \frac{e^2}{4\pi\varepsilon_0\varepsilon k_{\mathrm{B}}T}. \tag{2.68}$$

The Bjerrum length is defined as the distance at which the Coulomb interaction energy between two elementary charges is equal to the thermal energy [38] and it characterizes the strength of the electrostatic interactions in the solution. From Eqn. 2.65 immediately follows:

$$\lambda_{\mathrm{D}} = \frac{1}{\sqrt{4\pi\lambda_{\mathrm{B}}\sum_j z_j^2 c_j}}. \tag{2.69}$$

From Eqn. 2.67 it is evident that the charge cloud around a test ion results in a screening of the Coulomb interactions. The Debye length λ_{D} gives the range of the resulting effective potential.

Also for intrinsically flexible chains, the electrostatic interaction can cause a finite rigidity measured by the persistence length. The simplest way to introduce the concept of the persistence length into PELs is the so-called Odijk-Skolnick-Fixman (OSF) theory [39, 40, 41]. They considered a semi-flexible chain with a bare persistence length L_{p}^0 and linear charge density e/b^*, where b^* is the average distance between charges. The range of electrostatic interactions is assumed to be given by λ_{D}. Thus, at short distances, $\mid s - s' \mid \ll s_c$, the chain is unperturbed by the presence of electrostatic interactions and $L_{\mathrm{p}} = L_{\mathrm{p}}^0 = \bar{\kappa}/k_{\mathrm{B}}T$. At larger distances, $\mid s - s' \mid \gg s_c$, the effective persistence length is decomposed into two contributions:

$$L_{\mathrm{p}} = L_{\mathrm{p}}^0 + L_{\mathrm{p}}^{\mathrm{OSF}}, \tag{2.70}$$

where $L_{\rm p}^{\rm OSF}$ represents the stiffening of the chain due to long range Coulomb interaction:

$$L_{\rm p}^{\rm OSF} \simeq \frac{\lambda_{\rm B}\lambda_{\rm D}^2}{b^{*2}}. \tag{2.71}$$

Note that $L_{\rm p}^{\rm OSF} \propto \lambda_{\rm D}^2$, i.e. $L_{\rm p}^{\rm OSF}$ can become larger than screening length $\lambda_{\rm D}$. This means that the effect of the charges on the chain stiffness can extend beyond the range of electrostatic interactions. The crossover s_c between the two regimes can be estimated by comparing the energy needed to bend a small part of the chain whose length is $\Delta s = \mid s - s' \mid$ with the excess electrostatic energy associated with the bending. The bending energy can be estimated from Eqn. 2.28 and is (up to numerical prefactors) [39, 41]:

$$\frac{E_{\rm bend}}{k_{\rm B}T} \simeq L_{\rm p}^0 \left(\frac{\theta}{\Delta s}\right)^2 \Delta s \simeq \frac{L_{\rm p}^0}{\Delta s}\theta^2, \tag{2.72}$$

where θ is the deflection angle of the curve (see Fig. 2.4(b)). At small angles θ is proportional to $\mid \mathbf{t}(s+\Delta s) - \mathbf{t}(s) \mid$. In the weakly screened limit, $\Delta s \ll \lambda_{\rm D}$, and the excess electrostatic energy of the arc with respect to the straight line is (up to numerical prefactors):

$$\frac{E_{\rm el}}{k_{\rm B}T} \simeq \lambda_{\rm B}\frac{(\Delta s/b^*)^2}{(\Delta s/\theta)^2}\Delta s \simeq \frac{\lambda_{\rm B}}{b^{*2}}\,\Delta s\,\theta^2. \tag{2.73}$$

At the crossover distance, $\Delta s = s_c$, the two energies are of the same order of magnitude and we obtain

$$s_c \simeq \sqrt{\frac{L_{\rm p}^0}{\lambda_{\rm B}}}\,b^*. \tag{2.74}$$

The main result of this calculation is that at short length scales the chain keeps its original characteristics despite the electrostatic interactions. This approach is therefore consistent only for chains with an intrinsic rigidity $L_{\rm p}^0 \gg s_c$ leading to $L_{\rm p}^0 \gg b^{*2}/\lambda_{\rm B}$. This is the case, for example, for DNA molecules where $L_{\rm p} \sim 500$ Å while $b^* \sim \lambda_{\rm B}/4$ and $\lambda_{\rm B} \sim 7$ Å, but not for flexible polymers where $L_{\rm p}$ is of the order of a few Angstroms. Note that at $L \gg L_{\rm p}$ the chain becomes again flexible. Thus, the structure of PELs may be quite different on different length scales.

2.2.1.2 Solvent effects

Let us consider a solution of charged flexible chains with degree of polymerization N and a monomer size b. For simplicity, let us restrict ourselves to monovalent charges on the chains and monovalent counterions. With f being the degree of charging the total charge of the chain is fN. In a highly dilute salt-free solution, the counterions are expected to be homogeneously distributed throughout the system volume, and the Debye screening length fulfills $\lambda_{\rm D} \gtrsim L$. Therefore, the charges on the chain interact via an unscreened Coulomb potential [42] and the conformation of the chain is expected to be an extended one [43, 44]. At $f \ll 1$, each macromolecule can be represented as a chain of electrostatic blobs, with blob size $\xi_{\rm e}$. Inside the blobs the statistics of the chain is determined by the volume interaction

between uncharged monomers. In good and Θ-solvents, the electrostatic energy of the blob is of the order of the thermal energy [43, 44]

$$\frac{g_{\rm e}^2 e^2 f^2}{4\pi\varepsilon_0\varepsilon\,\xi_{\rm e}} \simeq k_{\rm B}T \qquad\qquad {\rm T} \geq \Theta, \tag{2.75}$$

where $g_{\rm e}$ is the number of monomers inside an electrostatic blob. For poor solvent the electrostatic blob size $\xi_{\rm e}$ is determined by the balance between the electrostatic energy of a blob and the polymer/solvent interfacial energy [45]

$$\frac{g_{\rm e}^2 e^2 f^2}{4\pi\varepsilon_0\varepsilon\xi_{\rm e}} \simeq \gamma\xi_{\rm e}^2 \qquad\qquad {\rm T} < \Theta, \tag{2.76}$$

where surface tension γ is given by Eqn. 2.57. The conformation of a macromolecule inside the electrostatic blob is almost unperturbed by the electrostatic interaction, but depends on the quality of the solvent for the neutral polymer. Therefore, following Eqns. 2.52, 2.43, 2.45 and 2.50, the size of the electrostatic blob is

$$\xi_{\rm e} \simeq b \begin{cases} (g_{\rm e}/\tau)^{1/3} & T < \Theta \\ g_{\rm e}{}^{1/2} & T = \Theta \\ g_{\rm e}{}^{3/5} & T \gg \Theta. \end{cases} \tag{2.77}$$

Using Eqns. 2.75, 2.76, 2.77 the number of monomers inside the electrostatic blob is found to be:

$$g_{\rm e} \simeq \begin{cases} \tau\left(uf^2\right)^{-1} & T < \Theta \\ \left(uf^2\right)^{-2/3} & T = \Theta \\ \left(uf^2\right)^{-5/7} & T \gg \Theta \end{cases} \tag{2.78}$$

where the dimensionless coupling constant u is given by

$$u = \lambda_{\rm B}/b. \tag{2.79}$$

Finally, the size of the electrostatic blobs becomes

$$\xi_{\rm e} \simeq b \begin{cases} \left(uf^2\right)^{-1/3} & T \leq \Theta \\ \left(uf^2\right)^{-3/7} & T \gg \Theta. \end{cases} \tag{2.80}$$

On length scales larger than $\xi_{\rm e}$, electrostatic interactions dominate and the blobs repel each other to form a fully extended chain of electrostatic blobs of total length

$$R \simeq \frac{N}{g_{\rm e}}\xi_{\rm e} \simeq Nb \begin{cases} \left(uf^2\right)^{2/3}\,\tau^{-1} & T < \Theta \\ \left(uf^2\right)^{1/3} & T = \Theta \\ \left(uf^2\right)^{2/7} & T \gg \Theta. \end{cases} \tag{2.81}$$

Note that the effect of solvent quality is merely to change the electrostatic blobs, but the conformation of chain is always a rod-like assembly of electrostatic blobs ($uf^2 < 1$) [42] .

2.2.1.3 Pearl-necklace structure

As discussed above, a polymer chain in a poor solvent forms a globule. If the polymer is charged, the Coulomb repulsion between charged monomers could change the shape of the globule, but would not significantly affect its volume. The volume occupied by the molecule is still defined by the solvent quality, as in the case of the uncharged globule. Khokhlov [45] argued that if the Coulomb repulsion

$$F_{\text{Coul}} \simeq \frac{e^2 f^2 N^2}{4\pi\varepsilon_0\varepsilon R} \tag{2.82}$$

becomes comparable to the surface energy

$$F_{\text{sur}} \simeq \frac{k_{\text{B}} T R^2}{\xi_{\text{t}}^2}, \tag{2.83}$$

the total energy of the globule can be lowered by elongating it into a cylinder. This deformation occurs when the total charge fN becomes larger than $(N\tau/u)^{1/2}$, or

$$f > \left(\frac{\tau}{uN}\right)^{1/2}. \tag{2.84}$$

The size of the cylinder can be found by optimizing the sum of the surface energy [29, 36, 45, 46, 47]

$$F_{\text{sur}} \simeq \frac{k_{\text{B}} T L_{\text{cyl}} D}{\xi_{\text{t}}^2} \tag{2.85}$$

and Coulomb energy

$$F_{\text{Coul}} \simeq \frac{e^2 f^2 N^2}{4\pi\varepsilon_0\varepsilon L_{\text{cyl}}} \tag{2.86}$$

at fixed volume

$$L_{\text{cyl}} D^2 \simeq \frac{b^3 N}{\tau} \tag{2.87}$$

determined by the solvent quality. The minimization of the free energy $F_{\text{cyl}} = F_{\text{sur}} + F_{\text{Coul}}$ gives the length of cylinder (see also Eqn. 2.81)

$$L_{\text{cyl}} \simeq \frac{bN}{\tau}(uf^2)^{2/3} \tag{2.88}$$

and width

$$D \simeq \frac{b}{(uf^2)^{1/3}}. \tag{2.89}$$

Note that the width D of the cylinder is the length scale at which the Coulomb repulsion between charges becomes of the order of the surface energy (electrostatic blob in a poor

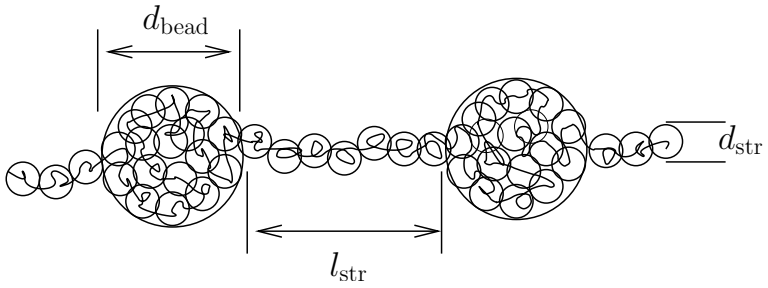

Figure 2.9: Schematic diagram of pearl-necklace structure. Beads are spherical with diameter $d_{\rm bead}$ and consists of $g_{\rm bead}$ monomers each. Strings are cylindrical with length $l_{\rm str}$ and diameter $d_{\rm str}$ and consists of $g_{\rm str}$ monomers each. The density of beads and string is the same-dense packing of thermal blobs of size $\xi_{\rm t}$.

solvent). The deformation-sensitive part of the free energy of the cylindrical globule of the optimal size $L_{\rm cyl}$ and width D given by Eqns. 2.88 and 2.89 is

$$\frac{F_{\rm cyl}}{k_{\rm B}T} \simeq \frac{\lambda_{\rm B} f^2 N^2}{L_{cyl}} \simeq \tau (u f^2)^{1/3} N. \tag{2.90}$$

However, Dobrynin, Rubinstein and Obukhov (DRO) [29] have demonstrated that the cylindrical globule is not the free energy minimum of a PEL chain in poor solvent (at $\tau > (uf^2)^{1/3}$). They argued that the total energy of the charged globule is lowered by splitting it into smaller globules such that neighbors are connected by a narrow string.

The problem of the shape of a charged globule is similar to the classical problem of the instability of a charged droplet, considered by Rayleigh [48, 49]. He showed that a spherical droplet with radius R and charge $Q > e\left(\frac{\gamma R^3}{k_{\rm B}T\lambda_{\rm B}}\right)^{1/2}$ (where γ is a surface tension) is locally unstable and will spontaneously split into smaller droplets. The equilibrium state is a set of small droplets each of which has charge lower than the critical one and placed at an infinite distance from each other. This state is impossible for PELs because the consist of monomers connected to chains by chemical bonds. In this case, the system can reduce its energy by splitting into a set of smaller charged globules connected by narrow strings. Kantor and Kardar [50, 51] who studied Rayleigh instability for polyampholytes called the resulting structure pearl-necklaces. Considering a pearl-necklace structure as drawn in Fig.2.9; with $N_{\rm bead}$ beads of size $d_{\rm bead}$ containing $g_{\rm bead}$ monomers in each ($d_{\rm bead} \simeq b\tau^{-1/3} g_{\rm bead}^{1/3}$) joined by $N_{\rm bead}-1$ strings of length $l_{\rm str}$ and width $d_{\rm str}$ containing $g_{\rm str}$ monomers each ($g_{\rm str} \simeq \rho l_{\rm str} d_{\rm str}^2$), the free energy is given by

$$\begin{aligned}\frac{F_{\rm nec}}{k_{\rm B}T} &\simeq N_{\rm bead}\left\{\frac{\lambda_{\rm B} f^2 g_{\rm bead}^2}{d_{\rm bead}} + \frac{d_{\rm bead}^2}{\xi_{\rm t}^2}\right\} \\ &\quad + (N_{\rm bead}-1)\left\{\frac{\lambda_{\rm B} f^2 g_{\rm str}^2}{d_{\rm str}} + \frac{d_{\rm str}^2}{\xi_{\rm t}^2}\right\} + \frac{\lambda_{\rm B} f^2 N^2}{L_{\rm nec}},\end{aligned} \tag{2.91}$$

where $L_{\rm nec} = (N_{\rm bead}-1) l_{\rm str} + N_{\rm bead} d_{\rm bead}$ is the total length of the necklace. The first term in Eqn. 2.91 is the electrostatic self-energy of the beads and the second term is the surface

energy of the beads. The third and fourth terms are the corresponding energies for the strings. The last term is the electrostatic repulsion between different beads and strings (up to logarithmic corrections). In Eqn. 2.91 all numerical prefactors are omitted. The total number of monomers in all strings and beads should be equal to the total number of monomers N

$$N_{\rm bead}\, g_{\rm bead} + (N_{\rm bead} - 1)\, g_{\rm str} = N_{\rm bead}\, g_{\rm bead} + M_{\rm str} = N, \tag{2.92}$$

where $M_{\rm str} = (N_{\rm bead} - 1) g_{\rm str}$ is the total number of monomers in all strings. In the limit of $l_{\rm str} \gg d_{\rm bead}$, Eqn. 2.91 becomes

$$\begin{aligned} \frac{F_{\rm nec}}{k_{\rm B}T} \;\simeq\; & \left\{ u f^2 \tau^{1/3} \frac{(N - M_{\rm str})^{5/3}}{N_{\rm bead}^{2/3}} + \tau^{4/3} N_{\rm bead}^{1/3} (N - M_{\rm str})^{2/3} \right\} + \\ & + \frac{\tau b}{d_{\rm str}} M_{\rm str} + u f^2 \tau \frac{N^2 d_{\rm str}^2}{b^2 M_{\rm str}}. \end{aligned} \tag{2.93}$$

The optimal values of $N_{\rm bead}, M_{\rm str}$ and $d_{\rm str}$ correspond to the minimum of the free energy. In Eqn. 2.93 only the first two terms depend on $N_{\rm bead}$. So, the minimization of Eqn. 2.93 with respect to $N_{\rm bead}$ yields

$$g_{\rm bead} \simeq \frac{\tau}{u f^2}, \tag{2.94}$$

and the size of the beads becomes

$$d_{\rm bead} \simeq \frac{b}{(u f^2)^{1/3}}. \tag{2.95}$$

In the optimal configuration the thickness of a string is of the order of the thermal blob size $d_{\rm str} \approx \xi_{\rm t}$ [29]. Balancing the Coulombic interaction between two beads with the surface energy of the connecting string, one gets the length of a string

$$l_{\rm str} \simeq \left(\frac{\tau}{u f^2} \right)^{1/2} b. \tag{2.96}$$

Using the monomer density in a thermal blob given in Eqn. 2.51, $\rho \simeq \tau / b^3 \simeq g_{\rm str} / (d_{\rm str}^2 l_{\rm str})$, the number of monomers in a string is found to be

$$g_{\rm str} \simeq \left(\tau u f^2 \right)^{-1/2}. \tag{2.97}$$

Because most of the mass is concentrated in beads, the number of beads along the PEL chain is estimated

$$N_{\rm bead} \simeq \frac{N}{g_{\rm bead}} \simeq N \frac{u f^2}{\tau}, \tag{2.98}$$

where $g_{\rm bead}$ is the same as $g_{\rm e}$ in poor solvent (see Eqn. 2.78). Finally the length of the pearl-necklace structure becomes

$$L_{\rm nec} \approx N_{\rm bead}\, l_{\rm str} \simeq N b \left(\frac{u f^2}{\tau} \right)^{1/2}. \tag{2.99}$$

The free energy of the necklace structure in this equilibrium state reads

$$\frac{F_{\rm nec}}{k_{\rm B}T} \simeq (N - M_{\rm str}) \tau u^{1/3} f^{2/3} + M_{\rm str} \frac{u}{\tau} f^2 + N f (\tau u)^{1/2}, \tag{2.100}$$

where

$$M_{\rm str} \simeq fN\left(u/\tau^3\right)^{1/2}. \tag{2.101}$$

The structure factor (Eqn. 2.24) can be rewritten for pearl-necklace structure. After averaging over all chain orientations, one gets [29]

$$S(\mathbf{q}) \approx \frac{g_{\rm bead}^2}{N}\left(N_{\rm bead} + 2\sum_{n=1}^{N_{\rm bead}-1}(N_{\rm bead}-n)\frac{\sin(ql_{\rm str}n)}{ql_{\rm str}n}\right) \times \left(3\frac{\sin(qR_{\rm bead}) - qR_{\rm bead}\cos(qR_{\rm bead})}{(qR_{\rm bead})^3}\right)^2, \tag{2.102}$$

with $R_{\rm bead} = d_{\rm bead}/2$. The second factor of Eqn. 2.102 corresponds to intrabead scattering (see Eqn. 2.46 for a sphere). The first factor represents the scattering between beads. Thus one predicts an increase of the scattering intensity on length scales of the order of

$$ql_{\rm str} \approx 2\pi k, \tag{2.103}$$

where k is an integer. Fig. 2.10 shows the structure factor for (i) pearl-necklace calculated

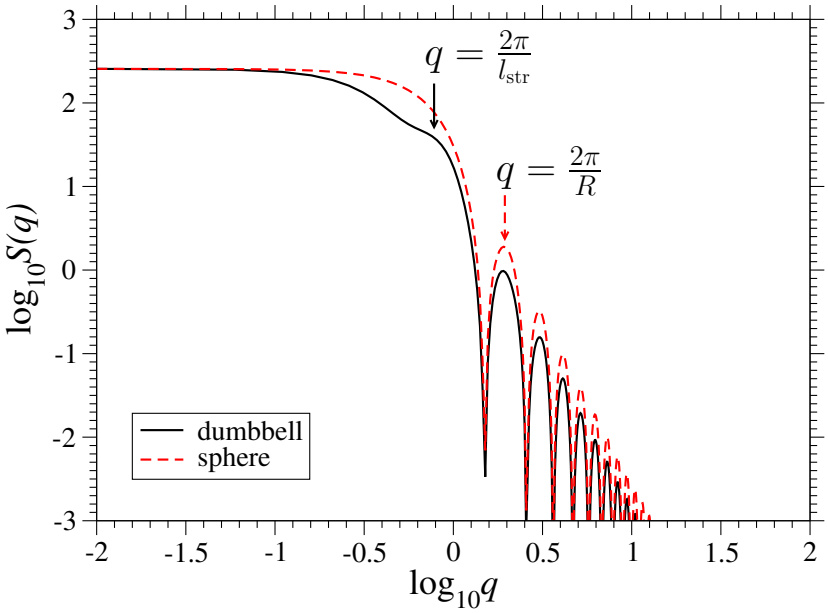

Figure 2.10: Structure factor calculated for a pearl-necklace with $N = 256$, $N_{\rm bead} = 2$, $d_{\rm bead} = 6$ and $l_{\rm str} = 8$ and for a solid sphere of $N = 256$ and with radius $R = 3$. The arrows give string length and sphere (or) bead size.

according to Eqn. 2.102 with $N = 256$, $N_{\rm bead} = 2$, $d_{\rm bead} = 6$ and $l_{\rm str} = 8$, where $g_{\rm bead} \times N_{\rm bead} \approx N$ and (ii) ensemble of solid spheres ($N = 256$) of radius $R = 3$ (Eqn. 2.46). The first arrow from left gives the position for bead-to-bead distance and the second one sphere (or bead) radius. The oscillations are due to intrapearl scattering, as expected for sphere.

To summarize the overall behavior of PEL chains in poor solvent the phase diagram in the (τ, f)-space is sketched in Fig. 2.11 ($N = 128$, $u = 1$).

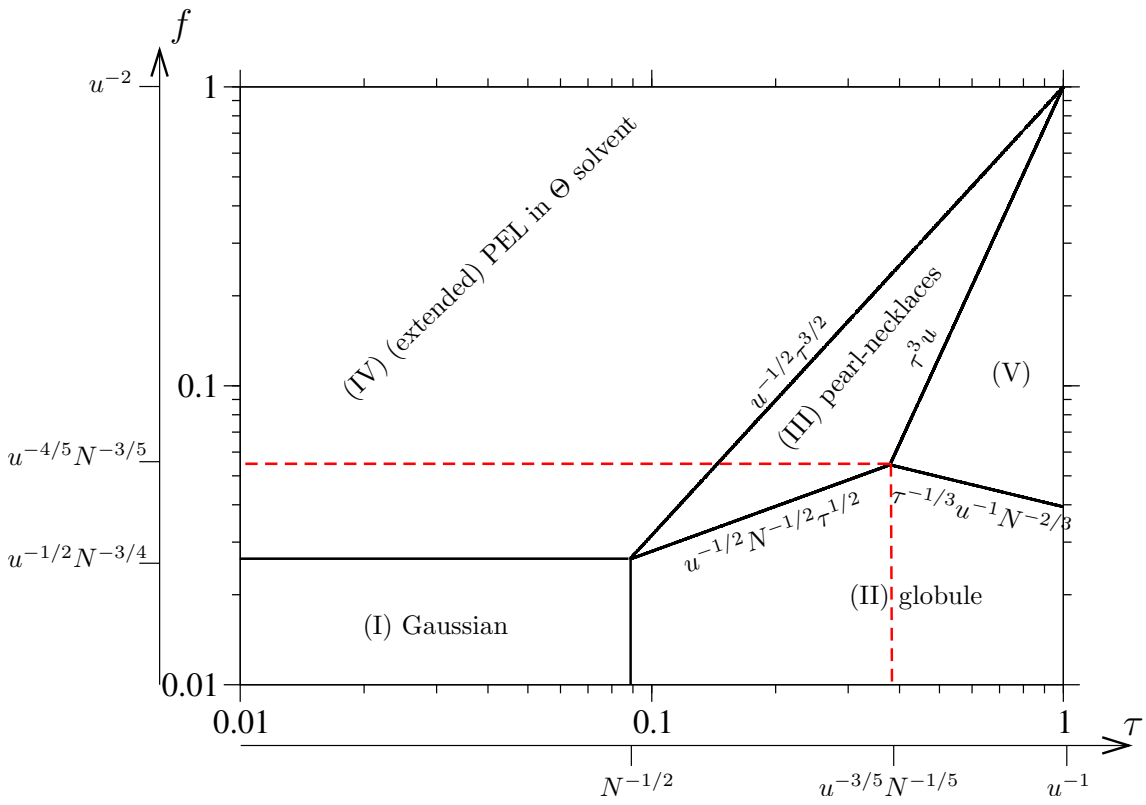

Figure 2.11: Diagram of states of a PEL chain $N = 128$ monomers in a poor solvent. The normalized Bjerrum length is $u = \lambda_B/b = 1.0$ (following [29]).

In region (I), close to the Θ temperature at weak charging, i.e.,

$$\tau < N^{-1/2} \text{ and } f < \tau^{1/2} N^{-1/2} u^{-1/2}, \tag{2.104}$$

the short-range attraction between monomers and the electrostatic repulsion between charges are too weak to deform the chain and it behaves like a Gaussian chain.

In region (II), deep in the poor solvent regime at low charge density, i.e.,

$$\tau > N^{-1/2} \text{ and } f < \tau^{1/2} N^{-1/2} u^{-1/2}, \tag{2.105}$$

the size of the thermal blob ξ_t is smaller the the Gaussian chain size $R_0 \simeq bN^{1/2}$, and the short-range attraction causes a collapse of the chain into a spherical globule. This globule is stable as long as its surface energy is larger than the electrostatic energy (see Eqn. 2.98 for $N_{\text{bead}} = 1$). The electrostatic free energy of such a globule is

$$\frac{F_{\text{el}}}{k_B T} \simeq f^2 N^{5/3} \tau^{1/3} u. \tag{2.106}$$

At higher charging, region (III), ($f > \tau^{1/2} N^{-1/2} u^{-1/2}$), the spherical globule is unstable with respect to capillary waves and first splits into a dumbbell with two smaller globules joined by a string of thermal blob width ξ_t. As the charge density f increases further, the necklace with two globules (dumbbell) splits into one with three smaller globules connected by two strings of diameter ξ_t and so on. This cascade of abrupt transitions between necklace

states with different numbers of pearls occurs at the boundaries given by Eqn. 2.98. At the upper boundary $f \simeq \tau^{3/2}u^{-1/2}$, the size of the beads $d_{\rm bead}$ is comparable to the width of the strings $\xi_{\rm t}$.

Region (IV) above the cascade zone at higher charging $f > \tau^{3/2}u^{-1/2}$ and smaller effective temperature τ corresponds to a $\Theta-$like state of the PEL chain which exhibits now a cylinder-like shape, the electrostatic free energy of which is

$$\frac{F_{\rm el}}{k_{\rm B}T} \simeq N f^{4/3} u^{2/3}. \tag{2.107}$$

In this regime the electrostatic blob size is the length scale at which electrostatic repulsion is of the order of thermal energy $k_{\rm B}T$, but still given by Eqn. 2.89 [7, 10, 29]. On length scales smaller than D, the chain is Gaussian. On larger length scales, the electrostatic repulsion forces the PEL into a linear array of electrostatic blobs. The length of the PEL in this regime is $R \simeq bN(uf^2)^{1/3}$ (see Eqn. 2.81). Note that at the boundary between regions (I) and (IV) (at $f \simeq u^{-1/2}N^{-3/4}$), the length of the chain crosses over its Gaussian size. To define the upper boundary of this region, at larger charging f one expects Manning condensation [30]. This condensation of counterions occurs at a linear charge density along the cylinder axis larger than $\lambda_{\rm B}^{-1} : f > u^{-2}$.

In region (V) of the diagram, the strong electrostatic attraction between counterions and charged groups on the polymer chain also results in counterion condensation. The crossover condition between condensed and free states of counterions can be found by comparing the thermal energy $k_{\rm B}T$ with the electrostatic interaction between a bead and a counterion for the necklace globule in regime (III) ($E_{\rm (III)} \simeq e^2 g_{\rm bead} f/4\pi\varepsilon_0\varepsilon d_{\rm bead}$) and between the globule and a counterion for a spherical globule in regime (II) ($E_{\rm (II)} \simeq e^2 N f/4\pi\varepsilon_0\varepsilon R$). These conditions give the upper, $f \simeq \tau^3 u$, and lower, $f \simeq \tau^{-1/3}u^{-1}N^{-2/3}$, boundaries of regime (V) in the diagram of states.

In this work PELs are studied within the Debye-Hückel model at infinite dilution. Therefore the generic quantities concern (i) the behavior at finite polymer concentration and (ii) the effect of counterions. In dilute and semidilute solutions, hydrophobic PELs form pearl-necklace structures. With increasing polymer concentration, the solutions of hydrophobic PELs may phase separate into concentrated and dilute phases or stay homogeneous depending on the value of the parameter $\epsilon_{\rm c} \approx (u/f)^{1/3}\tau$, which is the strength of the electrostatic interaction in units of the thermal energy $k_{\rm B}T$ between a bead and a counterion at its surface. At $\epsilon_{\rm c} \gg 1$ hydrophobic PELs are predicted to show phase separation into concentrated and dilute phases. The polymer concentration in the dilute phase is exponentially low for large values of the counterion condensation parameter $\epsilon_{\rm c}$. This phase separation is triggered by the counterion condensation inside beads. However, hydrophobic PELs, for which the value of the parameter $\epsilon_{\rm c}$ is smaller than unity, are stable with respect to phase separation throughout the entire concentration interval [52].

At the phase boundary of ion condensation the fraction of intruded and condensed ions can be quite high. In the regime that scaling theory refers to as "free counterions" a considerable fraction of ions has penetrated the beads or is condensed. Since the point at which ion condensation becomes relevant and the point at which the bead radius becomes infinite scale

identically, the range of stable beads in between is not accessible by scaling arguments which neglect prefactors [53].

2.2.2 Annealed polyelectrolytes

As mentioned above, for weak PELs, the total number of charges along PEL chain is not fixed, but it is tuned by changing the pH of the solution. Because of dissociation and recombination of ion pairs along the chain, one expects spatial and/or temporal fluctuations in the local degree of dissociation [34]. Such titrating PELs exhibit an annealed inhomogeneous charge distribution. In good and Θ solvents, a pronounced charge accumulation appears at chain ends because there are fewer neighbors for the charges to interact with and the penalty in energy is reduced. Although, at the level of scaling laws describing the statistical properties of polymer chains, the local charge distribution has only a weak effect on numerical prefactors [1], the extra degree of freedom for the charges leads to new and non-trivial features. The charge inhomogeneity can have a strong impact on process dominated by end-effects, such as the self-assembly of weakly charged linear micelles [54] and weak adsorption on charged surfaces [55].

An acid is a substance which produces hydrogen ions (H^+) by dissociation. For example $HCI \longrightarrow H^+ + CI^-$. The dissociation of a low molecular acid (HA) in an aqueous medium is given by the equilibrium reaction

$$HA + H_2O \rightleftharpoons H_3O^+ + A^- \tag{2.108}$$

or more simply

$$HA \rightleftharpoons H^+ + A^-. \tag{2.109}$$

The law of mass action yields the equilibrium constant (or dissociation constant)

$$K_a = \frac{[H^+][A^-]}{[HA]}, \tag{2.110}$$

where $[A^-], [HA], [H^+]$ are the (monomolar) concentrations of dissociated and undissociated acid and dissociated hydrogen, respectively. An interesting and extremely useful relationship between pH, and the dissociation constant K_a can be obtained simply by taking the logarithms of Eqn. 2.110. Using the standard notation $\mathrm{pH} = -\log_{10}[H^+]$, $\mathrm{p}K_a = -\log_{10}[K_a]$ and defining the degree of dissociation by

$$f = \frac{[A^-]}{[HA] + [A^-]}, \tag{2.111}$$

Eqn. 2.110 gives the well-known relation between the pH of the solution and degree of dissociation f of a simple acid

$$\mathrm{pH} = \mathrm{p}K_a + \log_{10}\left(\frac{f}{1-f}\right), \tag{2.112}$$

where $f =< f >= \left\langle (1/N)\sum_{i=1}^{N} f_i \right\rangle$ is the overall degree of dissociation. By using $\mathrm{p}K_a$ values, one is able to express the strength of an acid (i.e. its tendency to dissociate) with respect to the pH scale.

The dissociation behavior of polyacids can be described in a similar way, but the resulting $\mathrm{p}K_a$ value is now an apparent one (in the physico-chemical literature denoted by $\mathrm{p}K_{\mathrm{app}}$) [6]. In contrast to low-molecular-weight acids, the charged groups of polyacids are linked together along the chain. Therefore, the dissociation of one acid group is correlated in a complex way to the position and the number of other charged groups of the chain resulting in a masking of the intrinsic $\mathrm{p}K_a^0$ of a (polyelectrolyte) monomer ($\mathrm{p}K_a^0 = \left(\mu^0_{\mathrm{H}^+} + \mu^0_{\mathrm{A}^-} - \mu_{\mathrm{AH}^0}\right)/k_{\mathrm{B}}T$).

One may consider annealed PELs in very dilute solutions and focus on the potentiometric titration of a weak polyacid (HA) by a strong base. The monomer concentration is c and the concentration of small ion of species i (i=OH^-, H^+ and Na^+) is c_i. The two concentrations c and c_{Na^+} are fixed by the experimental conditions. The overall neutrality of the solution requires that

$$\left(\sum_i \epsilon_i c_i - fc\right) = 0, \tag{2.113}$$

where $\epsilon_i = \pm 1$ is the charge of the ions of species i. The thermodynamic potential that one has to minimize in order to obtain the equilibrium values of c_{H^+}, c_{OH^+} and f is [36]

$$\begin{aligned}\frac{F}{k_{\mathrm{B}}T} = & \sum_i c_i\left[\log c_i + \frac{\mu_i^0}{k_{\mathrm{B}}T} - \lambda\epsilon_i\right] \\ & + c\left[f\log f + (1-f)\log(1-f) + f\frac{\mu^0_{\mathrm{A}^-}}{k_{\mathrm{B}}T} + (1-f)\frac{\mu^0_{\mathrm{AH}}}{k_{\mathrm{B}}T} + \lambda f\right] \\ & + \frac{c}{N}\left[\log c + \frac{F_{\mathrm{el}}(f)}{k_{\mathrm{B}}T}\right],\end{aligned} \tag{2.114}$$

where F_{el} is the electrostatic energy of the chain given by Eqns. 2.90, 2.100, 2.106 and 2.107. μ^0_{AH}, $\mu^0_{\mathrm{A}^-}$ and μ_i^0 are the standard chemical potentials of an undissociated acidic group, of a dissociated acidic group and of an i-ion group, respectively. The free energy includes the translational entropy of the various small ions and of the polymer but also the entropy of the charged groups along the chain. The electroneutrality constraint has taken into account by introducing a Lagrange multiplier λ [36, 56].

Minimizing Eqn. 2.114 with respect to f one obtains the relation between the pH and the degree of dissociation f of a polyacid

$$\mathrm{pH} = \mathrm{p}K_a^0 + \frac{1}{k_B T}\,\mu(f), \tag{2.115}$$

where the chemical potential is given by

$$\mu(f) = k_{\mathrm{B}}T\log_{10}\left(\frac{1}{1-f}\right) + \frac{1}{N}\frac{\partial F_{\mathrm{el}}}{\partial f}. \tag{2.116}$$

Note that in the presence of screening of electrostatic interaction, in Eqn. 2.115 there appears an additional term $\lambda_{\mathrm{B}}/\lambda_{\mathrm{D}}$ [57, 58]. Eqn. 2.115 shows that by imposing the pH of the solution, one imposes the chemical potential of the charges. The chemical potential $\mu(f)$, which gives the free energy one has to pay for adding one extra charge at constant number of monomers, has two contributions:

1. An entropic one related to the mixing of charged and non-charged monomers along the chain,

2. An electrostatic one related to the interaction with charged monomers which form the local charge environment of an ionizable site.

If the solvent is not too poor ($\tau < N^{-1/5}u^{-3/5}$), the entropic term dominates and similarly to the good solvent case μ smoothly increases with f. Therefore, under this condition one would expect a continuous conformation of the globule which was thought to be described by Khokhlov's blob-cylinder model [45]. However later it was understood that such a structure is unstable with respect to the Rayleigh instability which drives the formation of pearl-necklaces [29].

On the other hand, in a rather poor solvent ($\tau > N^{-1/5}u^{-3/5}$) the chemical potential is a nonmonotonic function of f with a minimum value for

$$f_{\min} = \tau^3 u$$

and a maximum value for

$$f_{\max} = \frac{\tau^{1/2}}{N^{1/2}u^{1/2}}.$$

In between these two limits a given value of μ would correspond to three value of f. This result is clearly unphysical, the decreasing part of the curve is thermodynamically unstable. It is the signature of a first-order phase transition between collapsed chains with a charge density f_1 of order $f_{\max}$ and extended chains with a charge density f_2 of order $f_{\min}$. The precise values of f_1 and f_2 are obtained by the classical Maxwell equal-area construction. If the chemical potential is just a plateau value, one expects an equilibrium between extended and collapsed chains. This first-order transition could provide an explanation both for the behavior of the intrinsic viscosity that increases strongly when the chains are stretched and for the titration curve. Thus, annealed PELs in poor solvent are expected to undergo a discontinuous first-order collapse transition (in the limit of infinite molecular weights) between an extended state and globular one.

As mentioned above, in annealed PELs pearl-necklace can be stable if the solvent is not too poor ($\tau < N^{-1/5}u^{-3/5}$). The free energy of the annealed PEL in a necklace conformation reads:

$$\frac{F^{(\mathrm{nec})}_{\mathrm{annealed}}}{k_{\mathrm{B}}T} = \frac{F^{(\mathrm{nec})}_{\mathrm{quenched}}}{k_{\mathrm{B}}T} + Nf(\ln f - 1) - \mu_{\mathrm{el}}Nf, \tag{2.117}$$

where the second term is the entropy of the charges along the chain and the third term is associated to the exchanges with reservoir of charges of constant chemical potential. $F^{(\mathrm{nec})}_{\mathrm{quenched}}$ is given by Eqn 2.100. Minimizing Eqn. 2.117 with respect to f, the charge chemical potential reads [59]

$$\frac{\mu}{k_{\mathrm{B}}T} \simeq \ln f + \frac{N - M_{\mathrm{str}}}{N}\frac{\tau^{1/3}}{f^{1/3}} + \frac{M_{\mathrm{str}}}{N}\frac{u}{\tau}f + (\tau u)^{1/2}. \tag{2.118}$$

The charge fraction obtained from Eqn. 2.118 corresponds to a minimum of the free energy if

$$\frac{1}{f} - \frac{N - M_{\mathrm{str}}}{N}\frac{\tau u^{1/3}}{f^{4/3}} + \frac{M_{\mathrm{str}}}{N}\frac{u}{\tau} > 0. \tag{2.119}$$

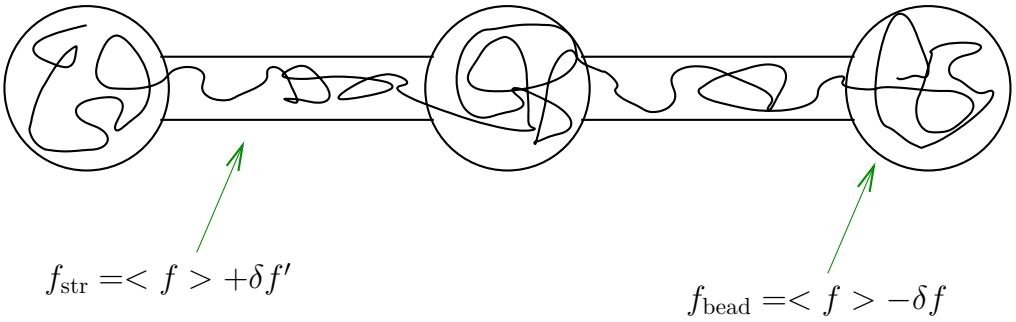

Figure 2.12: Necklace conformation: the inhomogeneity in charge distribution is observed by different charging of beads $f - \delta f$ and string $f + \delta f'$.

Up to lowest order in $\xi_{\rm t}/d_{\rm str}$, this inequality is rewritten as:

$$f^{1/3} > \tau u^{1/3}, \tag{2.120}$$

i.e., the model is correct as long as the system is far from the transition to stretched Gaussian chain behavior where the pearls disappear.

Castelnovo *et al.* [59] have discussed the equilibrium of charge distribution along the chain for pearl-necklace structures (see Fig. 2.12). They make the following simple estimation: Each monomer of the beads has a charge $f - \delta f$ and each monomer of strings has a charge $f + \delta f'$. The choice of the sign of the deviation around the average value f is motivated by the fact that charges are closer in beads than in stings.

Evaluating the change in the free energy

$$\Delta F = F^{\rm nec}_{\rm annealed}(f, \delta f, \delta f') - F^{\rm nec}_{\rm annealed}(f, 0, 0)$$

up to second order in δf and $\delta f'$ and minimizing ΔF with respect to δf and $\delta f'$, the reduction of the fraction of charged monomers in the pearls was found to be

$$\frac{\delta f}{f} \approx \left(\frac{f^2 u}{\tau^3}\right)^{1/2} \frac{\left(\frac{\tau^3 u}{f}\right)^{1/3}}{1 - \left(\frac{\tau^3 u}{f}\right)^{1/3}}, \tag{2.121}$$

where any numerical prefactor is neglected. The quantity $(\tau^3 u/f)^{1/3}$ is the electrostatic energy of a counterion at the surface of a pearl in units of $k_{\rm B}T$. If this energy is smaller than one (see Eqn. 2.120), the charge inhomogeneity $\delta f/f$ is small and the charge is almost uniform. For a finite value of this quantity (within the model the value is one), however, the denominator in Eqn. 2.121 becomes zero and the perturbation of charge distribution diverges. This is the signature of an instability of the pearl-necklace structure.

2.2.3 Effect of additional salt

When a finite concentration of salt is present in the solution, which is always the case in experiments at least because of water dissociation, the solution becomes a conducting, rather than a dielectric medium. The fundamental implication is that the Coulomb interaction

between charged monomers is screened by salt ions, i.e. the electrostatic potential created by a monomers, or a group of monomers, falls off exponentially rather than algebraically with distance. Thus distant parts of the chain do not interact, and in the asymptotic limit $N \to \infty$ the chain can be expected to behave as a random walk with short-ranged repulsive interactions [1].

It is a general result from the theory of charged solutions that charge fluctuations become uncorrelated (or, equivalently, that an external charge distribution is screened) over a typical distance λ_D, where λ_D is related to the thermodynamic properties of the solution [60]. In the case of dilute salt solutions, the Debye-Hückel theory can be used and the salt can be treated as ideal gas. Assuming a 1:1 monovalent salt as well as monovalent counterions, following Eqn. 2.69 the screening length is given by

$$\lambda_D = \frac{1}{\sqrt{4\pi\lambda_B(2c_s + c_{ci})}} \tag{2.122}$$

where c_s and c_{ci} are salt and counterion concentration (number density), respectively. The short-range interaction potential, Eqn. 2.66, is the starting point of many theoretical studies on PEL solutions. However, the application of an effective Debye-Hückel potential requires two conditions: (i) the ionic solution is dilute, (ii) the perturbation of the ion distribution caused by the macroion is weak. While condition (i) is more or less under control, condition (ii) requires a careful consideration. Although the potential in Eqn. 2.66 is short-ranged, its range λ_D can be much larger than the monomer size, which is typically interaction length in neutral polymers. Depending on the ionic strength, λ_D can vary typically from less than 1 nm to larger than 100 nm.

2.2.3.1 Quenched polyelectrolytes

(i) Good solvent: When the electrostatic screening length λ_D is smaller than the size of the chain, a new hierarchy of electrostatic screening blobs of size λ_D is introduced (each blob consists of g_{sc} monomers) (Fig.2.125) [61]. The structure of the chain at distances smaller than the screening length is the same as unscreened case where N is replaced by g_{sc}. The number of monomers inside one electrostatic screening blob is written

$$g_{sc} \simeq \frac{\lambda_D}{\xi_e} g_e. \tag{2.123}$$

Using Eqns. 2.80 and 2.78 for $T \gg \Theta$,

$$g_{sc} \simeq \frac{\lambda_D}{b(uf^2)^{2/7}}. \tag{2.124}$$

Since the repulsion between these electrostatic blobs acts on the same length scale as their radius it can be treated as excluded volume repulsion and the total size of the chain R scales as [42]

$$R \simeq \lambda_D \left(\frac{N}{g_{sc}}\right)^{3/5}. \tag{2.125}$$

Inserting Eqn.2.124 into 2.125, one gets

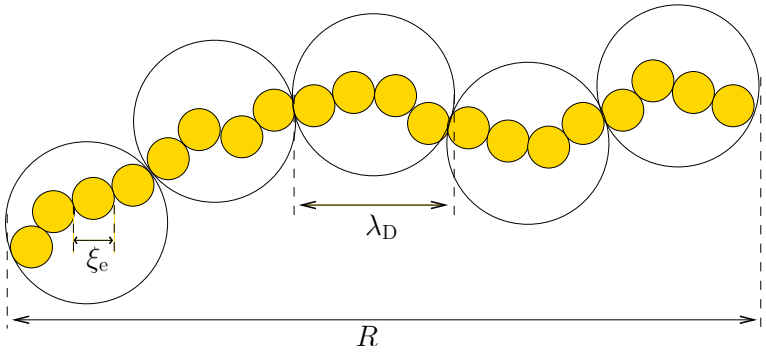

Figure 2.13: Blob picture in the presence of screening. Inside the electrostatic blobs, at length scales $r \lesssim \xi_e$, the behavior is dominated by the short-range monomer-monomer interactions and is solvent-dependent. Inside the electrostatic screening blobs, at length scales $\xi_e \lesssim r \lesssim \lambda_D$, electrostatic interactions dominate and the interaction blobs line up in an extended conformation. At larger length scales $\lambda_D \lesssim r \lesssim R$ the electrostatic interactions are screened and the electrostatic screening blobs interact via a short-range excluded volume interaction.

$$R \simeq \lambda_D^{2/5} (Nb)^{3/5} (uf^2)^{6/35}. \tag{2.126}$$

When $\lambda_D \sim \xi_e = b(uf^2)^{-3/7}$, electrostatic interaction is fully screened and Eqn. 2.126 yields $R \simeq bN^{3/5}$: the PEL chain behaves the same as a neutral chain. At $\lambda_D \gtrsim R$, one obtains the same size as in Eqn. 2.81 (for a simulation work see, for example, ref. [62]).

(ii) Slightly below the Θ point: Now a PEL chain conformation is considered at $0 < \tau < (uf^2)^{1/3}$, where according to Eqn. 2.104 it is supposed to be an elongated blob chain. For small salt concentrations one expects the salt to affect the flexibility of the chain of blobs rather than changing the behavior on the level of the blob. Thus, the short-range behavior of the blob chain should remain independent of the salt concentration as long as $\lambda_D > \xi_e$. However, the salt affects the long range behavior of the chain by introducing a finite persistence length L_p for the chain of blobs. For $\tau = 0$, this has been calculated by Khokhlov and Khachaturian [44] by modifying the original theory of Odijk and Houwaard [40] for strongly charged PELs. Following Odijk and replacing b by $\xi_e/(fg_e)$ the persistence length reads

$$L_p^{OSF} \simeq \lambda_B \left(\frac{\lambda_D}{b}\right)^2 \Rightarrow \frac{\lambda_B \lambda_D^2 f^2 g_e^2}{\xi_e^2} \simeq \frac{(uf^2)^{1/3} \lambda_D^2}{b}. \tag{2.127}$$

As long as $\lambda_D > R_0 \sim N^{1/2} b$, one has $L_p^{OSF} > R$ and the conformation of the blob chain is not effected. For $\lambda_D < R_0$, the blob chain becomes flexible with a persistence length L_p^{OSF} given by Eqn. 2.127. When λ_D equals the blob size ξ_e the persistence length shrinks to ξ_e and the notion of electrostatic blobs looses its meaning. If the concentration of added

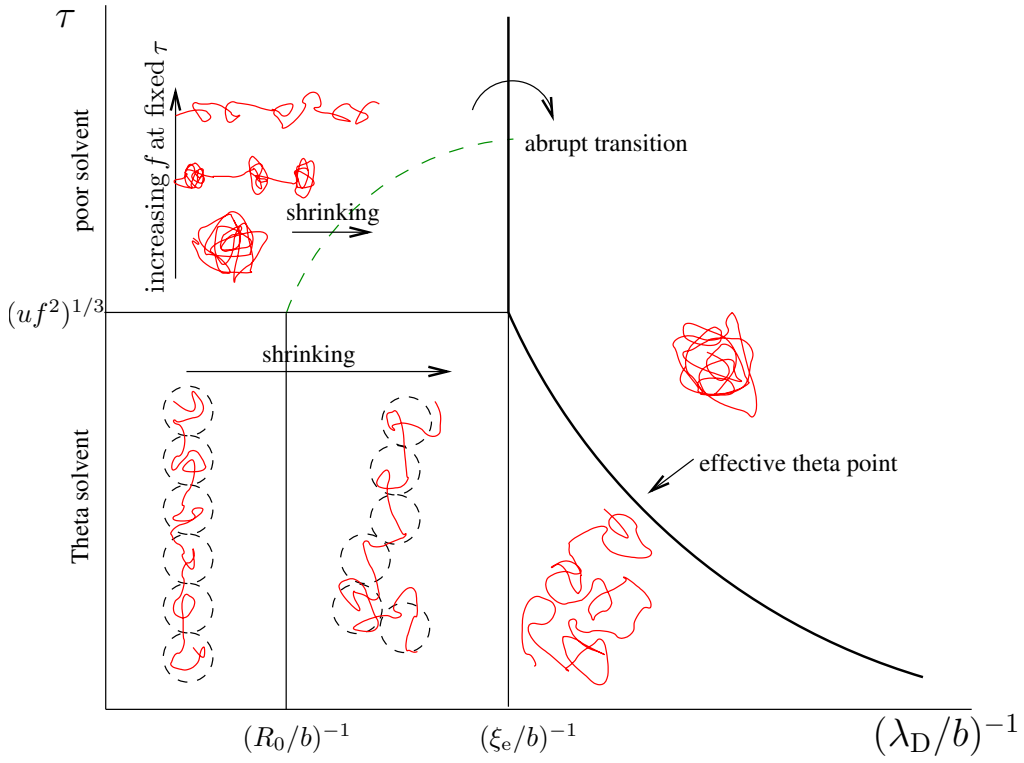

Figure 2.14: Conformations of a PEL chain in Θ and poor solvent as a function of solvent quality τ and inverse screening length (according to [46]).

salt increases more and the screened Coulomb interaction becomes rather short-ranged. The theory predicts that it may be replaced by an excluded volume pseudopotential ($v_{\rm el}\,\delta(r)$) and the chain behaves like a swollen chain with electrostatic excluded volume [44]

$$v_{\rm el} = 4\pi\lambda_{\rm B}\lambda_{\rm D}^2 f^2. \tag{2.128}$$

At $\tau > 0$ and $\xi_{\rm e}/\lambda_{\rm D} > 1$, the electrostatic excluded volume competes with the short-range attraction. Then the chain is governed by an effective excluded volume [46]

$$v_{\rm eff} \simeq b^3(4\pi u f^2\lambda_{\rm D}^2/b^2 - \tau). \tag{2.129}$$

For small τ, this quantity is positive but if $b^2/\lambda_{\rm D}^2 > uf^2/\tau$ it becomes negative. The chain therefore changes smoothly from swollen to collapsed on the addition of salt, passing through an effective Θ point (see Fig. 2.14).

(iii) Deep in the poor solvent region: For $\tau > (uf^2)^{1/3}$, in the absence of salt, the chain exhibits a collapsed conformation. For small salt concentrations, again the salt affects the flexibility of the chain of blobs rather than changing the behavior on the level of one blob. In the poor solvent case the persistence length of the blob chain reads [46]

$$L_{\rm p}^{\rm OSF} \simeq \frac{\lambda_{\rm B}\lambda_{\rm D}^2 f^2 g_{\rm e}^2}{\xi_{\rm e}^2} \simeq \frac{\lambda_{\rm D}^2\tau^2}{b(uf^2)^{1/3}}. \tag{2.130}$$

Again at very low salt concentrations one has $L_{\rm p}^{\rm OSF} > R$ and the conformation of the chain is not affected by screening. Using Eqns. 2.130 and 2.81, one finds that $L_{\rm p}^{\rm OSF}$ equals $R_{\rm poor}$ at

$$\tau \sim \left(N u f^2 b^2/\lambda_{\rm D}^2\right)^{1/3}, \tag{2.131}$$

shown as dashed line in Fig. 2.14. When the salt concentration increases, $L_{\rm p}^{\rm OSF}$ shrinks, but at $\xi_{\rm e}/\lambda_{\rm D} = 1$ or $b/\lambda_{\rm D} = (uf^2)^{1/3}$, the persistence length is still larger than $\xi_{\rm e}$. In fact on the upper part of the line at $b/\lambda_{\rm D} = (uf^2)^{1/3}$ in Fig. 2.14, i.e. at $\tau > (uf^2)^{1/3}$, one has $L_{\rm p}^{\rm OSF} > R$ and the chain exhibits still a quite elongated configuration. When $\xi_{\rm e}/\lambda_{\rm D} > 1$ or $b/\lambda_{\rm D} > (uf^2)^{1/3}$, the repulsion between neighboring blobs is screened and the argument leading to blob size $g_{\rm e}$ makes no further sense. Furthermore, the effective excluded volume is negative at this point and it should result in a collapsed conformation. So, one concludes that there occurs a discontinuous change at $\xi_{\rm e}/\lambda_{\rm D} = 1$ from a cylindrical configuration (or chain of blobs with large persistence length) to a spherical collapsed configuration with excluded volume $v_{\rm eff}$.

Supposing $N \gg g_{\rm e}$, the axial ratio L/D of the cylinder is large and one can neglect end effects. Omitting numerical prefactors, the free energy of the cylinder can be written

$$\frac{F_{\rm cyl}}{k_{\rm B}T} \simeq -N\tau^2 + \tau^2\frac{LD}{b^2} + f^2\tau^2\frac{\lambda_{\rm B}LD^4}{b^6}, \tag{2.132}$$

here the first term is the gain in energy ($k_{\rm B}T$ per thermal blob) when the chain collapses, which is the same as it would be for a neutral polymer. It is the real excluded volume $-\tau b^3$ which counts here, and not $v_{\rm eff}$, because the diameter is assumed to be smaller than the screening length. The second term is the surface energy, which is significant due to the large surface area of the cylinder. The charge inside the cylinder is $fe\rho$, hence an electrostatic energy of order $(fe\rho)^2D^4L/4\pi\varepsilon_0\varepsilon$, which is the third term of Eqn. 2.132. Note that a logarithmic factor has been neglected in the third term ($\sim \ln\frac{L}{D}$ in absence of salt, or $\ln\frac{\lambda_{\rm D}}{D}$ in presence of salt) because it will not significantly effect the scaling behavior. This is equivalent to Khokhlov's argument [45] that the electrostatic energy is dominated by the repulsion between nearest neighbor blobs of size D. Minimizing Eqn. 2.132 with respect to D at fixed volume $LD^2 \simeq Nb^3\tau^{-1}$ gives $D = \xi_{\rm e}$ while L is given by Eqn. 2.81. The minimum energy of any cylindrical configuration is therefore

$$\left\{\frac{F_{\rm cyl}}{k_{\rm B}T}\right\}_{\rm min} \simeq -N\tau^2 + N\tau(uf^2)^{1/3}. \tag{2.133}$$

On the other hand, for a sphere of radius $R > \lambda_{\rm D}$, screening is effective inside the sphere. Hence, the modified excluded volume relevant in this case (Eqn. 2.129). The sphere radius is therefore $R \simeq \left(Nb^3/v_{\rm eff}\right)^{1/3} b$. The energy gained on collapse reads

$$\frac{F_{\rm sph}}{k_{\rm B}T} \simeq -N\left(\tau - \frac{uf^2\lambda_{\rm D}^2}{b^2}\right)^2 \simeq -N\tau^2 + 2N\tau\frac{uf^2\lambda_{\rm D}^2}{b^2} - \ldots. \tag{2.134}$$

The surface energy for the sphere can be also ignored compared to other terms. However, due to the surface energy the sphere will always have a minimum in energy relative to

small increases of the axial ratio L/D. On the other hand, if the axial ratio is increased to such an extent that $D/\lambda_D < 1$, Eqn. 2.132 is applicable for the energy, not Eqn. 2.134. Therefore there is a second minimum in free energy as a function of L/D corresponding to the cylinder of Eqn. 2.133, provided $\xi_e/\lambda_D < 1$. Comparing Eqns. 2.133 and 2.134, it is evident that the cylinder is preferred if

$$N\tau \left(uf^2\right)^{1/3} < N\tau u f^2 \lambda_D^2/b^2, \tag{2.135}$$

i.e., the elongated configuration is stable at $\lambda_D > \xi_e$. For $\xi_e/\lambda_D > 1$, the sphere is preferred. Hence, a discontinuous transition is expected at $\xi_e/\lambda_D = 1$ [46]. Note that the elongated cylinder conformation might be unstable with respect to pearl-necklace conformation as pointed out by Dobrynin *et* (see Sec. 2.2.1.3).

2.2.3.2 Annealed polyelectrolytes

Above the degree of charging f was considered to be fixed while solvent quality τ and electrostatic screening length λ_D were variables. To derive corresponding relations for annealed PELs, let us assume τ to be fixed while f and λ_D are variables. The conjugated variable to the degree of charging f is the charge chemical potential μ which consists of an entropic part and an electrostatic one μ_{el} (see Sec. 2.2.2). The crucial point is that $\mu_{el}(f)$ is a nonmonotonic function for PELs in a poor solvent. This leads to the possible coexistence of two chain species with different charge fraction f which may result in a first-order phase transition (see Sec. 2.2.2). In absence of salt μ_{el} is a decreasing function of f in the range $\tau/N < uf^2 < \tau^3$ [63]. In the presence of salt the same arguments may be repeated. The results are [46]:

1. If $\tau > N^{-1/2}$ and $f < u^{-1/2}N^{-3/4}$, the electrostatics is weak and the PEL forms a globule (see Sec. 2.2.1.3). Following Eqn. 2.45 the size of the globule is

   $$R \simeq R_{glob} \simeq b\frac{N^{1/3}}{\tau^{1/3}}.$$

   If the screening length is larger than R_{glob} the interaction is unscreened inside the globule. Thus, at $\lambda_D > bN^{1/3}\tau^{-1/3}$ the behavior is identical to that without salt.

2. If the screening length is smaller than the globule size, but larger than the thermal blob size, i.e., at

   $$b/\tau < \lambda_D < bN^{1/3}/\tau^{1/3}, \tag{2.136}$$

   the range of f in which a cylindrical or pearl-necklace configuration exists is reduced, due to the abrupt collapse discussed above. Therefore μ_{el} decreases with f only in the range

   $$(\frac{b}{\lambda_D})^3 < uf^2 < \tau^3. \tag{2.137}$$

   When $b/\lambda_D > \tau$, this range shrinks to zero because the pearl-necklace configurations do not occur for any value of f.

   Strictly speaking the presence of a region where μ_{el} is decreasing with f is not sufficient to cause the instability, since it may be dominated by entropic factors [63]. In any case,

the first-order phase transition upon tuning μ_{el} and the anomalies in the titration curves should disappear in the presence of sufficient salt.

Chapter 3

Model and Simulation method

From a statistical physics point of view, one of the most important feature of polymers is that chain molecules can adopt a very large number of different conformations. Many of the unique properties of polymeric systems, such as flexibility and elasticity, originate in their large conformational entropy, which is a consequence of the large number of degrees of freedom. Moreover, different degrees of freedom can be related to quite different length and time scales; from highly localized bond vibrations, to long-range molecular relaxation and translation. The great advantage of simulations is to formulate a methodology which is, at least in principle, capable to sample effectively all degrees of freedom of an arbitrarily large system. A Monte Carlo (MC) simulation of a simple fluid is generally a rather straightforward task. However with increasing degrees of freedom a molecule has, one needs a more complex recipe for an efficient MC route.

3.1 Simulation method

Generally speaking, the Monte Carlo approach is a numerical technique making use of random numbers to solve a problem. Historically, the first large scale Monte Carlo work carried out dates back to the middle of the 20th century. Stanislav Ulam, John von Neumann and Enrico Fermi were the first who proposed and applied the Monte Carlo method as a numerical technique for solving practical problems. The earliest published work on Monte Carlo is probably the paper by Metropolis and Ulam from 1949 [64].

Thus, for carrying out a Monte Carlo simulation, a sequence of numbers is required, which have to be random, independent, real and uniformly distributed (in the range zero to one). In early Monte Carlo studies tables of random numbers have been used, which were generated directly from real random processes, e.g. radioactive decay or thermal noise in electronic devices. However such an approach is only practicable as long as Monte Carlo calculations are carried out manually. For computer calculations, the use of any predefined table seems to be impractical. Hence it is often desired to generate random numbers when required at certain steps of calculation, employing simple arithmetic operations that do not take much computer time. These numbers, generated by deterministic algorithms, are therefore predictable and reproducible. Hence, by no stretch of imagination they can be called, in a strict way, random. If they are uniformly distributed and independent over a rather large sequence, they are

considered to be pseudo-random. However, one has to bear in mind that the quality of random numbers generated by certain random number generator using a particular set of parameters can be quite different. That is, it is a good practice to check their quality by standard test of randomness before using them in real simulations.

3.2 Basic definition

Statistical physics deals with systems with many degrees of freedom. A typical task in statistical physics is to compute average values of macroscopic observables of systems, the Hamiltonian $\mathcal{H}(\mathbf{x})$ of which is known. In the canonical ensemble, the thermal average of any observable $A(\mathbf{x})$ is defined by

$$\langle A(\mathbf{x})\rangle_T = \frac{1}{Z}\int d\mathbf{x}\exp\left[-\mathcal{H}(\mathbf{x})/k_{\mathrm{B}}T\right]A(\mathbf{x}), \tag{3.1}$$

where Z is the partition function

$$Z = \int d\mathbf{x}\exp\left[-\mathcal{H}(\mathbf{x})/k_{\mathrm{B}}T\right]. \tag{3.2}$$

Note that $\mathbf{x}$ denotes the set of coordinates necessary to fix completely a point in the phase space. For a N-particle system, one has

$$d\mathbf{x} = dx_1\, dy_1\, dz_1\, dx_2 \ldots dz_N\, dp_{x_1}\, dp_{y_1}\, dp_{z_1} dp_{x_2} \ldots dp_{z_N}. \tag{3.3}$$

The normalized Boltzmann factor

$$p(\mathbf{x}) = \frac{1}{Z}\exp\left[-\mathcal{H}(\mathbf{x})/k_{\mathrm{B}}T\right] \tag{3.4}$$

plays the role of a probability density describing the statistical weight with which the configuration $\mathbf{x}$ occurs in thermal equilibrium.

In equilibrium statistical mechanics the Monte Carlo method starts from the idea of approximating the exact equation 3.1, where one integrates over all states $\{\mathbf{x}\}$ with their proper weights $p(\mathbf{x})$, by a finite sum integration using only a characteristic subset of phase space points $\{\mathbf{x}_1, \mathbf{x}_2, ..., \mathbf{x}_M\}$ which are used as statistical sample. Clearly, if one considers the limit $M \longrightarrow \infty$, the discrete sum

$$\langle A(\mathbf{x})\rangle = \frac{\sum_{l=1}^{M}\exp\left[-\mathcal{H}(\mathbf{x}_l)/k_{\mathrm{B}}T\right]A(\mathbf{x}_l)}{\sum_{l=1}^{M}\exp\left[-\mathcal{H}(\mathbf{x}_l)/k_{\mathrm{B}}T\right]} \tag{3.5}$$

must approximate Eqn. 3.1, just as in a numerical integration routines integrals are replaced by sums.

3.2.1 Simple sampling

Unlike to standard routines for solving one-dimensional integrals $\int f(x)dx$, where $f(x)$ is a function of one real variable x only instead of a high-dimensional vector $\mathbf{x}$, here it makes no sense to chose the points $\mathbf{x}_l$ according to a regular grid. A much better uniform and

representative distribution of grid points is obtained if the points $\mathbf{x}_l$ are chosen at random. This Monte Carlo method is called simple sampling. It works quite well for non-thermal problems, e.g. random walks, self-avoiding walks and percolation [65]. Besides its simplicity, the most important advantages of the simple sampling method are: (i) that the individual configurations are statistically independent of each other and therefore standard error analysis applies, (ii) that, for chain-like problems, in one simulation run one obtains information on the full range of values for chain length N up to some maximum length.

3.2.2 Importance sampling

Simple random sampling techniques are, however, not so useful for evaluating thermal averages such as Eqn. 3.5. See for example the case where in Eqn. 3.5 $A(\mathbf{x}_l)$ is the Hamiltonian $\mathcal{H}(\mathbf{x}_l)$ itself. In this case, the specific heat C per bond of the chain is given by

$$\frac{C}{k_B} = \frac{1}{N}\frac{\partial\left(\langle\mathcal{H}\rangle_T\right)}{\partial\left(k_{\mathrm{B}}T\right)} = \frac{\langle\mathcal{H}^2\rangle_T - \langle\mathcal{H}\rangle^2}{N(k_{\mathrm{B}}T)^2}, \tag{3.6}$$

which implies for the relative fluctuation

$$\frac{\langle\mathcal{H}^2\rangle_T - \langle\mathcal{H}\rangle^2}{\langle\mathcal{H}\rangle_T^2} \propto \frac{1}{N}.$$

Hence, for large N, the probability distribution $p(E)$ of the energy E per degree of freedom defined as

$$p(E) = \frac{1}{N}\int d\,\mathbf{x}\,\delta\left(\mathcal{H}(\mathbf{x}) - NE\right)\exp\left[-\mathcal{H}(\mathbf{x})/k_{\mathrm{B}}T\right] \tag{3.7}$$

is expected to be very sharply peaked. Writing

$$\langle\mathcal{H}\rangle_T = N\int_{-\infty}^{+\infty} E\,p(E)\,dE, \qquad \langle\mathcal{H}^2\rangle_T = N\int_{-\infty}^{+\infty} E^2\,p(E)\,dE \tag{3.8}$$

it becomes evident that $p(E)$ must have a peak of height $\sqrt{N}$ and width $1/\sqrt{N}$ near $E = \langle\mathcal{H}\rangle_T/N$. In fact, off second- or first-order phase transitions one can show that $p(E)$ is actually Gaussian. Therefore, using simple sampling, the probability of generating states with E in the relevant region near $\langle\mathcal{H}/N\rangle$ is exponentially small. Or in other words: Most of the phase space prints $\{\mathbf{x}_l\}$ enter Eqn. 3.5 with an exponentially small weight factor $p(x)$. So what is needed is a more efficient technique that samples the configurations $\mathbf{x}_l$ included in the average Eqn. 3.5 not completely random, but preferentially from that regime of phase space which is important at temperature T. Suppose we consider a process where the phase space points $\mathbf{x}_l$ are selected according to some possibility $P(\mathbf{x}_l)$. Choosing the set $\{\mathbf{x}_l\}$ according to a given probability distribution $P(\mathbf{x}_l)$ one has to correct the averaging for the bias and

$$\langle A(\mathbf{x})\rangle = \frac{\sum_{l=1}^{M}\exp\left[-\mathcal{H}(\mathbf{x}_l)/k_{\mathrm{B}}T\right]A(\mathbf{x}_l)/P(\mathbf{x}_l)}{\sum_{l=1}^{M}\exp\left[-\mathcal{H}(\mathbf{x}_l)/k_{\mathrm{B}}T\right]/P(\mathbf{x}_l)}. \tag{3.9}$$

A simple and most natural choice for $P(\mathbf{x}_l)$ would be $P(\mathbf{x}_l) \propto \exp\left[-\mathcal{H}(\mathbf{x}_l)/k_{\mathrm{B}}T\right]$; then the

Boltzmann factor cancels out, and Eqn. 3.9 reduces to a simple arithmetic average

$$\langle A(\mathbf{x})\rangle = \frac{1}{M}\sum_{l=1}^{M} A(\mathbf{x}_l). \tag{3.10}$$

The problem is, of course, to find a procedure which practically realizes this so-called *importance sampling* [66]. Metropolis *et al.* suggested not to choose the successive states $\{\mathbf{x}_l\}$ independently of each other, but to construct a Markov process where each state $\{\mathbf{x}_{l+1}\}$ is constructed from a previous state $\{\mathbf{x}_l\}$ via a suitable transition probability

$$W(\mathbf{x}_l \rightarrow \mathbf{x}_{l+1}).$$

They pointed out that it is possible to choose the transition probability W such that in the limit $M \rightarrow \infty$ the distribution function of the states generated by this Markov process tends towards the equilibrium distribution

$$P_{\mathrm{eq}}(\mathbf{x}_l) = \frac{1}{Z}\exp\left(-\frac{\mathcal{H}(\mathbf{x}_l)}{k_{\mathrm{B}}T}\right) \tag{3.11}$$

as desired. A sufficient condition to achieve this is to impose the principle of detailed balance

$$P_{\mathrm{eq}}(\mathbf{x}_l)W(\mathbf{x}_l \rightarrow \mathbf{x}_{l'}) = P_{\mathrm{eq}}(\mathbf{x}_{l'})W(\mathbf{x}_{l'} \rightarrow \mathbf{x}_l). \tag{3.12}$$

Eqn. 3.12 implies that the ratio of transition probabilities for a "move" $\mathbf{x}_l \rightarrow \mathbf{x}_{l'}$ and the inverse move $\mathbf{x}_{l'} \rightarrow \mathbf{x}_l$ depend only on the energy change $\delta\mathcal{H} = \mathcal{H}(\mathbf{x}_{l'}) - \mathcal{H}(\mathbf{x}_l)$,

$$\frac{W(\mathbf{x}_l \rightarrow \mathbf{x}_{l'})}{W(\mathbf{x}_{l'} \rightarrow \mathbf{x}_l)} = \exp\left(-\frac{\delta\mathcal{H}}{k_{\mathrm{B}}T}\right). \tag{3.13}$$

Eqn. 3.13 obviously does not specify $W(\mathbf{x}_l \rightarrow \mathbf{x}_{l'})$ uniquely, and some arbitrariness in the explicit choice of W remains. The most frequently used choice is [67, 68]

$$W(\mathbf{x}_l \rightarrow \mathbf{x}_{l'}) = \begin{cases} \exp\left(-\delta\mathcal{H}/k_{\mathrm{B}}T\right) & \text{if} \quad \delta\mathcal{H} > 0, \\ \\ 1 & \text{otherwise.} \end{cases} \tag{3.14}$$

Thus, the importance sampling algorithm looks as follows: At any given time the current state of the system (i.e. its position in the search space) is denoted state-0. It has an energy of ϵ_0 and a property value of A_0. After a random move the system will be in a new trial state (state-1) with an energy of ϵ_1 and a property value of A_1. The simulation proceeds as follows. Independently whether this trial state will be accepted or rejected the attempt is counted as one Monte Carlo step. The acceptance criterion is given by Eqn. 3.14, i.e.,

- if $\epsilon_1 < \epsilon_0$: the trial state is accepted with probability 1 and becomes the new state-0. In addition, the property of the new state is added to the sum ($A_{\mathrm{sum}} = A_{\mathrm{sum}} + A_1$),

– if $\epsilon_1 > \epsilon_0$: the trial state is accepted with probability $\exp\left[-(\epsilon_1 - \epsilon_0)/k_{\mathrm{B}}T\right]$, i.e., if accepted the trial state becomes the new state-0, if it is rejected then the system remains in the old state-0 which is counted once more. Technically the acceptance with probability $\exp\left[-(\epsilon_1 - \epsilon_0)/k_{\mathrm{B}}T\right]$ is solved by comparing it with a random number $0 \leq \zeta \leq 1$. If $\exp\left[-(\epsilon_1 - \epsilon_0)/k_{\mathrm{B}}T\right] > \zeta$ the trial state is accepted.

Note that now, i.e., using importance sampling, the different states are not independent any more. Hence, standard error analysis cannot be applied directly.

3.3 Model

A freely-jointed bead-spring chain [69] of N beads (monomers) is considered. Neighboring monomers are connected by a harmonic spring, the potential of which is given by Eqn. 2.16,

$$U_{\mathrm{bond}}(r) = \frac{3k_{\mathrm{B}}T}{2}\frac{r^2}{b_0^2},$$

with b_0 being the (bare) average bond length. The nonelectrostatic interaction between all the monomers is described by a modified Lennard-Jones potential [70]

$$U_{\mathrm{LJ}}^{(\mathrm{m})}(r) = \begin{cases} 4\varepsilon\left\{\left[\left(\frac{\sigma}{r}\right)^{12} - \left(\frac{\sigma}{r}\right)^{6} + \frac{1}{4}\right] + \beta\left[\cos\left(2\pi r/r_c\right) - 1\right]\right\}, & r < r_c \\ 0, & r > r_c \end{cases} \tag{3.15}$$

with $r_c = 2^{1/6}\sigma$. For $\beta > 0$, this potential includes a very narrow attractive part such that the range of interaction remains short; making a significant advantage in simulation time. The quality of solvent or the strength of the attractive part is tuned by parameter β (see Fig. 3.1). The scaled temperature in Eqn. 2.40 reads now

$$\tau = \frac{\beta - \beta_\Theta}{\beta_\Theta}, \tag{3.16}$$

where β_Θ is the β value corresponding to the Θ point. b_0 is used as the unit of length, ε as the unit of energy, and the monomer mass m as the unit of mass. All quantities are expressed in this unit system. The simulations are performed at $k_{\mathrm{B}}T = 1.2$. To ensure that the bond length distribution will be only weakly perturbed by the short-range interaction, but remains almost Gaussian, σ is set to 1/2. In Fig. 3.2, the bond length distribution function of a neutral chain is shown at different values of σ. The bold line is plotted according to Eqn. 2.10; i.e., the theoretical bond length distribution of the Gaussian chain.

In addition to the short-range interaction, all charged monomers interact with each other via the screened Coulomb (Debye-Hückel) potential

$$U_{\mathrm{DH}} = k_{\mathrm{B}}T\lambda_{\mathrm{B}}\frac{e^{-r/\lambda_{\mathrm{D}}}}{r}.$$

The PELs are considered at infinite dilution and therefore the screening length λ_{D} is determined only by the concentration of added salt but not by the charges on the polymer or the

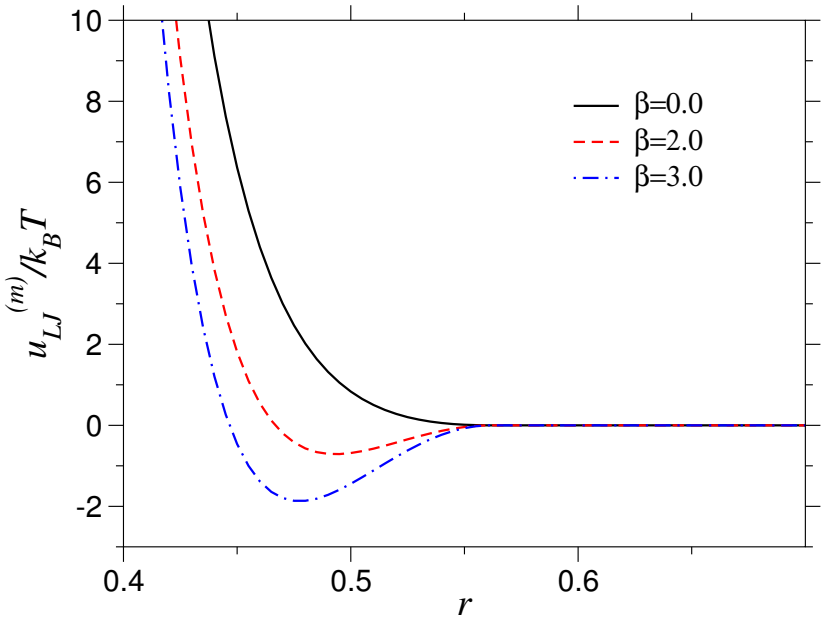

Figure 3.1: Modified Lennard-Jones potential between one pair of monomers. β establishes the quality of solvent. $\sigma = 0.5, \varepsilon = 1.0$ and $k_{\mathrm{B}}T = 1.2$.

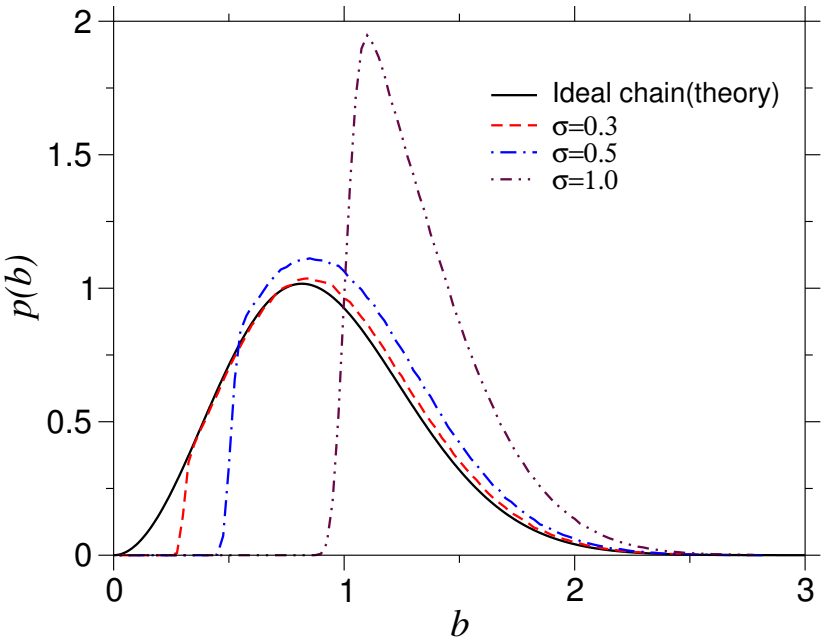

Figure 3.2: Bond length distribution of a neutral chain, of N=1000 monomers, for different values of σ and comparison to the theoretical bond length distribution of the ideal chain. $\sigma = 0.5$ is the value chosen in this study.

counterions. Because the study is focused to annealed PELs, the monomer charge density and distribution along the chain is not fixed. However, within the framework of the model, the screening length can be kept constant while the chemical potential μ and the average degree of charging are varying (Sec. 4.1.2). Except otherwise mentioned, throughout sections 4.1 and 4.2, λ_D is set to $10b_0$ and $N = 256$. The exponentially decaying interaction enables the introduction of a cutoff which is chosen as $r_c = 5\lambda_D$. The chain is simulated in a (semi-)grand canonical ensemble where it is in contact with a reservoir of charges of constant chemical potential μ.

3.4 Simulation details

Adopting a freely jointed bead-spring model with a dynamic distribution of charges along the chain, a set of different MC moves must be included to equilibrate the system. A set consisting of *local displacement, pivot, reptation* and *charge moves* was found to be appropriate to produce equilibrium values at reasonable times:

- **Local displacement move:** A monomer of the chain is chosen at random and moved by a random displacement vector (see Fig. 3.3(a)). This move is required to equilibrate bond length distribution. Local displacements are very effective especially for compact structures as, e.g. neutral chains or very weakly charged PELs in poor solvent. Sometimes one needs to tune the maximum amount of displacement in order to accelerate the simulation.

- **Pivot move:** One monomer is picked randomly and one chain end, e.g. to the right of the picked monomer is rotated as a rigid body at a random orientation and angles (see Fig. 3.3(b)). This move is very effective in simulating highly diluted polymer solutions. It is the fastest way to equilibrate large length scales. But, the acceptance rate drops down at higher polymer densities. That is why one can omit it if the system is close to its equilibrium as a compact structure. However, if the system is swollen or the simulation have just started from an elongated state, the pivot move is highly preferable.

- **Reptation move:** One end of the chain is randomly chosen, it is cut and appended to the other end with a random orientation (segment length is kept fixed) (see Fig. 3.3(c)).

- **Charge move:** Additionally to the configurational MC moves introduced above the algorithm is completed with a charge move by which the charge state of a randomly chosen monomer is switched; Fig. 3.3(d).

  The energy change of a complete MC move reads

$$\Delta E = \Delta E_{\text{conf}} \pm \mu, \tag{3.17}$$

  where ΔE_{conf} is the change in configurational energy due to ΔU_{bond}, ΔU_{LJ}, and ΔU_{DH}. The plus sign is used when the monomer is to be neutralized (protonated) and the minus sign when it is to be charged (deprotonated).

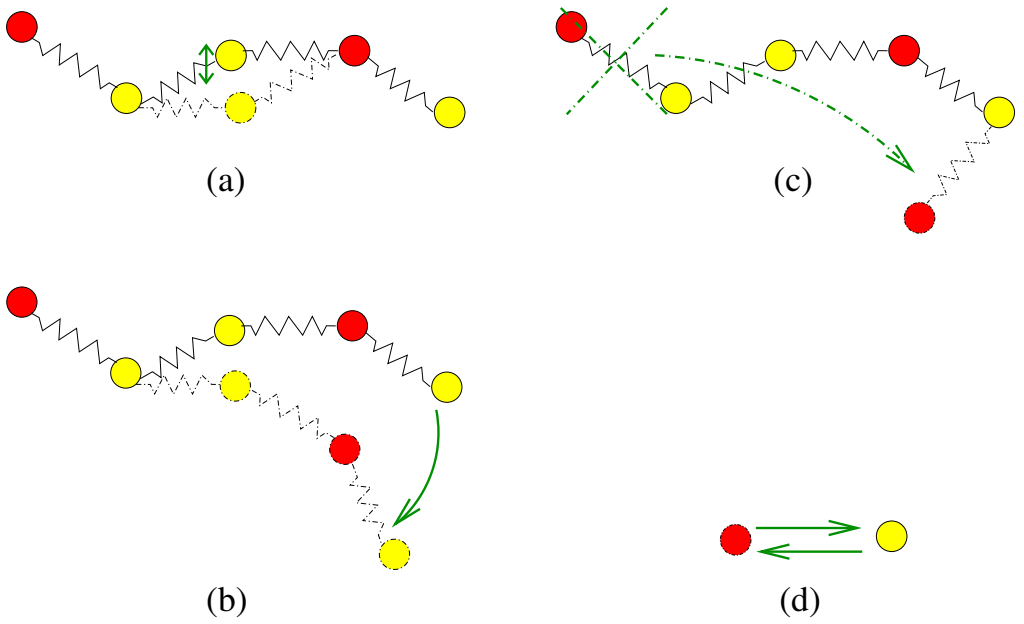

Figure 3.3: Trial moves used in the simulation; (a) local move, (b) pivot move, (c) reptation move and (d) charge move. Red color denotes charged monomers and yellow color denotes uncharged monomers.

It is noted that in the simulations at different values of β, including good, Θ and poor solvent regimes, the maximum displacement vector is tuned. For this process, the acceptance rate of the local displacement move can be used to tune the maximum length of local displacement during the simulation. For example, the maximum displacement length was set 0.5 for $\beta = 2.40$ and 2.615, but 0.1 for $\beta = 3.0$ and higher β.

To ensure that the simulation generates equilibrium data the simulation runs were started with different configurations: random coil and straight line (good solvent) or random coil, dumbbell and globule (poor solvent). After appropriate relaxation, these runs yield identical averaged quantities. Depending on the type of starting configuration different mixing of the configurational MC moves is necessary [71]. Furthermore, in particular for not too large τ and $Nb/\lambda_{\mathrm{D}} \gg 1$, during relaxation one has to take care that the chains are not accidentally charged up while the structure becomes trapped in local energy minima corresponding to highly stretched states. That is why the frequency of charge moves is temporarily reduced at such points.

Doing so, equilibrium structures were obtained after typically $3 \cdot 10^6$ (combined) Monte Carlo steps per monomer (MCM). After reaching extended equilibrium states a pivot move is added after 200 (combined) MC moves. In collapsed equilibrium states pivot move is omitted because of its vanishing acceptance rate. To estimate the statistical inefficiency of the runs, the autocorrelation function (see Sec. 3.5) of the end-to-end distance is calculated. In the highly charged extended state the corresponding correlation time is about 15 MCM. In the globular state it can become substantially larger ranging from about 15 MCM (at $\tau = 0.19$) up to about 200 MCM (at $\tau = 0.26$). Ensemble-averaged properties are taken as average over trajectories of lengths between $10 \cdot 10^6$ MCM and $25 \cdot 10^6$ MCM corresponding to renewal

times between $4 \cdot 10^4$ and $170 \cdot 10^4$. In this way the relative error of the m.s. end-to-end distance $R = \langle \mathbf{R}^2 \rangle = \langle (\mathbf{r}_N - \mathbf{r}_1)^2 \rangle$ was found to be less than 1% in the collapsed state and less than 8% in the extended state. The number of charges are reproducible within less than 1% independently of the conformation of the polyelectrolyte.

3.5 Analyzing simulation results

As mentioned already above, MC simulation data generated by importance sampling are no statistically independent. Therefore error analysis has to be done carefully [67, 68]. Suppose n successive observations A_k, $k = 1, ..., n$ of a quantity A have been stored, with $n \gg 1$. One can consider the expectation value of the square of the statistical error

$$\begin{aligned} \left\langle (\delta A)^2 \right\rangle &= \left\langle \left[\frac{1}{n} \sum_{k=1}^{n} (A_k - \langle A \rangle) \right]^2 \right\rangle = \frac{1}{n^2} \sum_{k=1}^{n} \left\langle (A_k - \langle A \rangle)^2 \right\rangle \\ &+ \frac{2}{n^2} \sum_{k_1=1}^{n} \sum_{k_2=k_1+1}^{n} \left(\langle A_{k_1} A_{k_2} \rangle - \langle A \rangle^2 \right). \end{aligned} \tag{3.18}$$

Changing the summation index k_2 to $k_2 + k$, Eqn. 3.18 can be written as

$$\left\langle (\delta A)^2 \right\rangle = \frac{1}{n} \left[\langle A^2 \rangle - \langle A \rangle^2 + 2 \sum_{k=1}^{n} \left(1 - \frac{k}{n} \right) \left(\langle A_0 A_k \rangle - \langle A \rangle^2 \right) \right]. \tag{3.19}$$

A time $t_k = \delta t_k$ is associated with the Monte Carlo process, δt being the time interval between two successive observations A_k, A_{k+1}. Transforming the summation into a time integration and dropping index k from t_k, one obtains

$$\begin{aligned} \left\langle (\delta A)^2 \right\rangle &= \frac{1}{n} \left[\langle A^2 \rangle - \langle A \rangle^2 + 2 \frac{1}{\delta t} \int_0^{t_n} \left(1 - \frac{t}{t_n} \right) \left[\langle A(0) A(t) \rangle - \langle A \rangle^2 \right] dt \right] \\ &= \frac{1}{n} \left(\langle A^2 \rangle - \langle A \rangle^2 \right) \left[1 + \frac{2}{\delta t} \int_0^{t_n} \left(1 - \frac{t}{t_n} \right) \frac{\langle A(0) A(t) \rangle - \langle A \rangle^2}{\langle A^2 \rangle - \langle A \rangle^2} dt \right]. \end{aligned} \tag{3.20}$$

Next the normalized relaxation function (autocorrelation function) of the quantity A is introduced

$$C_A(t) = \frac{\langle A(0) A(t) \rangle - \langle A \rangle^2}{\langle A^2 \rangle - \langle A \rangle^2}. \tag{3.21}$$

Note that $C_A(0) = 1$ and $C_A(t)$ decays to zero as $t \to \infty$. Assuming that $C_A(t)$ decays to zero on a time-scale t_R

$$t_R = \int_0^{\infty} C_A(t) dt, \tag{3.22}$$

called correlation time with $t_R \ll t_n$, Eqn. 3.20 can be approximated. Because $C_A(t)$ differs from zero appreciably only for time $t \ll t_n$, the term t/t_n in Eqn. 3.20 can be neglected and the upper limit of the integration is replaced by infinity. This yields

$$\left\langle (\delta A)^2 \right\rangle = \frac{1}{n} \left[\langle A^2 \rangle - \langle A \rangle^2 \right] \left(1 + 2 \frac{t_R}{\delta t} \right). \tag{3.23}$$

If $\delta t \gg t_R$, then the last factor in Eqn. 3.23 is unity to a very good approximation and the statistical error has just the same from as encountered due to standard error analysis. In the inverse case, where $\delta t \ll t_R$, one finds instead ($n\delta t = t_{\text{obs}}$ is the time over which the averaging is extended)

$$\left\langle (\delta A)^2 \right\rangle \approx \frac{2t_R}{n\delta t} \left[\left\langle A^2 \right\rangle - \langle A \rangle^2 \right] = 2\frac{t_R}{t_{\text{obs}}} \left[\left\langle A^2 \right\rangle - \langle A \rangle^2 \right], \tag{3.24}$$

which shows that the *statistical error* is independent of the choice of the *time interval* δt [67, 72]. Although for a given averaging time t_n a choice of a smaller value δt results in a correspondingly larger value of the number n observations, it does not increase the statistical error; only the ratio between the relaxation time t_R and the observation time t_{obs} matters. The fact that $\langle (\delta A)^2 \rangle$ in general is not given by the simple sampling result $\left[\langle A^2 \rangle - \langle A \rangle^2 \right] / n$, but is enhanced by some factor and therefore the enhancement factor is also called the "statistical inefficiency" of the method [73].

Chapter 4

Simulation results

The behavior of annealed PELs in a poor solvent has been studied by Monte Carlo simulation. To equilibrate the system in a reasonable CPU time and to prevent possible bottlenecks the Monte Carlo moves described above are mixed in a optimized way depending on the specific evolution of chain structure. The code has been written in Fortran90 language and the simulations were carried out on Compaq Alpha servers, with EV67/883 MHZ processors. First the code was verified by reproducing well-known features of uncharged polymers and quenched PELs.

4.1 Development and testing of the code

4.1.1 Neutral chain

4.1.1.1 Gaussian chain

A Gaussian chain is the simplest polymer system one can imagine (Sec. 2.1.1). A chain of $N = 1000$ monomers connected by harmonic springs has been simulated. The bond potential is given by Eqn. 2.16. Only local displacement and pivot moves are applied in a 1:1 mixing.

For a Gaussian chain, the scaling relation predicts that the size of the coil grows with the square root of the chain length, i.e.

$$\frac{\langle R^2 \rangle^{1/2}}{b} \propto N^{1/2}.$$

Evaluating the intrachain form factor in the Porod region $2\pi/R_{\mathrm{g}} < q < 2\pi/b$ the predicted behavior reads

$$S(q) \propto q^{-1/\nu} \propto q^{-2}.$$

Fig. 4.1 shows the chain length dependence of the end-to-end distance which exhibits a perfect fitting with exponent $\nu = 1/2$. The spherically averaged intrachain structure factor (see Eqn. 2.24) is plotted in Fig. 4.2. In the Porod region, $S(q)$ shows a perfect asymptotic behavior with $\nu = 1/2$. Additionally, the intersecting point with y-axis gives the degree of polymerization.

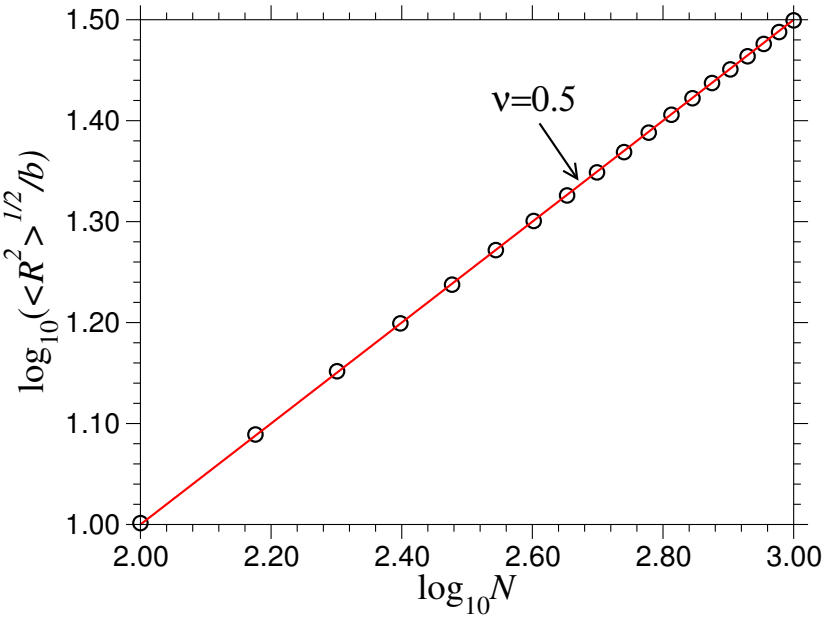

Figure 4.1: Coil size dependence R versus N of an ideal chain. The line indicates a power law $N^{1/2}$.

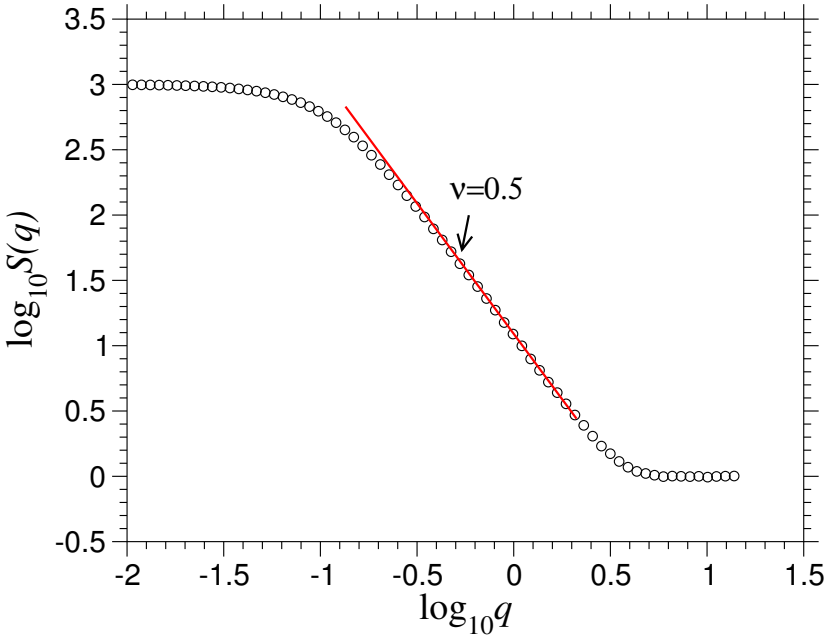

Figure 4.2: Spherically averaged intrachain structure factor of an ideal chain (N=1000). The line indicates the asymptotic behavior $S(q) \propto q^{-2}$.

Performing numerical simulations in statistical physics one importing problem is: Are equilibrium states reached in reasonable times? This test is done, for example, by starting the simulation with quite different configurations, e.g., with one starting from a random coil and another one starting from an elongated chain. Independently from the starting configuration, all simulation runs should approach the same equilibrium structure. In Fig. 4.3, the running

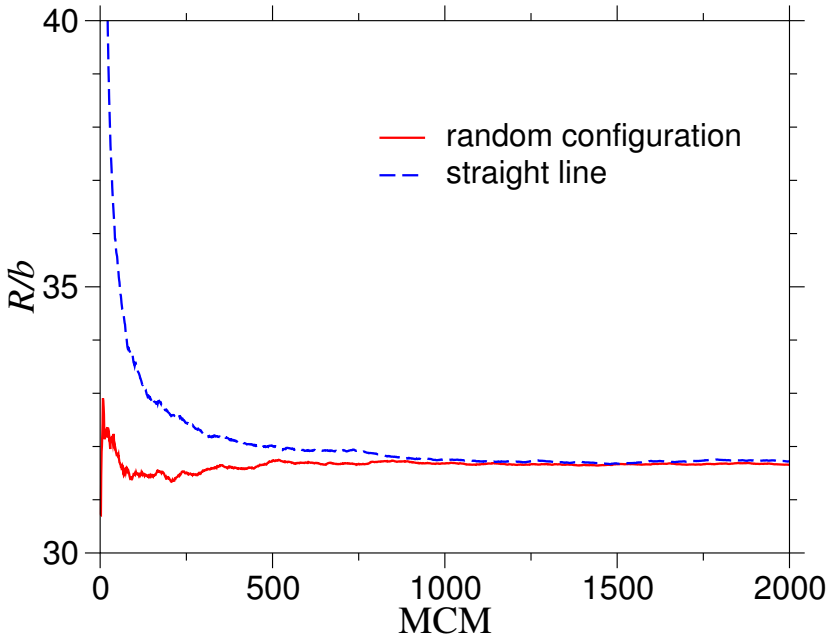

Figure 4.3: Running averages of m.s. end-to-end distance, starting with a random conformation and with a straight line, $N = 1000$.

averages of m.s. end-to-end distance versus Monte Carlo steps per monomer (MCM) are shown. The two runs from a random coil configuration and a completely stretched chain, respectively approach each other after about 1000 MCM. To estimate the typical relaxation times this kind of test has been always performed whenever the physical system was changed.

4.1.1.2 Swollen chain with excluded volume

Including excluded volume effects, i.e., simulating a polymer chain in a good solvent one expects a swelling of the coil which is reflected by a Flory exponent $\nu \approx 0.6$.

The good solvent is modeled by setting $\beta = 0.0$ in Eqn. 3.15, i.e. no attraction at all. A mixing of local displacement moves and pivot moves is appropriate to equilibrate the system in reasonable times. The acceptance rates of both local displacement and pivot moves are about 30%.

In Fig. 4.4, the chain length dependence of the m.s. end-to-end distance is collected for three different values of σ. The corresponding spherically averaged form factors are plotted in Fig 4.5. For $\sigma = 1.0$ and $\sigma = 0.5$ the behavior fits rather well the scaling theoretically expected, i.e. $\nu \approx 0.6$, while for $\sigma = 0.3$, the chain exhibits a cross over to the behavior of an ideal chain. Note that $\sigma = 0.5$ was used in order to allow a bond length distribution which is almost Gaussian (see Sec. 3.3). To include both features in our main study, $\sigma = 0.5$ is preferred in the investigation of annealed PELs in poor solvent.

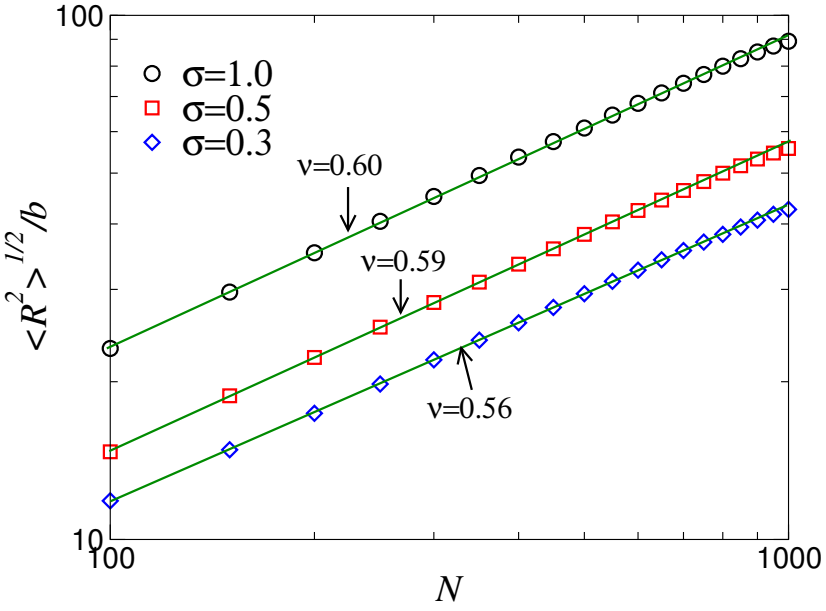

Figure 4.4: Chain length dependence of a neutral chain ($N = 1000$) in good solvent for different σ.

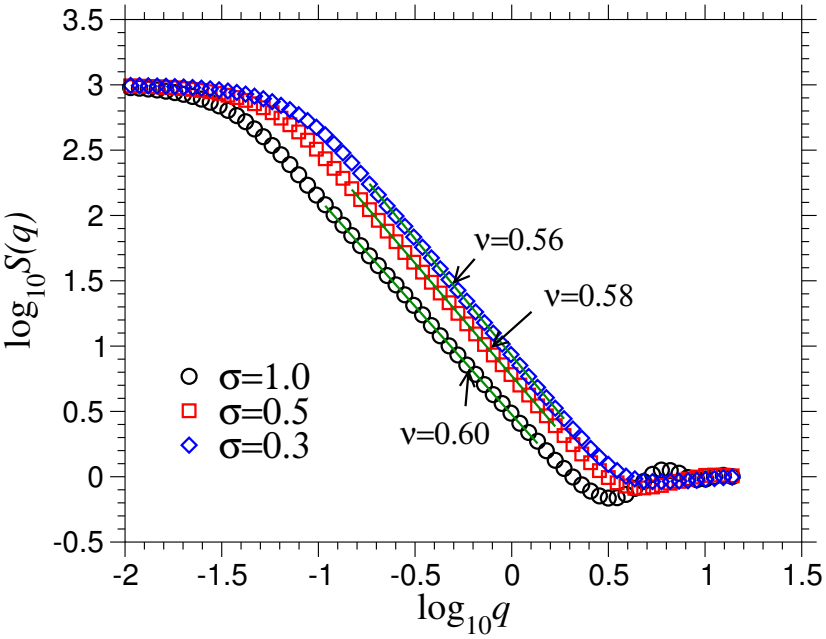

Figure 4.5: Spherically averaged structure factor of a neutral chain in good solvent for different σ (N=1000).

4.1.1.3 Determination of the Θ point

Within the model used in this study the quality of the solvent is tuned by parameter β (see Eqn. 3.15). To determine the Θ point one can use the different chain length dependences below, above and at the Θ point, respectively. For large β, the attractive part of the potential (Eqn. 3.15) dominates the behavior of the chain which will collapse into a globular structure. On the other hand, at sufficiently small β the attraction becomes rather weak and the chain

is expected to form a swollen coil due to repulsive excluded volume. In between, i.e., at β_Θ both interactions cancel each other and the chain exhibits the behavior of an ideal chain. Hence, following the general scaling predictions (see Eqns. 2.43, 2.45 and 2.50), one expects the asymptotic behavior

$$R \propto bN^{\nu} \quad \text{with} \quad \nu \begin{cases} \approx 0.6 & \text{at} \quad \beta < \beta_\Theta, \\ = 1/2 & \text{at} \quad \beta = \beta_\Theta, \\ = 1/3 & \text{at} \quad \beta > \beta_\Theta. \end{cases}$$

Thus, plotting $\langle R^2 \rangle / (Nb^2)$ versus $1/N$ for varying β the curves should flatten off at $\beta = \beta_\Theta$ in the asymptotic region $1/N \to 0$. The simulation results for chains of length N=4, 8, 16, 32, 64, 128, 256 at $2.0 \leq \beta \leq 2.8$ are plotted in Fig. 4.6 and 4.7. In fact, both for the m.s. end-to-end distance and the radius of gyration the chain length dependences obey Gaussian behavior $\langle R^2 \rangle / Nb^2 = \text{const}$ at a certain β. In this way, it is found that

$$\beta_\Theta = 2.615 \pm 0.015.$$

Due to (i) different bond potential and (ii) different setting of σ, β_Θ is slightly larger than that obtained in ref. [70].

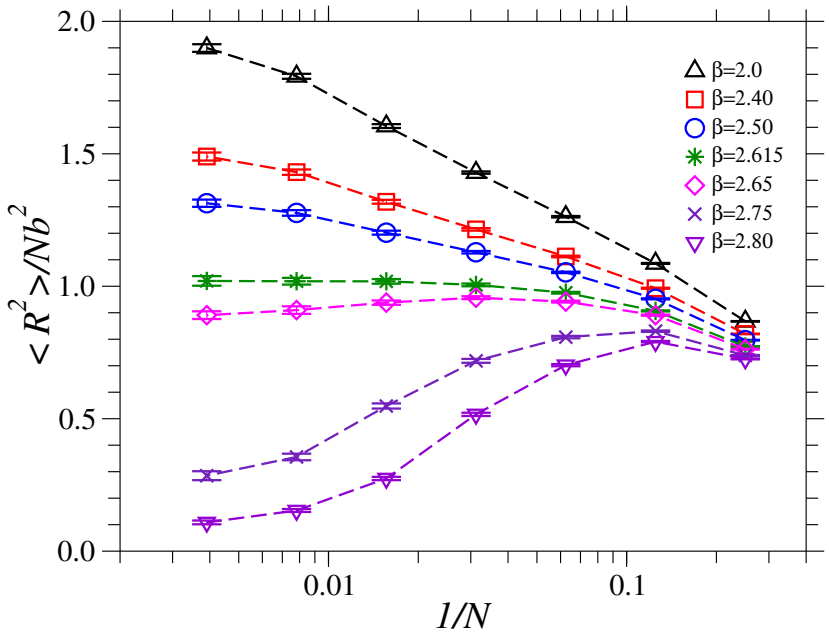

Figure 4.6: Chain length dependence of the normalized end-to-end distance for a neutral chain at different values of β.

The value of β_Θ can be counterchecked by plotting $\langle R^2 \rangle / Nb^2$ versus β for different chain lengths. For large N, all curves should have a common intersection point at $\beta = \beta_\Theta$ where the order of the curves is changing [74, 75]: at $\beta < \beta_\Theta$ the ratio $\langle R^2 \rangle / b^2 N$ is increasing while N becomes larger, since the exponent $2\nu - 1$ is positive, while at $\beta > \beta_\Theta$ the ratio $\langle R^2 \rangle / b^2 N$ is decreasing while N becomes larger. In this way, Fig. 4.8 proves that $\beta_\Theta = 2.615$, corresponds to the Θ point indeed.

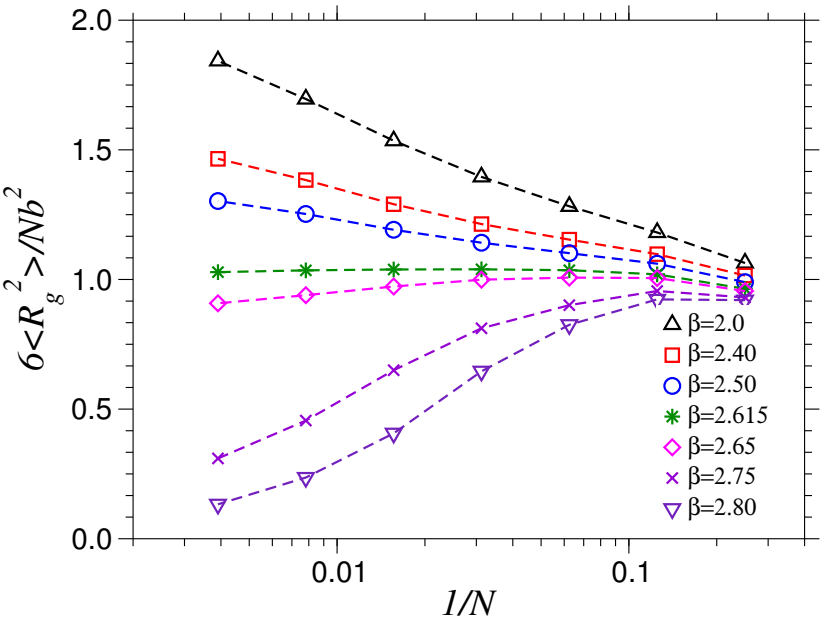

Figure 4.7: Chain length dependence of the normalized radius of gyration at different values of β.

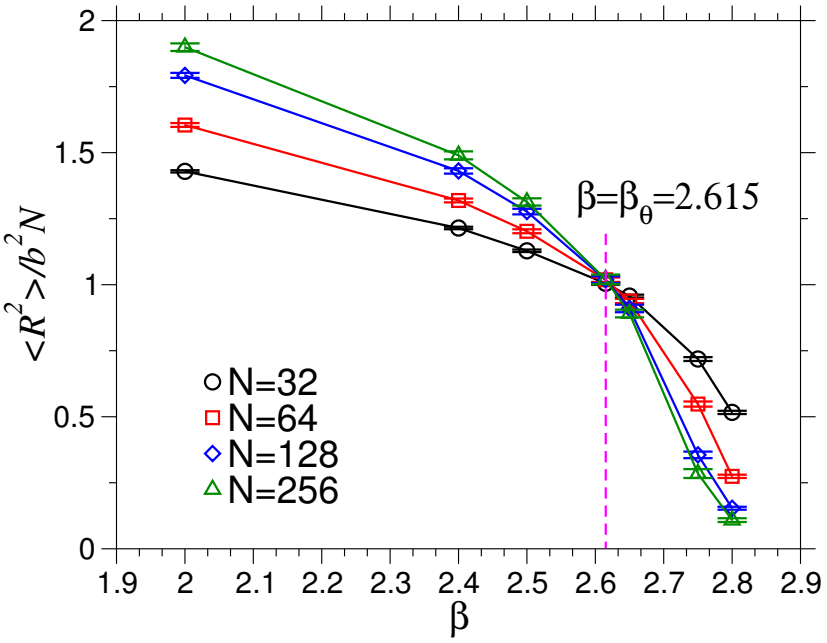

Figure 4.8: The normalized end-to-end distance $\langle R^2\rangle/b^2N$ vs. β at different chain lengths. For large N, all the curves intersect in a common point $\beta_\Theta = 2.615$.

4.1.1.4 Varying solvent quality

For β values larger than β_Θ, the neutral chain will collapse into a globular structure. However, for β very close to β_Θ, the globular structure is yet not realized for the model of a flexible chain used here. The first clear globule could be observed at $\beta \approx 2.90$, which corresponds to

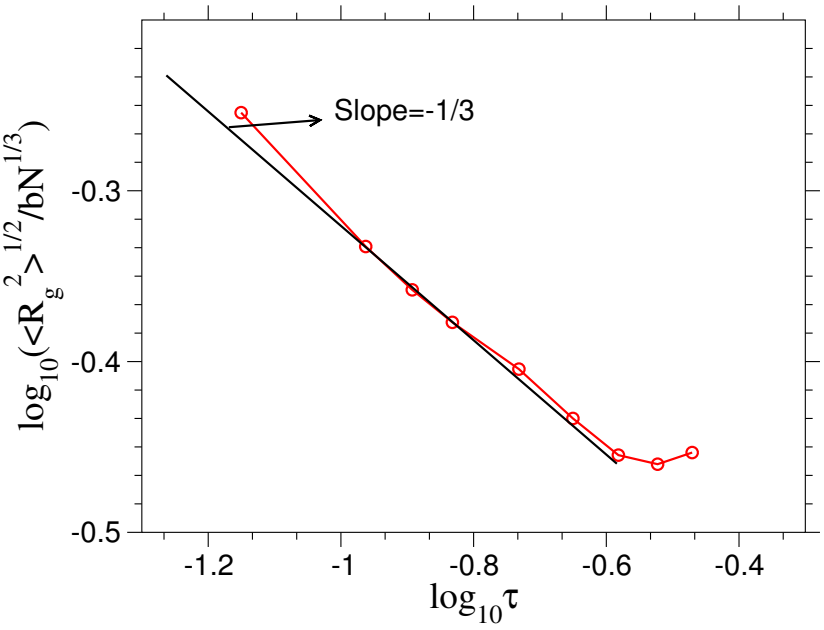

Figure 4.9: The normalized radius of gyration of a neutral chain of $N = 256$ versus τ in poor solvents.

$\tau \approx 0.10$. For poor solvents, the scaling relation on τ reads

$$\frac{\langle R_g^2 \rangle^{1/2}}{bN^{1/3}} \propto \tau^{-1/3}. \tag{4.1}$$

Fig. 4.9 displays the corresponding plot. In the region $0.10 \leq \tau \leq 0.15$ one obtains agreement with the scaling predictions. At larger τ the dependence of $\langle R_g^2 \rangle^{1/2}$ on τ deviates from the theoretically predicted one given by Eqn. 4.1. The reason is that for strong attraction the monomers become effectively close-packed, such that no further shrinking is possible. Using the corresponding radius of gyration $R_g \approx 1.6$ and taking into account that for a spherical globule with uniform density the relation between the radius R and R_g reads $R_g = (3/5)^{1/2} R$, the radius of the globule is estimated as $R = 2.1$, which corresponds to a very high density where typically simulations of polymer melts are performed [76] (Note that the end-to-end distance measured directly in the simulation is 2.0).

Fig. 4.10(a) shows the single chain structure factors at different β close to Θ point. While the behavior at the good solvent side is very close to that in Θ solvent, at the poor solvent side the behavior is drastically changed. Fig. 4.10(b) exhibits the conformational features of chains in rather poor solvents. There appears a new length scale in the problem: The peak seen at $\log_{10} q \approx 0.5$ gives the size of the globules:

$$R = \frac{2\pi}{q} \Longrightarrow R \approx 2.0,$$

which agrees well with the estimation made above and confirms that the globule is becoming more compact, up to a certain limit, for poorer solvent. Note that depending on τ, the end-to-end distances measured directly range from 1.9 to 2.2. Starting from Θ point and increasing β the first stable globule was found at $\beta = 2.90$ or $\tau = 0.10$. However at such a relative

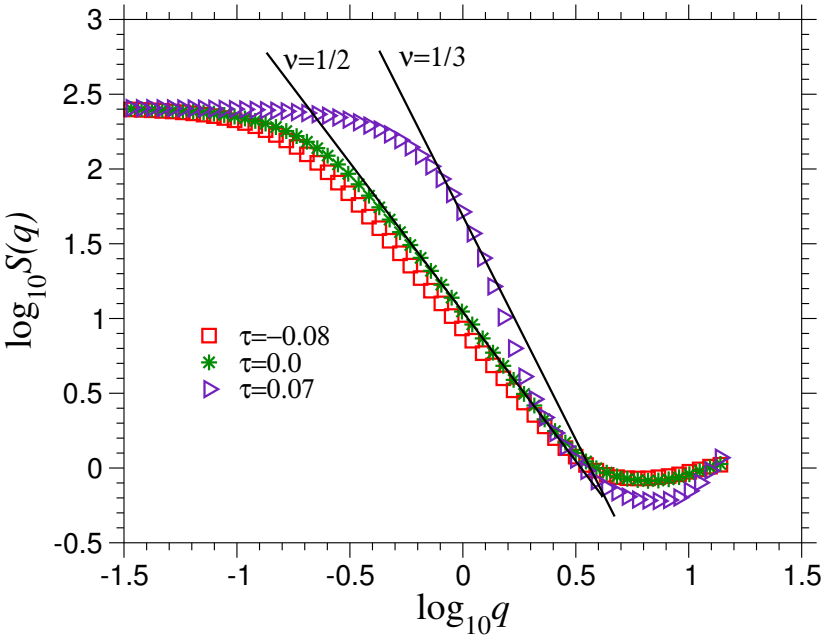

(a)

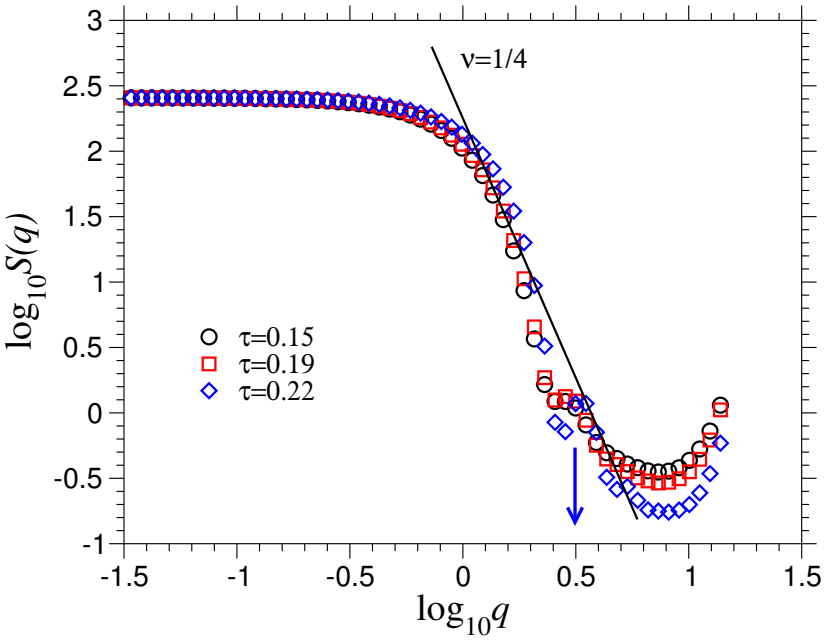

(b)

Figure 4.10: Structure factor of a neutral chain at different solvent qualities ($N = 256$). (a) close to Θ point; $\tau = -0.08, 0.0,$ and 0.07; (b) far below Θ point; $\tau = 0.15, 0.19,$ and 0.22. Arrow points peak corresponding to globule size. Straight lines indicate certain asymptotic scaling.

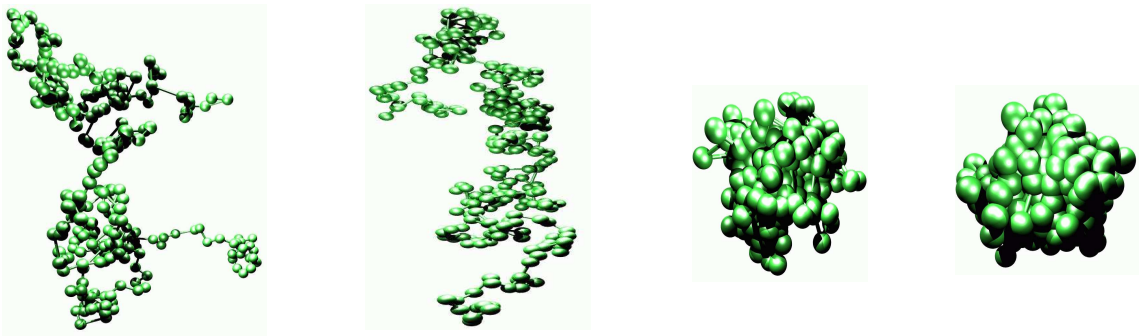

Figure 4.11: Sample pictures of a neutral chain in different solvent conditions; (a) $\beta = 2.40$, (b) $\beta = 2.615$, (c) $\beta = 2.90$ and (d) $\beta = 3.0$.

small distance from Θ point the fluctuations of the structure are still large. This feature is also indicated in the snapshots shown in Fig. 4.11. On the other hand, deeper in the poor solvent region at $\beta = 3.0, \tau = 0.15$, there remain only weak fluctuations of the globule. To estimate the statistical inefficiency of the simulation data, the correlation function of $\langle R^2 \rangle$ is calculated at different solvent quality. Fig. 4.12 shows the autocorrelation function of $\langle R^2 \rangle$ of neutral chains with different chain lengths; Fig. 4.12(a) for $\beta = 2.40$ which corresponds to a good solvent ($\tau = -0.08$), Fig. 4.12(b) for the Θ-solvent and Fig. 4.12(c) for $\beta = 2.75$ which corresponds to a poor solvent ($\tau = 0.05$). For simplicity, the correlation times are taken as the intersecting points with $1/e$. The corresponding correlation times t_{R} in units of Monte Carlo steps are given in Table 4.1. Because the relaxation is slowing down for the compact structures (see Fig.4.12(c)) it becomes more and more difficult to calculate the correlation function, especially for larger chains when β is increased.

N	$\tau = -0.08$ $t_R \approx$	$\tau = 0.0$ $t_R \approx$	$\tau = 0.05$ $t_R \approx$
256	8	22	120*
128	16	57	200*
64	35	71	280
32	65	121	330
16	124	194	417
8	250	264	545
4	445	829	1195

Table 4.1: Correlation times in units of MC steps for various neutral chains at different β. (*: the corresponding t_R's are obtained by extrapolation of the simulation data).

Before finishing the discussion of neutral chains in a poor solvent, the time evolution of the structure of a neutral chain after immersing in a poor solvent is illustrated in Fig. 4.13. The starting configuration is a random coil (good solvent). The equilibrium state of the globule is

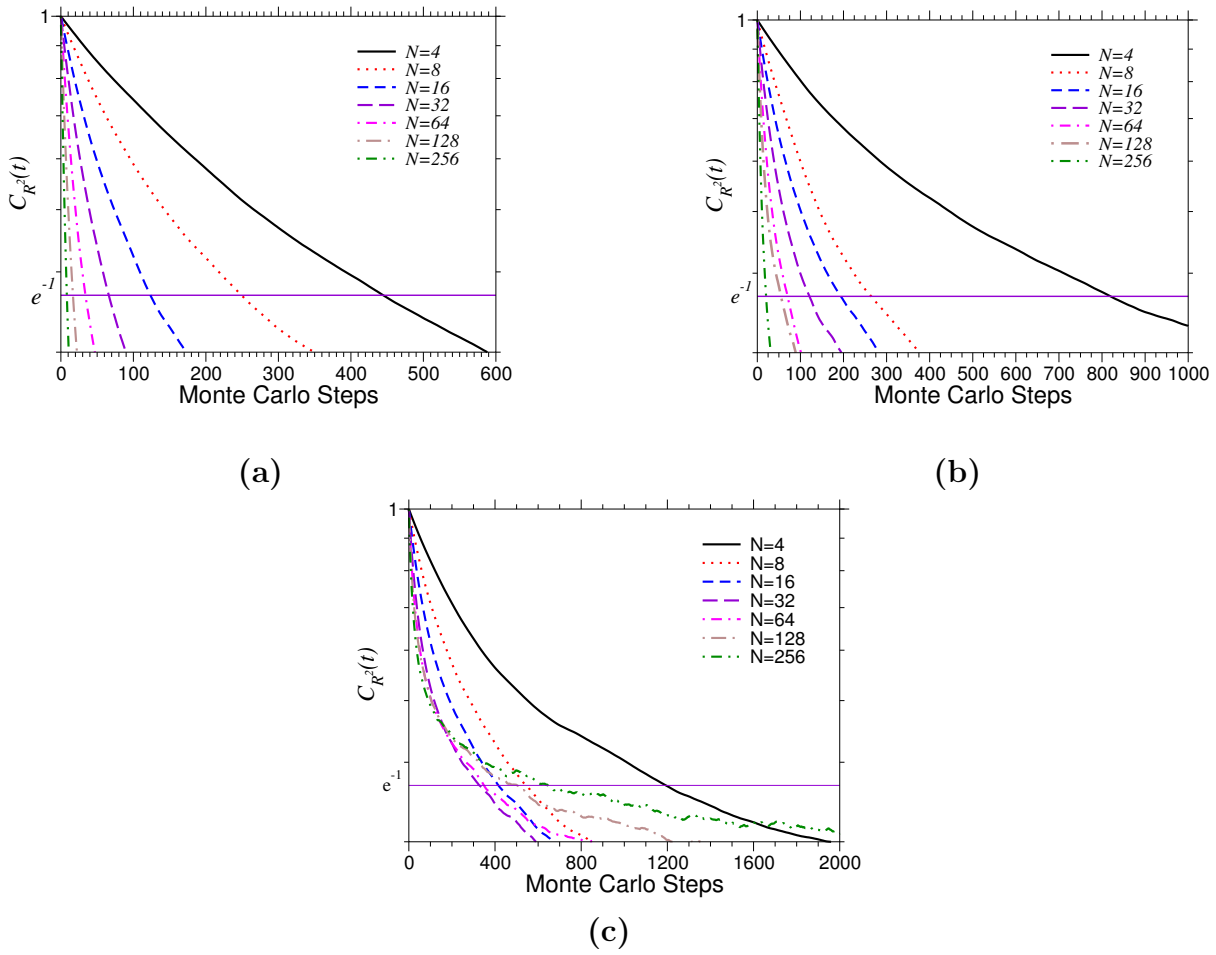

Figure 4.12: Autocorrelation function of $\langle R^2 \rangle$ of a neutral chain under different solvent conditions. (a) $\tau = -0.08$ ($\beta = 2.40$, good solvent), (b) $\tau = 0.0$ ($\beta = 2.615, \Theta$-solvent) and (c) $\tau = 0.05$ ($\beta = 2.75$, poor solvent) for various chain lengths. (Note the different scale of x-axes.)

reached via a deformed compact structure. This coil-globule transition process is reversible. The snapshots were taken at $\beta = 3.0, \tau = 0.15$ and $N = 256$.

4.1.2 Quenched polyelectrolytes

In the case of quenched PEL, the polymer chain is charged with a certain degree and the positions of the charges are fixed, i.e., the system has no freedom in the charge distribution. In a good solvent, PELs are stretched on different length scales depending on the degree of charging. Provided strong charging and vanishing screening the chain can be almost fully stretched. If the PEL chain is in a poor solvent, it can exhibit so-called pearl-necklace structures [29, 70].

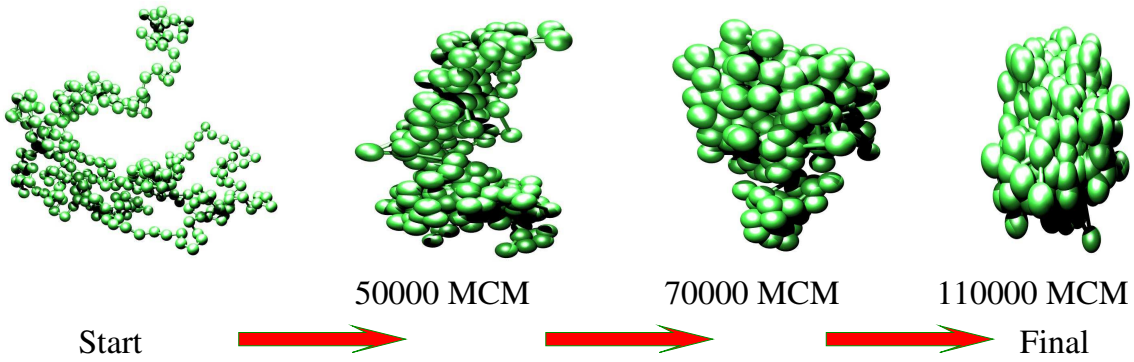

Figure 4.13: Evolution of coil-globule transition. The snapshots were taken from the simulation of a neutral chain ($N = 256$) in poor solvent ($\tau = 0.15$). MCM is one (mixed) Monte Carlo step per monomer.

4.1.2.1 Completely charged PELs in good solvent

All monomers are charged ($f = 1$) carrying one elementary charge and interacting with the Debye Hückel potential (Eqn. 2.67). The good solvent is modeled by a purely repulsive Lennard-Jones potential given in Eqn. 3.15 with $\beta = 0.0$. Depending on the degree of screening the chain is expected to be stretched on a varying length scale. Fig. 4.14 displays the chain length dependence of the m.s. end-to-end distance of a fully charged PEL chain at different λ_D. At weak screening, when almost all charged units are interacting with each other, in the asymptotic region the size of the chain scales as

$$\langle R^2 \rangle^{1/2} \simeq bN,$$

i.e., the chain is strongly stretched and its end-to-end distance is proportional to contour length. On the other hand, at strong screening the PEL chain behaves more or less like a neutral one, i.e.

$$\langle R^2 \rangle^{1/2} \simeq bN^{0.6}.$$

The corresponding spherically averaged structure factors $S(q)$ are shown in Fig. 4.15. In the Porod region, $2\pi/R \ll q \ll 2\pi/b$, the behavior of $S(q)$ is predicted in analogy to the neutral chain case, where $S(q)$ scales as $q^{-1/\nu}$, with ν being the exponent of the N dependence of the chain radii. The exponent ν estimated from $S(q)$ are given in Table 4.2. Except the case $\lambda_D = 500$, $S(q)$ clearly indicates different scaling on different length scales. This behavior appears due to the finite range of the screened Coulomb interaction. At large length scales $r \gg \lambda_D$ the PEL chain scales scales like a neutral one.

Additionally to the stretching at large length scales discussed above, also the bond length distribution differs substantially with increasing screening length. The bond length distributions at different screening are shown in Fig. 4.16. In the highly stretched case, the bond length distribution is shifted to larger b with an average bond length increased by about $\sim 40\%$. Note that this is a feature of the Gaussian chain model used in this study. At strong screening the distribution function is almost unperturbed compared to a neutral chain.

The snapshots of the simulations at the four different Debye lengths are presented in Fig. 4.17. Note the different scale used to plot the snapshots.

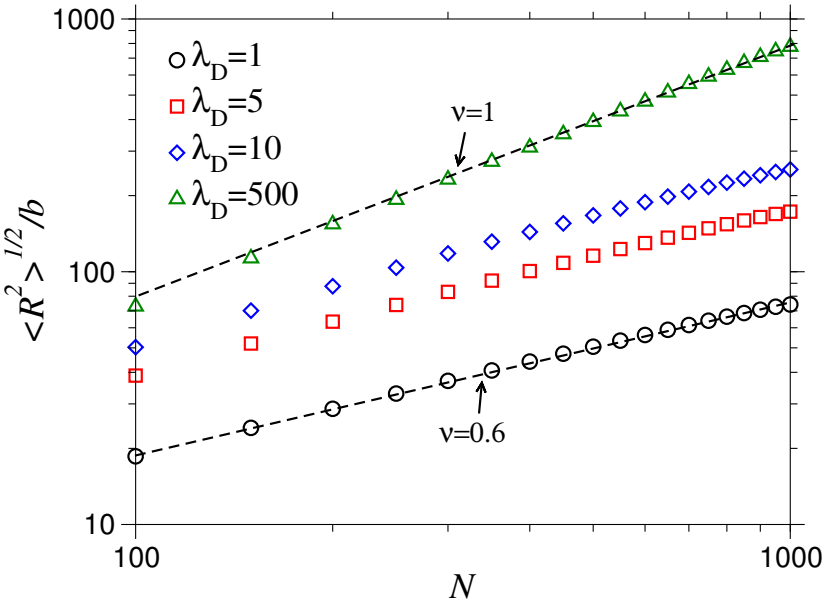

Figure 4.14: Chain length dependence of the end-to-end distance of a fully charged PEL chain at varying Debye length ($N = 1000$).

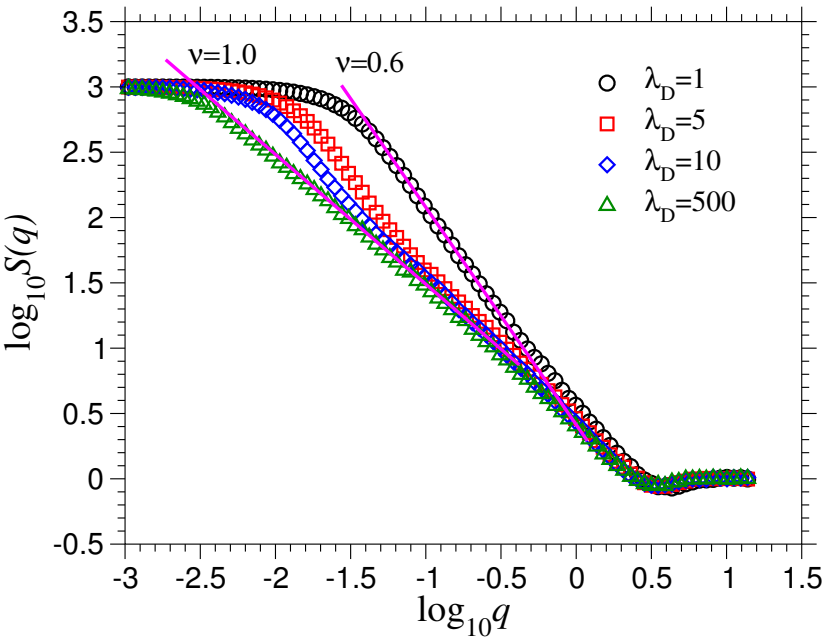

Figure 4.15: Spherically averaged structure factor for a fully charged PEL chain ($N = 1000$) at varying Debye lengths. The straight lines give the two limiting scaling relations.

λ_D	λ_D/b	λ_D/L	λ_D/R	ν
1	0.95	0.001	0.013	0.61
5	4.13	0.005	0.029	0.85
10	7.94	0.01	0.039	0.93
500	357.14	0.5	0.65	0.99

Table 4.2: Estimated exponent ν for a fully charged PEL chain ($N = 1000$) at different screening lengths. In the second column λ_D is scaled by bond length, third one by contour length of the chain and in the fourth one by m.s. end-to-end distance of the chain.

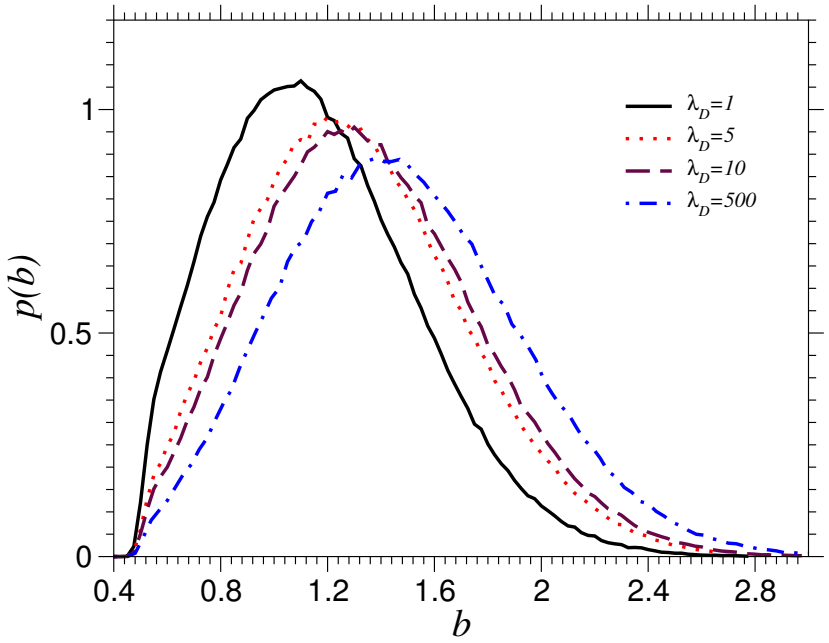

Figure 4.16: Bond length distributions for a fully charged PEL chain ($N = 1000$) at different Debye lengths.

4.1.2.2 Weakly charged PELs in poor solvent

In this section simulations on weakly charged, quenched PELs in a poor solvent are reported. The case of weak interaction strength, $uf^2 \ll 1$ and at rather poor solvents $\tau > N^{-1/2}$ is considered ($N = 128$ and $N = 256$). The solvent quality is tuned between $\tau = 0.0$, i.e. Θ-solvent, and $\tau = 0.26$, which is a rather poor solvent quality indeed.

In sufficiently poor solvents, the chain forms a compact structure if the electrostatic interaction is weak. With increasing Coulomb interaction the chain starts to change its shape. Depending on the electrostatic interaction, the chain passes through a number of pearl-necklace states toward a stretched configuration [29].

Fig. 4.18 shows the normalized end-to-end distance versus the scaling variable uf^2. It is obvious that the chains behave quite differently depending on the solvent quality. At small τ and not too small uf^2, the chain structure follows the behavior of a PEL chain in Θ-solvent,

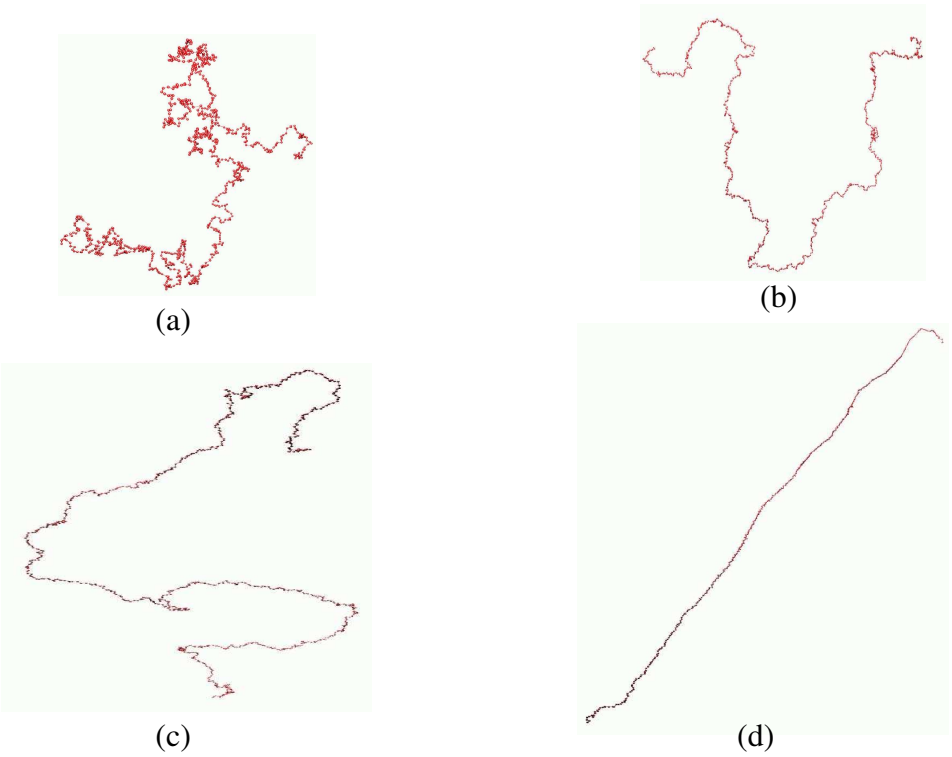

Figure 4.17: Simulation snapshots of a fully charged PEL chain of $N = 1000$ monomers in a good solvent at different Debye length: (a) $\lambda_D = 1$, (b) $\lambda_D = 5$, (c) $\lambda_D = 10$, and (d) $\lambda_D = 500$.

i.e., following Eqn. 2.81,

$$R \simeq bN \left(uf^2\right)^{1/3}.$$

A similar result for a charged chain near Θ point was obtained in ref. [47]; Higgs *et al.* simulated the chains of 10-100 monomers and plotted $< R^2 >$ versus u (f was set to 1) and they observed that $< R^2 >^{1/2}$ is independent of u for small u and increases with $u^{1/3}$ for large u.

At $\tau \gg N^{-1/2}$, which becomes roughly $\tau > 0.10$ for $N = 128$, the chain structure is drastically changed: For small uf^2, the electrostatic interaction is too weak to perturb significantly the poor solvent behavior, i.e., similarly to neutral chain one obtains globular structures which become independent of the value of uf^2. With increasing strength uf^2, however, the chain undergoes a transition into a coil structure. This sharp increase is interpreted as the formation of a necklace out of the globule. This increase is seen well in Fig. 4.19, which shows the reduced radius of gyration as a function of the parameter Nuf^2/τ. The rescaling is done for pearl-necklace scaling (see Eqn. 2.99). Hence, for pearl-necklace structures there should appear a constant plateau (see dashed line). The transition point from globule to pearl-necklace structure is located at $Nuf^2/\tau \approx 11$, which means that one requires more electrostatic strength for larger τ to split the globule to smaller beads connected by strings. At $Nuf^2/\tau > 90$ in Fig. 4.19, the PEL chain behaves like in a Θ solvent. The parameter range where pearl-necklaces occur agrees with the theoretical prediction (see Sec. 2.2.1.3). Also the parameter ranges where the other regimes exist (Gaussian coil, globule and extended

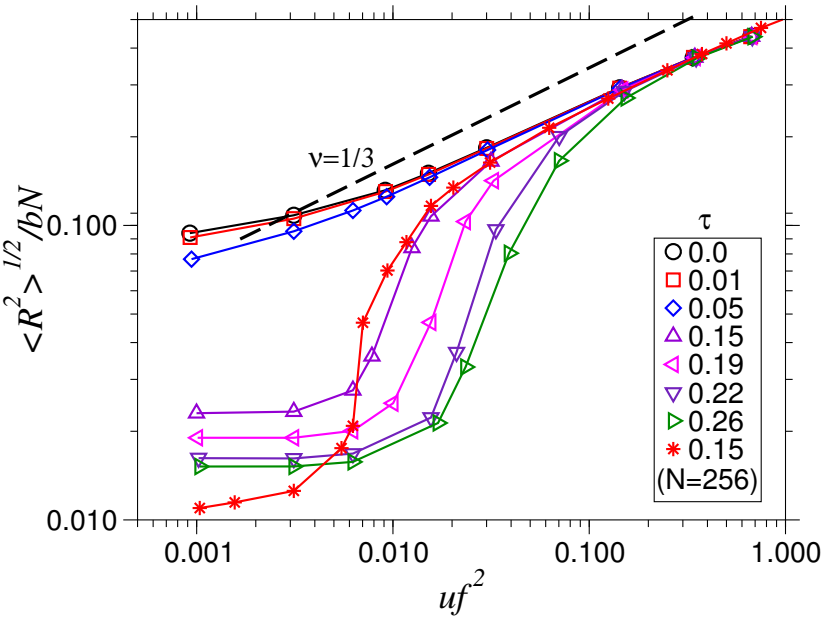

Figure 4.18: Normalized end-to-end distance versus the electrostatic interaction strength for different values of τ at $f = 1/8$ ($N = 128$, except one case stated in the legend).

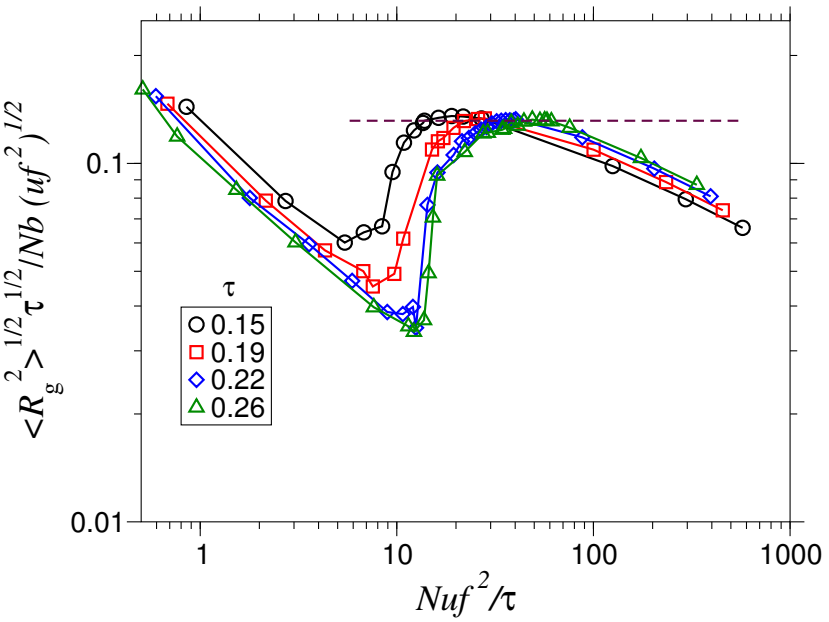

Figure 4.19: Reduced radius of gyration as function of Nuf^2/τ. The normalization is done such that the curve should be one constant for pearl-necklace scaling ($N = 128, f = 1/8$). (Dashed line shows the plateau according to the pearl-necklace scaling).

PEL) are in agreement with predictions given in Fig. 2.11, which was drawn for $N = 128$ and $u = 1$ (one should bear in mind that any prefactor has been ignored in Fig. 2.11).

Finally, in the limit of large uf^2 one finds again the universal behavior of PEL chains in a

Θ-solvent and the chain size becomes independent of τ. This behavior is in good agreement with scaling theory predictions which claim that Θ-solvent conditions are realized if $\xi_e \ll \xi_t$, i.e., at $uf^2 \gg \tau^3$. Note that obviously both for chain length $N = 128$ and $N = 256$ the coil-globule transition is influenced by finite size effects.

Fig. 4.20 shows the spherically averaged structure factor of the $N = 128$ chain at different solvent conditions for various uf^2 values; Fig. 4.20(a) for the Θ point and 4.20(b) for a poor solvent. At the Θ point, when the electrostatic interaction is rather weak, the behavior of PEL chain in the Porod region is similar to that of Gaussian one. With increasing electrostatic interaction, the chain is extended. On the other hand, the chain in a rather poor solvent looks like a compact globule if Coulomb interaction is weak. In the structure factor plot, Fig. 4.20(b), the curve at $uf^2 = 0.001$ corresponds to a globular structure for the PEL chain. However, a peak which one expects at a high q value for a globular structure is now slightly smeared: although the global view of the chain at this weak electrostatic interaction is a compact globule, now the structure is deformed at some level compared to the neutral globule in a poor solvent (see Fig.4.10(b)). On the other hand, a shoulder, seen at $\log_{10} q \approx -0.07$ for $uf^2 = 0.033$, corresponds to a pearl-necklace conformation and one can go into a more refined analysis of the structure (see, for example, Sec. 4.2.2).

The snapshots shown in Fig. 4.21 give typical chain conformations of PELs in a poor solvent over the whole range of interaction strength uf^2 (The scaling of the snapshots is different).

4.2 Annealed polyelectrolytes in poor solvent

PELs can be distinguished in terms of their dissociation behavior [1, 8]. For annealed PELs, i.e., for polyacids and polybases, the total charge on the polymer is not fixed, but it can be tuned by changing the pH of the solution. The positions of the charges along the polymer chain are also not fixed, but self-adjusted due to the local environment.

In this section, the simulation results for annealed PEL chains in a poor solvent will be represented. Three topics are discussed in the following three subsections:

(i) the behavior in a rather poor solvent, where a first-order phase transition occurs between a weakly charged globule and a strongly charged stretched conformation,

(ii) the behavior close to Θ-temperature, where pearl-necklace structures are observed,

(iii) the influence of additional salt ions.

4.2.1 Rather poor solvents

Depending on the distance from the Θ point the behavior of annealed PELs in poor solvents can be quite different (see Sec. 2.2.2). Theory predicts that, as long as the solvent quality is not too poor, i.e., at

$$\tau < \tau^* \simeq N^{-1/5} u^{-3/5}, \tag{4.2}$$

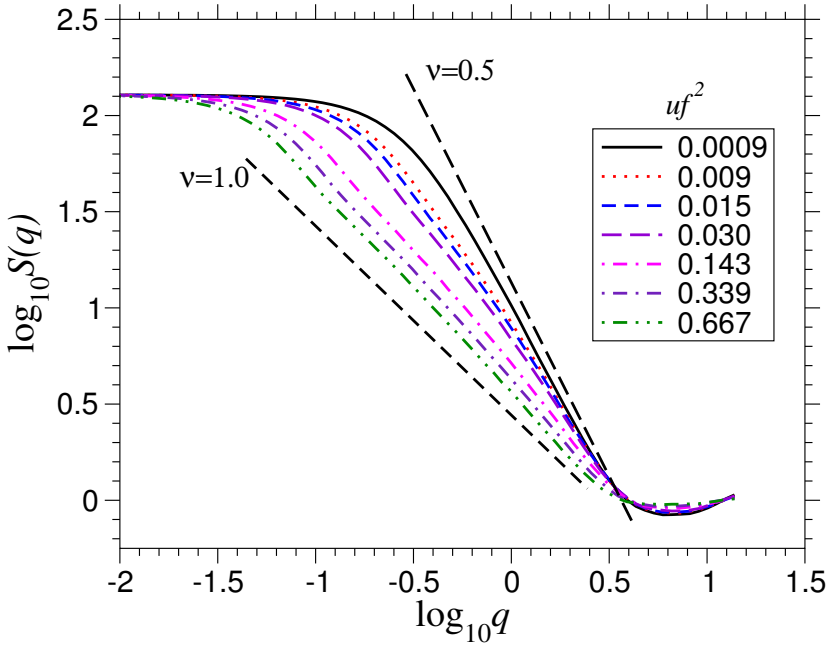

(a)

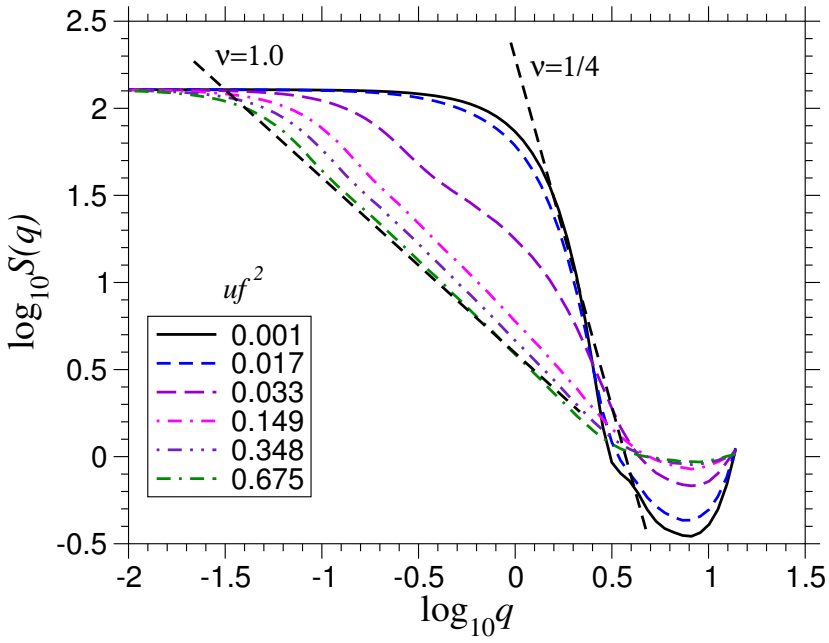

(b)

Figure 4.20: Spherically averaged structure factor ($N = 128$) for different values of uf^2: (a) at the Θ point ($\beta = 2.615$), (b) for $\tau = 0.15$ ($\beta = 3.1$). The dashed lines indicate the limiting scaling laws.

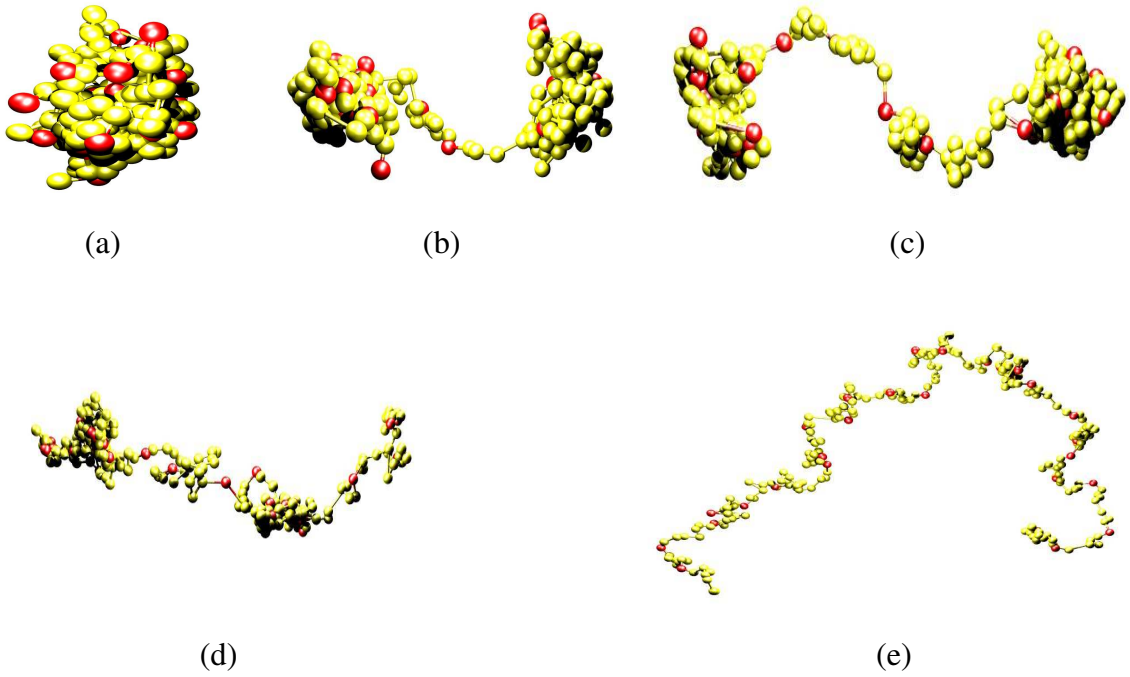

Figure 4.21: Typical snapshots from the simulation of a weakly charged, quenched PEL ($f = 1/8$, $N = 256$) in a solvent ($\tau = 0.15$). (a) $uf^2 = 0.0063$, (b) $uf^2 = 0.0078$, (c) $uf^2 = 0.0094$, (d) $uf^2 = 0.0156$ and (e) $uf^2 = 0.031$. Charged monomers are red colored while uncharged ones are yellow.

the entropic term still dominates the charge chemical potential μ which remains a smooth increasing function of f. Pearl-necklaces (or any other sub-structures) can occur in this region. However, at $\tau \geq \tau^*$ the chemical potential becomes a non-monotonic function of f due to the electrostatic contribution to μ, resulting in a first-order phase transition between a collapsed weakly charged conformation and an extended strongly charged state.

Titration experiments are an widespread approach to characterize weak PELs. The overall shape of the titration curve depends on the nature of the PEL that is titrated [77]. In particular, PELs in poor solvent show a pronounced plateau [78, 79] where the pH remains almost constant. This plateau has been related to a discontinuous transition between collapsed and stretched states [36]. Pronounced anomalies of the titration curves, which has been assigned to a conformational change, were found for poly(methacrylic acid) and related copolymers [80] as well as for copolymers of maleic acid [81].

On the other hand it has been shown that peculiarities of the titration curves can be also explained by including correlations between the charges without relying on conformational transitions. There are both studies for rigid rods with nearest-neighbor interaction [82, 83, 84] as well as with the full (screened) long-range one [58] and studies for semi-dilute solutions [79].

In this subsection simulations of annealed PELs in sufficiently poor solvents ($\tau \geq \tau^*$) are reported. Because PELs are studied at infinite dilution the screening length λ_D is determined only by the concentration of added salt but not by the charges on the polymer or the counterions. That is why λ_D can be considered to be constant at varying μ. In the simulations reported here Debye screening length has been set $\lambda_D = 10$. If not otherwise stated the chain

length is $N = 256$.

The results demonstrate clearly the relation between the transition in the degree of dissociation and the conformational one which occur simultaneously at a certain chemical potential $\mu^*(\tau, \lambda_B)$ [85]. Contrary to a previous simulation [86], which claimed that the transition between weakly charged globules and strongly charged stretched chains is continuous, it is shown that it is indeed of first order as predicted by theory [36]. Analyzing finite size effects, it becomes evident, that previous results were strongly influenced by the relatively short chain length used in ref. [86].

Simulations have been done in a parameter range sufficiently deep in the poor solvent region, i.e., the corresponding neutral chain is collapsing into a globular state. Here data obtained for τ values between 0.19 and 0.26 are reported. At Bjerrum length $\lambda_B = 1$ the variation of the chemical potential between $\mu = 4.0$ and $\mu = 9.0$ was found to be appropriate to cover all the substantial changes in the structure of the PEL.

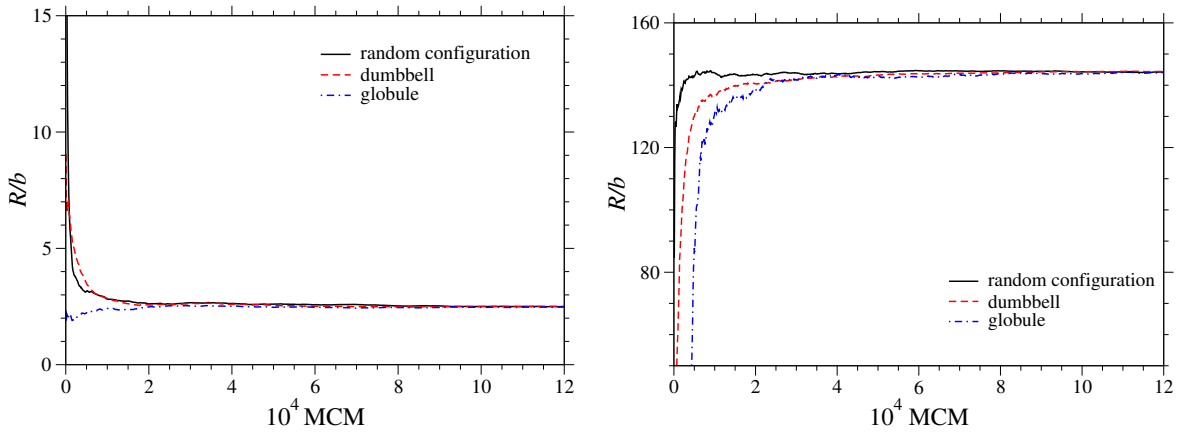

Figure 4.22: Running averages of end-to-end distance, starting with random configuration, dumbbell and globule. (a) $\mu = 4.0$ where the equilibrium state is a compact globule, (b) $\mu = 8.0$ where the equilibrium state is a stretched configuration ($N = 256$, $\tau = 0.19$).

Fig. 4.22 displays running averages of end-to-end distance at $\tau = 0.19$ with three different starting configurations: random coil, dumbbell and globule. In Fig. 4.22(a) $\mu = 4.0$ at which the equilibrium state is a compact globule, while in Fig. 4.22(b) $\mu = 8.0$ at which the equilibrium is a stretched configuration. The different runs from random coil, dumbbell and globule approach each other after about 40000 MCM.

Fig. 4.23 shows both degree of charging and m.s. end-to-end distance as a function of chemical potential, which is the pH of the solution except a trivial additive constant (see Sec. 2.2.2). At small μ a weakly charged globular state is obtained. A corresponding simulation snapshot is shown in Fig. 4.24 a). On the other hand, a completely charged, highly stretched state (see Fig. 4.24 b)) is found in the large μ limit. The discontinuous transition between

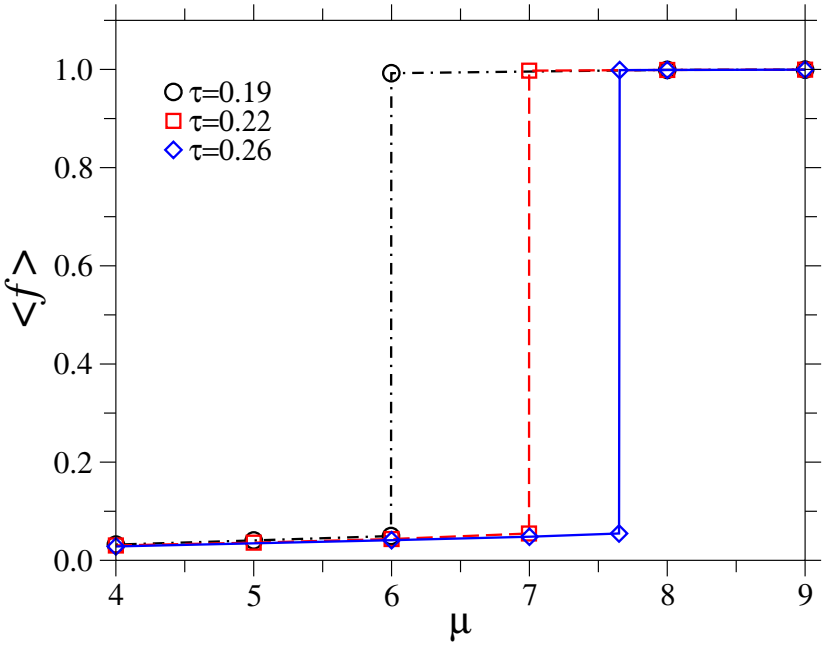

(a)

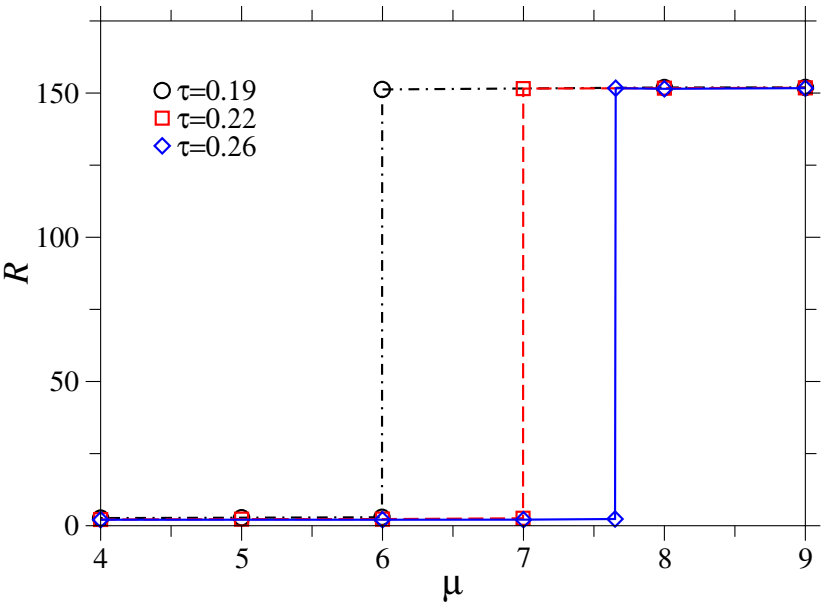

(b)

Figure 4.23: Simulation results at $\lambda_B = 1$ and varying solvent quality: $\tau = 0.19$ (circles), $\tau = 0.22$ (squares), and $\tau = 0.26$ (diamonds). a) Degree of charging *vs.* chemical potential (titration curves), b) m.s. end-to-end distance *vs.* chemical potential.

Figure 4.24: Simulation snapshots at constant solvent quality ($\tau = 0.22$): a) weakly charged, collapsed chain at $\mu = 4.0$ (charged monomers are colored red and uncharged ones are colored yellow), b) completely charged, extended chain at $\mu = 9.0$.

the two states takes place simultaneously in the degree of charging and in the conformation of the PEL at a well-defined chemical potential μ^* the value of which depends of the solvent quality τ. It is found that $\mu^* = 5.9971 \pm 0.0010$ at $\tau = 0.19$, $\mu^* = 6.9977 \pm 0.0008$ at $\tau = 0.22$, and $\mu^* = 7.6501 \pm 0.0001$ at $\tau = 0.26$.

A simple and direct way to determine the order of a phase transition is the histogram method of Lee and Kosterlitz [87] for the energy distribution function $P(E)$. Since the partition function is given by the sum of the Boltzmann factors, one can directly estimate free energy barriers. For a canonical ensemble, the normalized distribution function $P(E)$ is related to the free energy via

$$\frac{F}{k_{\mathrm{B}}T} = -\ln P(E). \tag{4.3}$$

For a second-order transition, at the transition point $P(E)$ displays a broad single maximum around the mean value of E. Off the transition point the distribution function becomes more narrow. For first-order transitions there is not such a continuous shift and broadening but a second peak develops at lower/higher energy. The phase transition point can be determined as the point where the states have the same free energy (or the same peak height in the energy distribution function). Note once more that the simulations reported here are done within a semi-grand canonical ensemble where the number of particles is fixed, but the charges are in contact with a reservoir of constant chemical potential μ. Hence, in this case the relevant energy is $E = E_{\mathrm{conf}} + \mu N_{\mathrm{c}}$ with N_{c} being the number of charged monomers. Applying Eqn. 4.3 the distribution function $P(E)$ is related to the semi-grand potential (or semi-grand free energy). In Fig. 4.25 the distribution function is plotted for three chemical potentials close to the transition point.

The double-minima structure provides direct evidence for the first-order nature of the transition in agreement with the theoretical prediction by Raphael and Joanny [36]. The minimum at small values of E is related to the globule and the one at larger E corresponds to the stretched chain. As μ increases, the global minimum jumps from the collapse to the stretched state. At the transition point the two minima have the same depth, i.e., both states have the same semi-grand canonical free energy. In the case presented in Fig. 4.25 this appears at $\mu^* = 4.093$ ($N = 64$). For larger chains μ^* is increased.

Fig. 4.26(a) shows the degree of charging as a function of μ for different chain lengths while Fig. 4.26(b) shows the normalized m.s. end-to-end distance versus the chemical potential for different chain lengths. For shorter chains the influence of finite size effects is evident. In particular, at $N = 32$ there remains no indication of a discontinuous transition. This explains

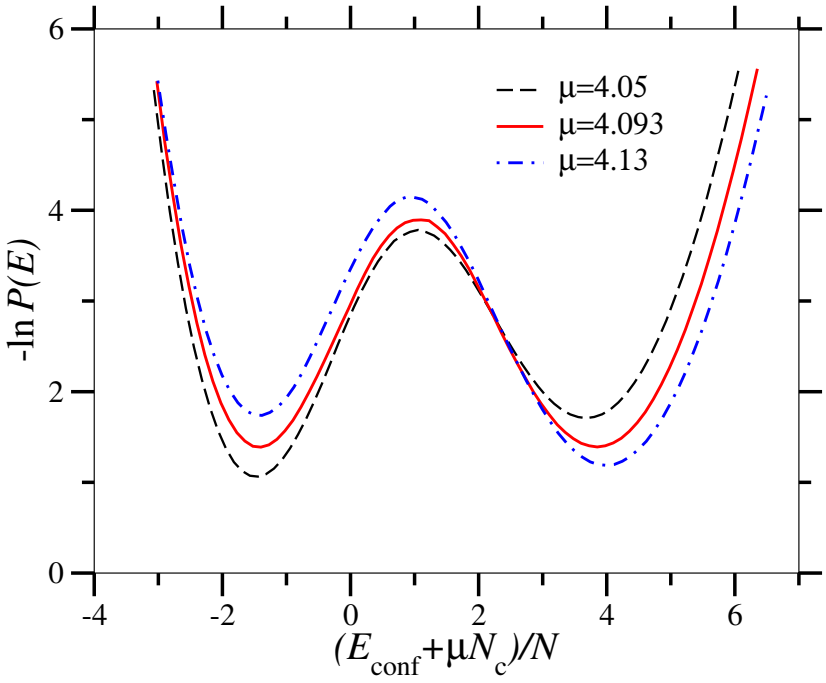

Figure 4.25: Simulation results at $\lambda_B = 1$ and $\tau = 0.19$. Energy distribution function $P(E)$ at $\mu = 4.05$ (dashed), $\mu^* = 4.093$ (solid), $\mu = 4.13$ (dot-dashed) for chain length $N = 64$,

why in a former simulation study [86] with chains of length 40 were considered the authors claimed to see a continuous transition, contrary to the theoretical expectation.

According to Raphael and Joanny [36] a phase transition is expected to occur at $\tau > \tau^*$. Taking into account enlarged average bond length in the stretched conformation, Eqn. 4.2 yields a characteristic distance from the Θ point $\tau^* \approx 0.28 \ldots 0.33$, i.e., values which are of the same order of magnitude as the τ's considered in the simulations. Note that Eqn. 4.2 is based on a scaling theory approach, i.e., any numbers are omitted. Thus, the transition observed is in qualitative agreement with theory. Across the phase transition the theory predicts a jump from $f_1 \cong \tau^3 u$ to $f_2 \cong \tau^{1/2} N^{-1/2} u^{-1/2}$ [36]. For the lower value, the simulation data yield $f_1 \approx 5\%$ which is in a good agreement with the theoretical prediction that gives $f_1 \approx 1\% - 2\%$. For the upper value f_2, there appears an obvious disagreement between scaling theory and simulation data. While the simulations yield almost complete charging with $f_2 > 99\%$ the theory predicts $f_2 \approx 3\% - 4\%$.

In Fig. 4.27 the spherically averaged form factor is plotted for four different chemical potentials (at $\tau = 0.22$): (i) one far below and one just before the transition, (ii) one just after and one far above the transition point. The corresponding pairs of curves below or above the transition point, respectively, map almost perfectly onto each other reflecting the discrete nature of the phase transition.

Quite similar to the behavior of neutral chains discussed in Sec. 4.1.1.4 the peak in the structure factor at $\log_{10} q \approx 0.50$ occurring below the transition point is a fingerprint of a globule of size $R \approx 2.0$. Above the transition one obtains a chain which is almost completely

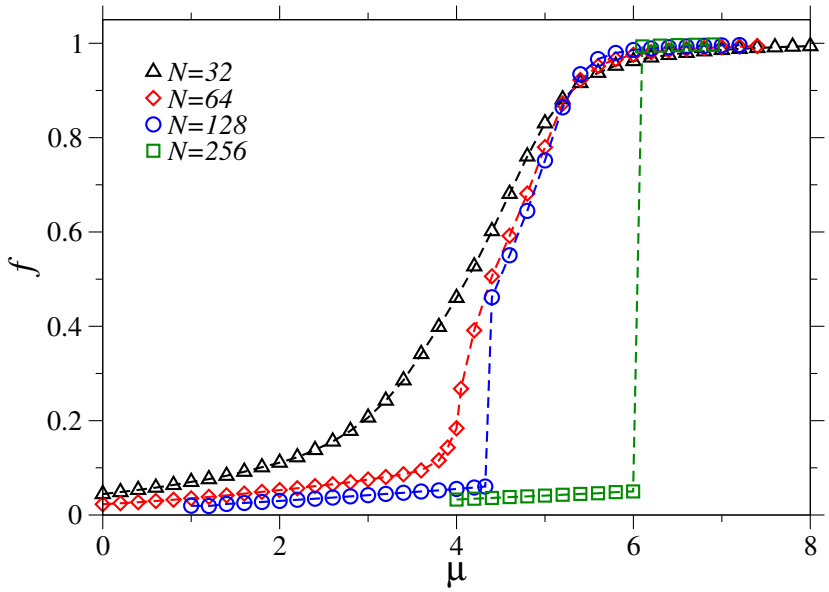

(a)

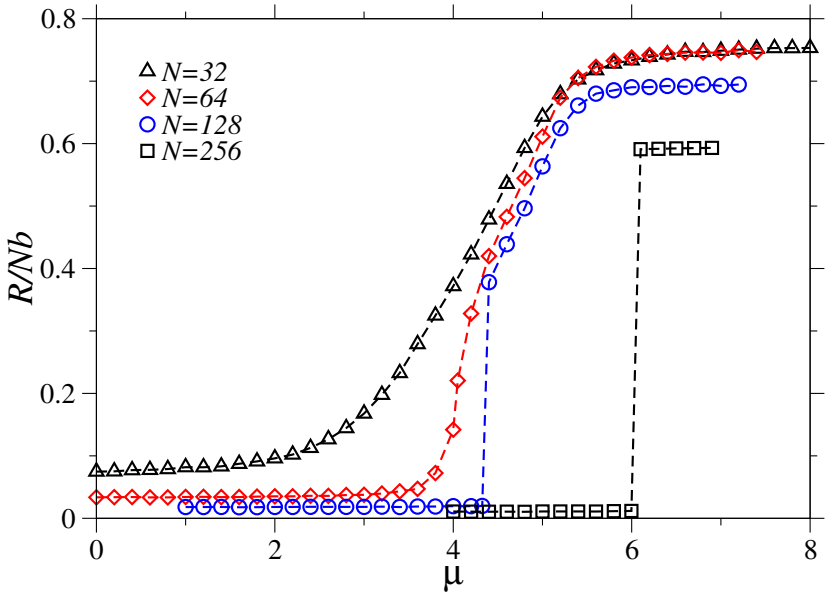

(b)

Figure 4.26: Simulation results at $\lambda_B = 1$ and $\tau = 0.19$: a) degree of charging and b) normalized chain size *vs.* chemical potential at $N = 32$ (triangles), 64 (diamonds), 128 (circles), 256 (squares).

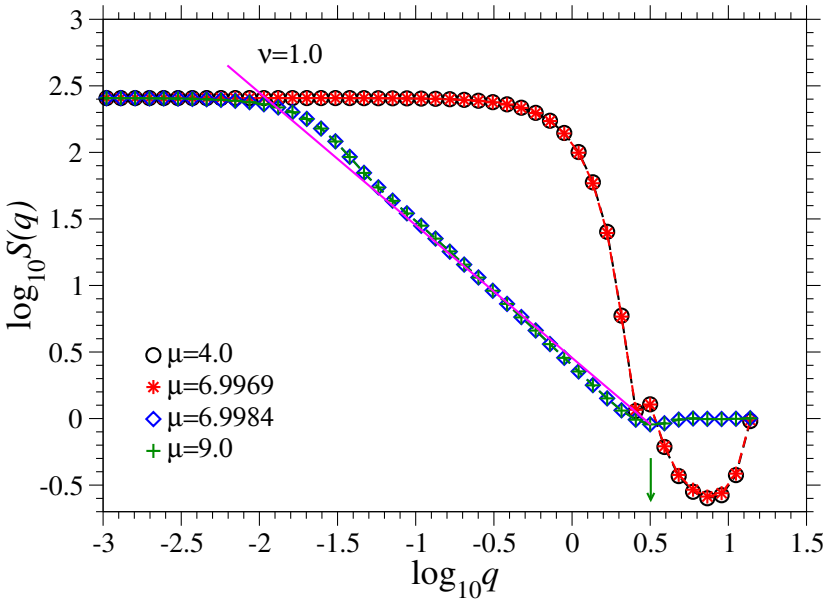

Figure 4.27: Spherically averaged form factor ($\tau = 0.22$, $N = 256$, $\lambda_B = 1.0$) for various chemical potentials. The straight line gives the scaling behavior of a completely stretched chain. The arrow indicates the q value giving the size of globule.

stretched.

Performing MC simulations of annealed PELs in poor solvent, it has been shown that discontinuous transitions in the degree of charging are closely associated with discontinuous conformational transitions. For the first time, the first-order nature of the transition has been proved by simulation. The PEL can be caused to collapse by decreasing the charge chemical potential μ, which can be easily done in experiment by reducing the pH of the solution, as well as by increasing the coupling strength u. Experimentally the latter route can be attained by reducing the distance between the ionizable groups in, e.g., block-copolymers.

4.2.2 Close to Θ point

To detect possible substructures like pearl-necklaces one has to approach the region close to Θ point $\tau < \tau^*$. Obviously, there are two choices to do that: (i) reducing τ, i.e., coming really closer to Θ point or (ii) increasing τ^*, i.e., fixing the absolute distance to Θ point, but enlarging the width of the specific region close to Θ point. The first route is difficult to realize in simulation studies: Close to Θ point the simulation becomes unstable due to huge fluctuations. However, the second route seems promising. According to Eqn. 4.2 τ^* can be enlarged both by reducing chain length N and coupling strength u. The use of shorter chain lengths obviously would restrict the search for pearl-necklaces. Therefore, in the following the coupling strength u is varied to study the behavior of annealed PELs close to Θ point. Weaker coupling strengths are easily attained in simulations by reducing Bjerrum length λ_B. In experimental studies a realistic way to reduce u is to enlarge the distance between ionizable

groups by synthesizing block copolymers.

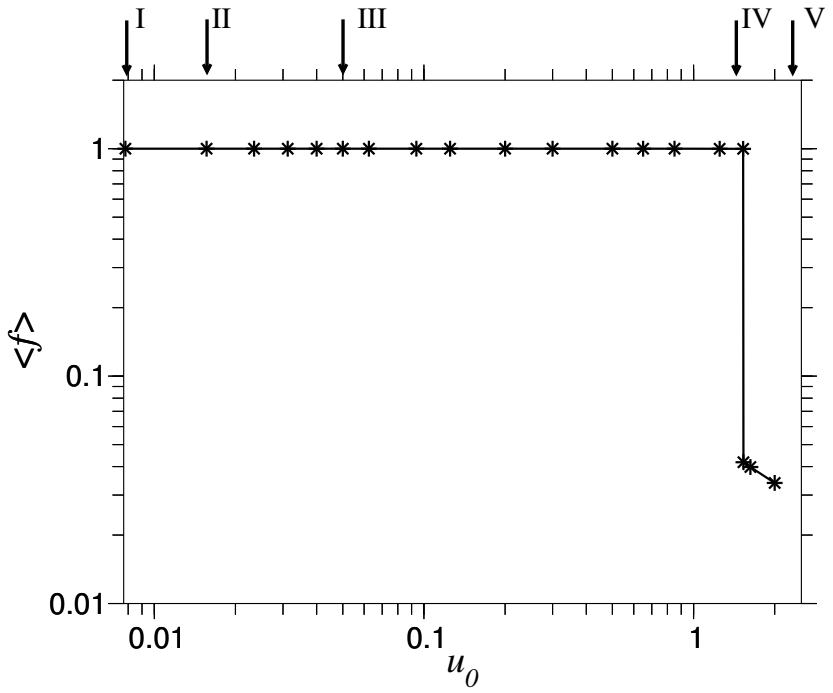

Figure 4.28: Degree of charging versus the coupling parameter for $\tau = 0.26$ and $\mu = 9.0$ ($N = 256$).

Fig. 4.28 shows the degree of charging versus coupling strength in the range $0.08 \lesssim u \lesssim 1.5$ for a relatively large chemical potential ($\mu = 9.0$). The distance from Θ point is $\tau = 0.26$ ($N = 256$). With these parameters and following Eqn. 4.2 the critical coupling strength above which pearl-necklaces are unstable becomes

$$u^* \simeq N^{-1/3}\tau^{-5/3} \simeq 1.5.$$

Hence, within the range of u considered here pearl-necklaces might appear.

In Fig. 4.29 the corresponding behavior of the m.s. end-to-end distance is plotted. Typical snapshots are presented in Fig. 4.30. From the snapshots one can see that there occur pearl-necklaces indeed. Beside that, the influence of coupling strength exhibits various interesting features: Although the chain is completely charged due to the large μ value at weak interaction strength it is collapsed into a globule (point I). With increasing u the globule becomes deformed and splits into several pearls. Pearl-necklace structures are formed between points II ($u_0 = 0.016$) and III ($u_0 = 0.05$). Note that the m.s. end-to-end distance is drastically enlarged in this region. Beyond point III all the pearls are pulled out and the chain exhibits a stretched but more or less homogeneous configuration. Following de Gennes *et al.* [43] the chain extension is expected to grow as $R \propto (uf^2)^{1/3}$ which is nicely confirmed by the simulation result. Up to that point there is no difference to the behavior of quenched PELs (Note that for a completely charged chain there is no difference between annealed and quenched case). However, at a certain u^* the Coulomb energy per charged monomer becomes larger than the penalty for neutralizing a charge. Consequently the PEL minimizes its energy by neutralizing almost all charges and collapsing back into a nearly uncharged globule

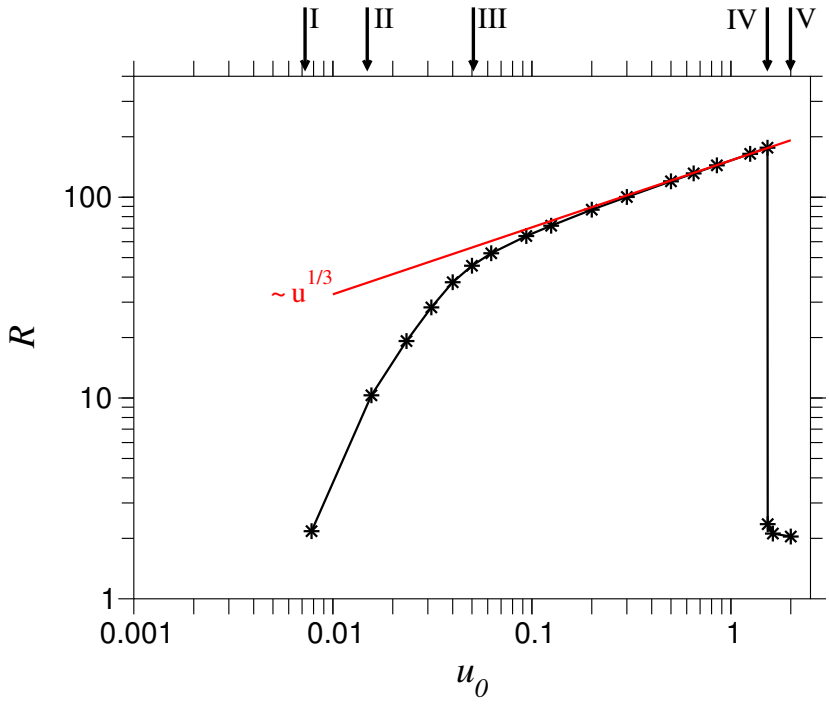

Figure 4.29: End-to-end distance versus the coupling parameter for $\tau = 0.26$ and $\mu = 9.0$ ($N = 256$).

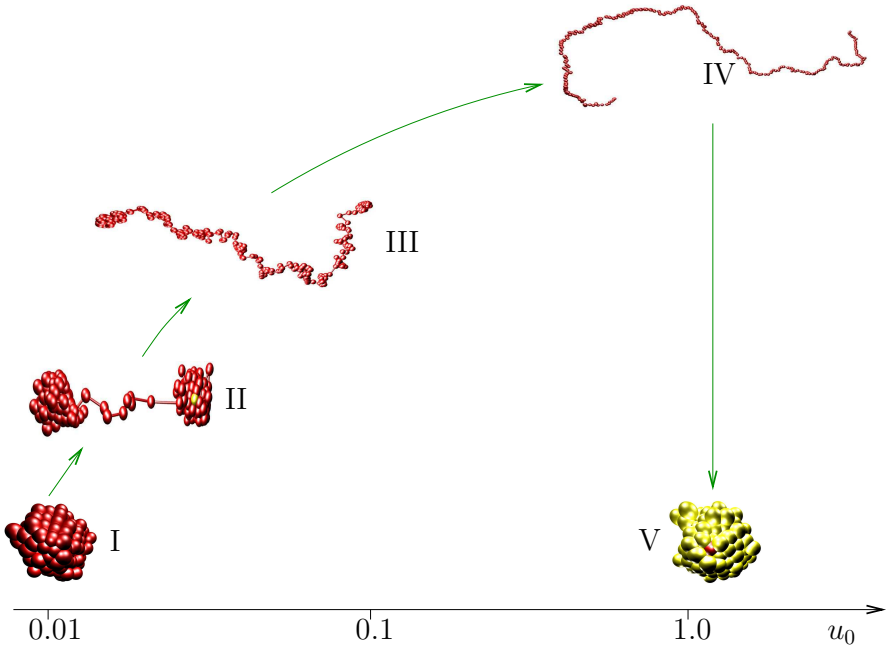

Figure 4.30: Snapshots demonstrating the transitions which occur when the coupling strength is increased at constant τ, μ ($\tau = 0.26, \mu = 9.0$). Charged monomers are colored red, uncharged ones yellow.

(point V, $u_0 = 1.53$). Similarly to the discontinuous transition discussed above a simultaneous transition both in degree of charging and chain stretching is observed. In Fig. 4.31 $S(q)$ is

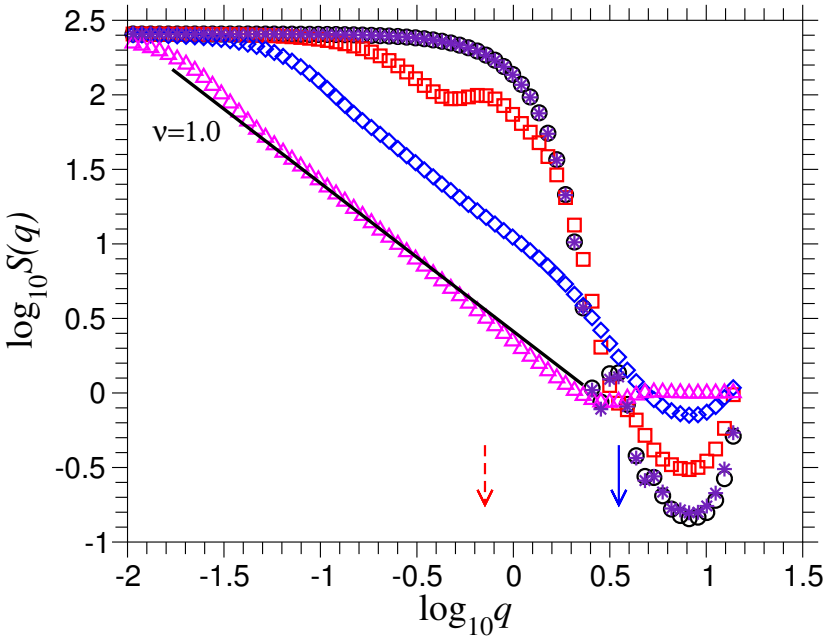

Figure 4.31: Spherically averaged structure factor at $\tau = 0.26$, $\mu = 9.0$ and varying coupling strength: Circles for point I, squares for II, diamonds for III, triangle-ups for IV and stars for point V. The straight line indicates the limiting scaling law. The arrows point to the additional peaks, solid for globular structure and dashed for dumbbell.

plotted for the five points discussed above: I at zero coupling parameter; i.e. no electrostatic interaction and compact globule, II at very small coupling strength with a nice dumbbell structure, III coupling a bit stronger, forming a number of pearls connected by strings, IV just before the discontinuous coil-globule transition, a highly stretched chain and V at any coupling strength beyond the point IV; chain collapsed back a compact globule. Note that for the cases I to IV, the chain is almost fully charged while at point V, the charge on the chain can be neglected. In terms of weakness of electrostatics, points I and V can be considered as identical ones. In these globular cases, where $S(q)$ is almost identical, an additional peak occurs at $\log_{10} q \approx 0.54$ which is related to a globule diameter $R \approx 1.8$. Note that globule size is the same as discussed for neutral chain at $\tau = 0.22$ in Sec. 4.1.1.4. For point II, one observes a pronounced shoulder at $q \approx 0.7$, which is related to the string length in the dumbbell structure (for detailed consideration see below).

The pearl-necklace structures around point II are analyzed by using a cluster search algorithm (see Appendix A), which is optimized for analyzing pearl-necklace structures up to five pearls. The results are collected in Table 4.3, with g_{bead} being the averaged number of monomers in a bead and g_{str} the number of monomers in a string. d_{bead} is the bead size, l_{str} the length of a string, f_{bead} is the average degree of charging of beads and f_{str} corresponding charging of strings. In the table, only the structures are included with a weight of at least 1 %. The number of pearls increases with the coupling parameter u. With increasing u_0 there occurs more fluctuations between necklace structures with different pearl numbers, since the

energy difference between them is reduced. (Note that the case $N_{\mathrm{bead}} = 6$ is beyond the range where the cluster search routine gives reliable results). Using the theoretically predicted re-

u_0	N_{bead}	weight (%)	g_{bead}	g_{str}	d_{bead}	l_{str}	f_{bead}	f_{str}
0.016	2	99.9	124.1 ± 7.9	7.7 ± 0.1	3.36 ± 0.04	4.87 ± 0.03	0.999982	1.0
0.023	3	70.9	77.3 ± 5.1	11.2 ± 0.1	3.16 ± 0.04	5.61 ± 0.07	0.999979	1.0
	4	27.8	58.8 ± 3.8	6.9 ± 0.1	2.90 ± 0.03	3.45 ± 0.03	0.999997	0.999960
0.030	3	10.3	62.52 ± 4.6	34.21 ± 0.7	3.30 ± 0.05	10.49 ± 0.1	0.998462	0.999159
	4	65.0	51.91 ± 3.6	15.90 ± 0.1	2.95 ± 0.05	6.11 ± 0.09	0.998651	0.999316
	5	24.0	43.43 ± 2.9	9.72 ± 0.1	2.72 ± 0.02	4.11 ± 0.04	0.99842	0.999488
0.040	2	2.5	40.3 ± 4.5	175.2 ± 1.3	3.62 ± 0.02	36.54 ± 0.06	1.0	1.0
	3	20.7	37.6 ± 3.5	71.6 ± 0.2	3.22 ± 0.02	17.89 ± 0.11	0.999986	0.999987
	4	38.8	34.5 ± 2.9	39.3 ± 0.1	2.97 ± 0.02	11.23 ± 0.08	0.999992	0.999994
	5	28.6	32.0 ± 2.5	23.9 ± 0.1	2.79 ± 0.02	7.75 ± 0.06	0.999979	0.999997
	6	8.2	29.9 ± 2.2	15.2 ± 0.1	–	–	0.999974	0.999980

Table 4.3: Analysis of pearl-necklace structures at $\tau = 0.26$ and $\mu = 9.0$. The third column gives the weight of the various peal-necklace structures, g_{bead} is the number of monomers per bead and g_{str} the number of monomers per string, d_{bead} is the size of one bead, l_{str} the length of one string, f_{bead} is the average degree of charging of beads and f_{str} that of strings.

lations for $N_{\mathrm{bead}}, g_{\mathrm{bead}}, g_{\mathrm{str}}, d_{\mathrm{bead}}$ and l_{str} given in Sec.2.2.1.3 (Eqns. 2.98, 2.94, 2.97, 2.95 and 2.96, respectively) and choosing $u_0 = 0.016$ as reference state, for calculating the prefactors omitted in the scaling relations, one obtains the quantitative predictions collected in Table 4.4.

Comparing simulation results (Table 4.3) and theoretical predictions (Table 4.4), good agreement is observed for the number of pearls N_{bead}. The behavior of both g_{bead} and d_{bead} is found to be in agreement; both have a tendency to decrease with increasing coupling strength. However, disagreement appears for g_{str} and l_{str}: while the theory (see Eqn. 2.96) predicts that they should decrease with increasing coupling strength, the simulation results show

u_0	N_{bead}	g_{bead}	g_{str}	d_{bead}	l_{str}
0.023	2.9	86.36	6.33	2.99	4.03
0.03	4.0	66.21	5.55	2.73	3.53
0.04	5.1	49.66	4.80	2.49	3.06

Table 4.4: According to Eqns. 2.98, 2.94, 2.97, 2.95 and 2.96 predicted quantities for pearl-necklace structures at $\tau = 0.26$ and $f = 1$ ($N = 256$). N_{bead} is the number of beads, g_{bead} the number of monomers per bead, g_{str} the number of monomers per string, d_{bead} the size of one bead and l_{str} the length of of string. The prefactors are calculated by choosing the case $u_0 = 0.016$ as reference state.

the opposite tendency. Nevertheless, considering the total size of the pearl-necklace structure which is basically given by the total string length, one obtains a rather nice agreement between theory and simulation data. According to Eqn. 2.99 the pearl-necklace length should grow as $R \simeq N_{\mathrm{bead}} l_{\mathrm{str}} \propto (uf^2/\tau)^{1/2}$. Plotting the average m.s. end-to-end distance *vs.* $(uf^2)^{1/2}$, which is shown in Fig. 4.32 (τ is constant), one obtain a nearly linear behavior. This is

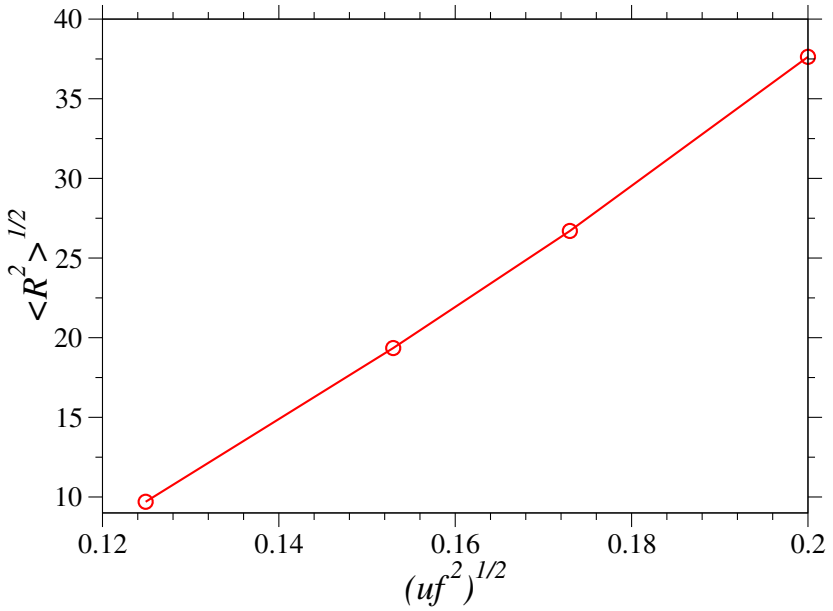

Figure 4.32: Average m.s. end-to-end distance for pearl-necklace structures *vs.* $(uf^2)^{1/2}$ ($\tau = 0.26$, $N = 256$).

rather surprising because the higher order structures at large u exhibit strong fluctuations. Note that this discrepancy, i.e., agreement in the total size but disagreement in the string quantities is already known from simulation results on quenched PELs [88].

The average degrees of charging in Table 4.3 are in qualitative agreement with the theoretical discussion by Castelnovo *et al.*. In many cases the average charge of beads is observed to be smaller than the corresponding charge of strings.

At this point, one experimental work on the pearl-necklace structures is mentioned: In a

recent work Kirwan *et al.* [89] gave the first direct experimental evidence that the variation of charge on an annealed PEL can be a direct tool to induce pearl-necklaces between globular and coil-like structures. Conformational changes of poly(vinylamine) (PVA) upon adsorption onto mica from solution with varying pH were determined by AFM. PVA is a weak cationic PEL. Its charge density can be tuned by the pH from completely neutral (pH > 10) to fully ionized (pH < 3) as demonstrated by titration experiments [90]. In Fig. 4.33, the original

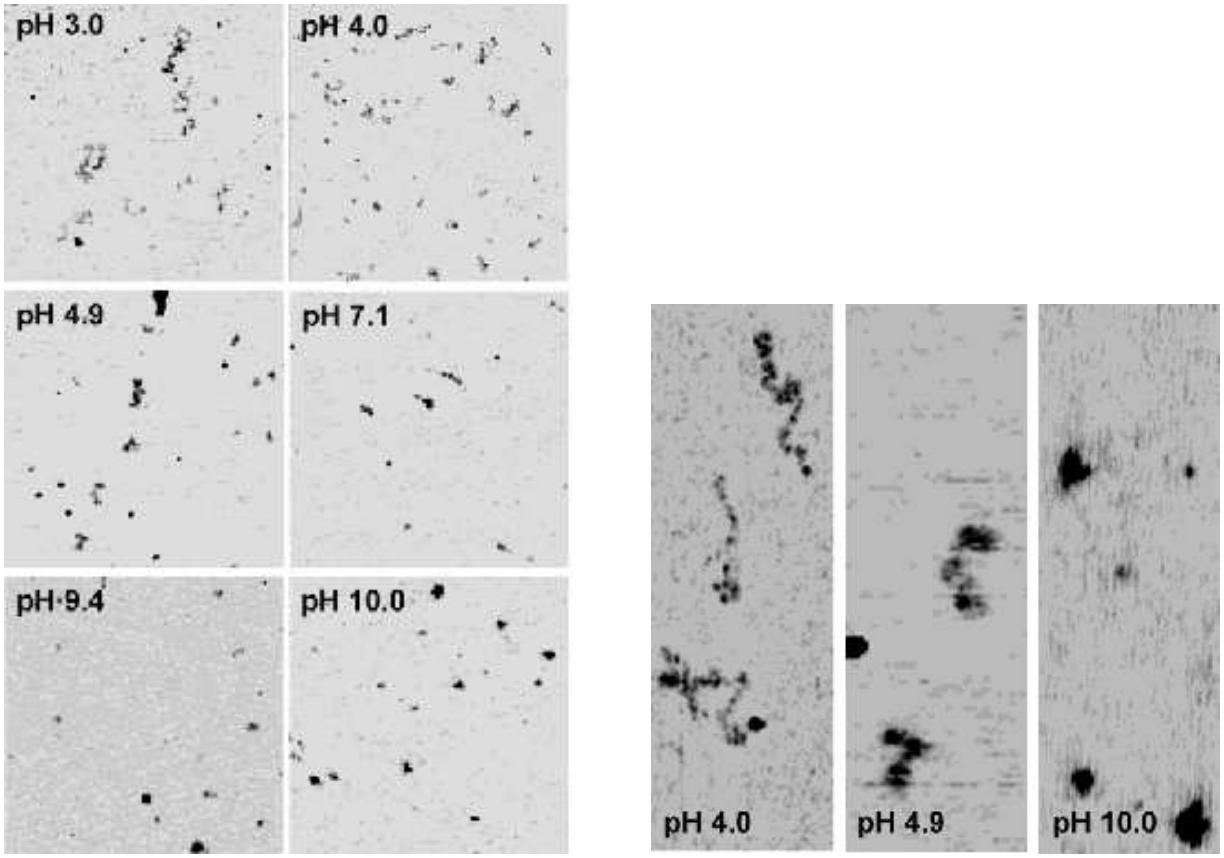

(a) (b)

Figure 4.33: Configuration of an annealed PEL at varying pH. (a) AFM images showing the extended coil-to-globular conformational transition of poly(vinylamine) (PVA), achieved by adsorption onto mica from solutions of varying pH. (b) Expanded view of selected molecules highlights the structural transition as a function of solution pH. The pearl-necklace structures can be clearly seen at pH = 4.0 and 4.9 (Figures from [89]).

figures from ref. [89] are shown: Fig. 4.33(a) shows representative AFM images (1×1 μm scans) visualizing the coil-to-globule transition of PVA as a function of pH. Selected zoomed sections of these scans are given in Fig. 4.33(b). At pH = 3.0 and 4.0, the PVA is fully ionized. The extended conformations of the chains can be noticed. At pH = 4.9 a significant decrease in the degree of ionization of PVA sets in and a marked change in conformation is observed. This picture clearly confirms the existence of pearl-necklace structures during the

conformational coil-to-globule transition. At pH = 7.1 about half of the groups are ionized, and more elongated, globular conformations are observed. At pH = 9.4 and 10 the chain is only weakly charged, and collapsed globular structures can be seen [1].

Above it has been shown that pearl-necklaces exist indeed in annealed PELs provided the solvent quality is not too poor. The width τ^* of the region close to Θ is determined by chain length N and coupling strength u (see Eqn. 4.2). For small u, τ^* can become rather large. In this way, at a given solvent quality τ one can shift the system from "rather poor" behavior (no pearl-necklaces) to "close to Θ" behavior (stable pearl-necklaces). This is easily done in simulation, but obviously it requires large effort in experiment. Therefore the interesting question is, will globule-necklace transitions also occur in a kind of titration "experiment", i.e., simulating the system at constant u and $\tau < \tau^*$, but varying μ. This problem which is similar to the experimental study discussed above is addressed in the remaining part of the section.

At $\tau = 0.26$ two coupling strengths are chosen: (i) $u_0 = 0.016$, (ii) $u_0 = 0.03$. For both cases the condition $\tau < \tau^*$ is fulfilled. Fig. 4.34 shows the average degree of charging as a function of chemical potential μ. The corresponding behavior of the m.s. end-to-end distance is plotted in Fig. 4.35 and typical snapshots are given in Fig. 4.36.

The unusual behavior represented in the figures can be summarized as follows:

(i) At small μ the degree of charging increases linearly with growing chemical potential (pH). The larger the coupling constant u the smaller is the slope. Note that the slope is very small at $u_0 = 1$ (see Sec. 4.2.1). While increasing the degree of charging from zero up to about 0.5 (at $u_0 = 0.03$) or 0.77 (at $u_0 = 0016$), respectively, the shape of the chain is not changed. It remains a globule independent of u, only the size of which is very weakly growing with f.

(ii) Reaching a certain degree of charging f^* the globule becomes unstable. It splits into several pearls the number of which depends on coupling strength u. However, for annealed PELs the structure instability is coupled with a charge instability. At $\mu = \mu^*(f^*)$ the chain jumps into a completely charged state. This transition is very similar to the first order transition discussed in Sec.4.2.1. However, now the interaction is too weak to stretch the chain completely and it stays in the multi-pearl state corresponding to complete charging at the specific coupling strength. For $u_0 = 0.016$, one obtains a dumbbell. A higher-order pearl-necklace appears for $u_0 = 0.03$. The positions of the globule-to-

[1] To mention experimental works on pearl-necklace structures in strong PELs: Partially sulfonated polystyrenefulfonate (PSS), a typical hydrophobic PEL, was studied by ref [91] and pearl-necklace size was observed to be related to the charge fraction. In ref. [92] migrosegregation in individual single chains of T4 DNA in solutions of poly(2-vinylpyrrolidone) (PVP) was observed by fluorescent microscopy. After mixing solutions of DNA with PVP, single chains exhibited intrachain segregation with multiple mini-globules connected by narrow flexible chains. Similar results were obtained when DNA was induced by polyethylene glycol with pendant amino groups (PEG-A) in ref. [93]. Refs. [94, 95] also include similar results from fluorescence images of large DNA molecules. Besides these ref. [96] gives an indirect evidence for the case of cationic PELs by small angle X-ray scattering. Recently such structures have been also visualized for linear PELs by imaging adsorbed poly(2-vinyl pyridine) and poly(methacryloyloxyethyl dimethyl benyl ammonium chloride) (PMB) with atomic force microscopy (AFM) [97, 98].

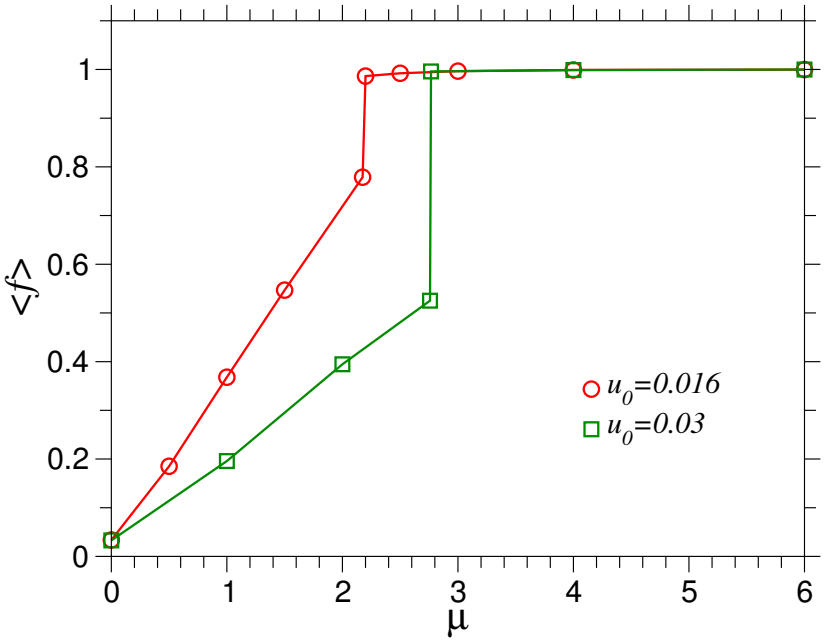

Figure 4.34: Average degree of charging versus chemical potential at small coupling strength ($N = 256$, $\tau = 0.26$).

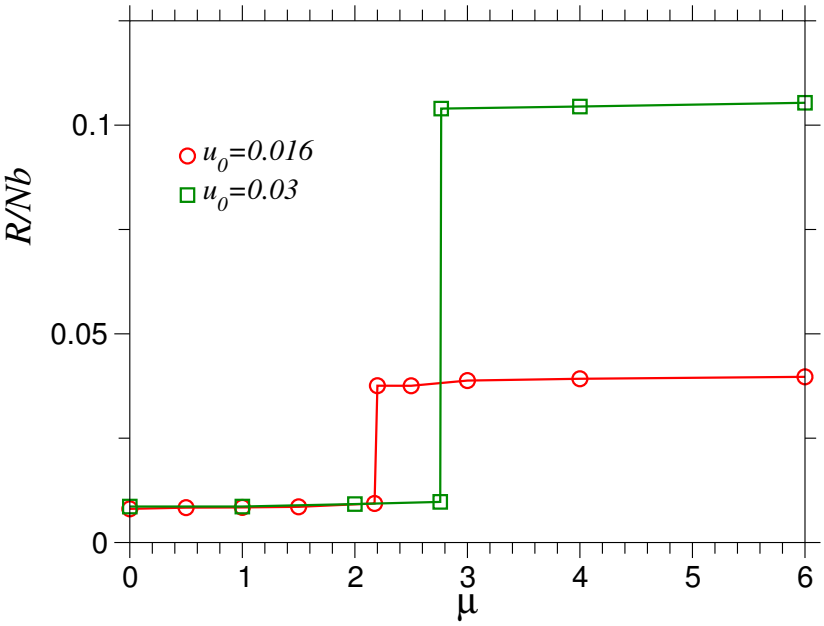

Figure 4.35: End-to-end distance versus chemical potential at small coupling strength ($N = 256$, $\tau = 0.26$).

necklace transition are given in Table 4.5. Since the instability occurs at $f^* \simeq (\tau/uN)^{1/2}$ the critical degrees of charging are expected to obey

$$\frac{f_1^*}{f_2^*} = \left(\frac{u_2}{u_1}\right)^{1/2} \simeq 1.4$$

which is fulfilled indeed quite well.

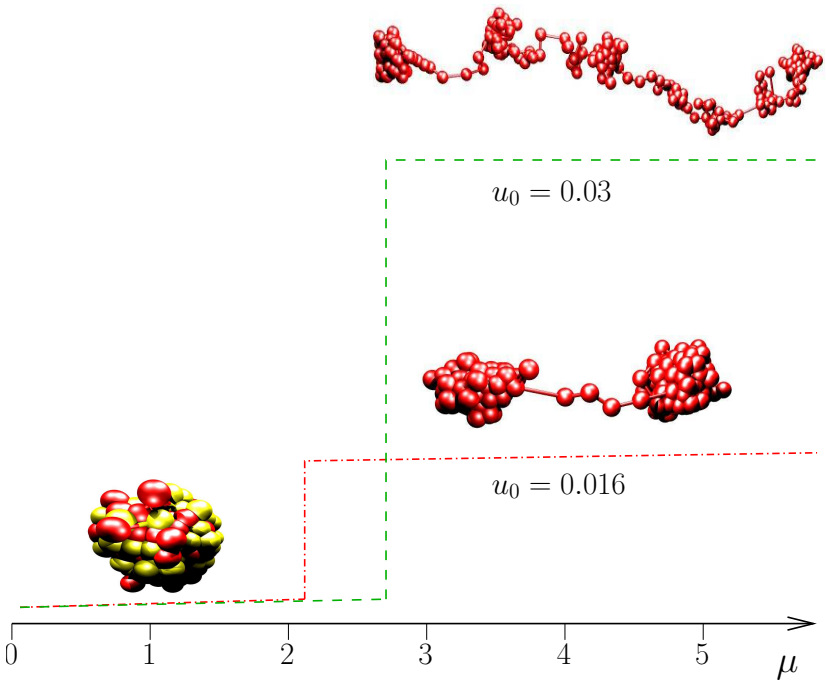

Figure 4.36: Weak coupling region, typical snapshots at different charge chemical potentials (see also Figs. 4.34 and 4.35).

u_0	μ^*	$\langle f^* \rangle$
0.016	2.19 ± 0.01	0.77
0.03	2.76 ± 0.01	0.54

Table 4.5: Position of globule-to-necklace transition. Chemical potential μ^* and averaged degree of charging $\langle f^* \rangle$ at the coupling strengths $u_0 = 0.016$ and $u_0 = 0.03$ ($\tau = 0.26$, $N = 256$).

(iii) Because complete charging is reached no changes occur at $\mu > \mu^*$. Note the strong fluctuations on the number of pearls in the case $u_0 = 0.03$. Fig. 4.37 represents the frequency of the various pearl-necklace states during the simulation together with the corresponding m.s. end-to-end distance. The chain fluctuates basically between pearl-necklaces with 3 pearls at minimum and 5 pearls at maximum. The weight of the four-pearl structure is 65%, five- and three-pearl chains appear with about 24% and 10%, respectively. The end-to-end distance is correlating in a reasonable way with the structure type: R fluctuates basically between about 19 and 33.

The m.s. end-to-end distances R measured directly from the simulation data are 9.6 and 26.7 for $u_0 = 0.016$ and 0.03, respectively. The total length of the pearl-necklace structures given by

$$L_{\text{nec}} = N_{\text{bead}} \times d_{\text{bead}} + (N_{\text{bead}} - 1) \times l_{\text{str}} \tag{4.4}$$

are calculated as 10.7 and 30.2 for $u_0 = 0.016$ and 0.03, respectively. Basically, the

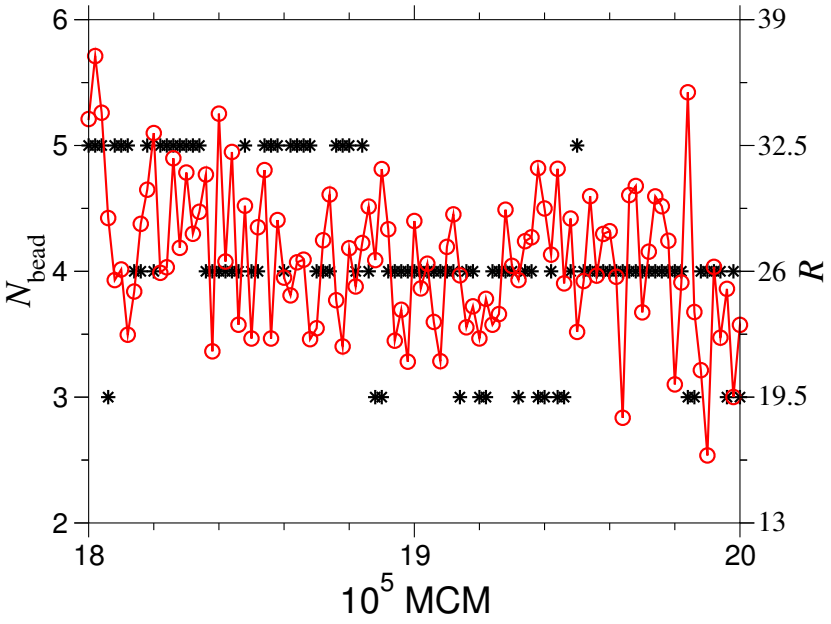

Figure 4.37: Occurrence of different pearl-necklace states and corresponding end-to-end distances during the simulation ($N = 256$, $u_0 = 0.03$, $\mu = 4.0$).

deviations from the chain m.s. end-to-end distances have the following reason: The pearl-necklace chain is mostly not in a straight conformation as assumed in Eqn. 4.4. Therefore the real end-to-end distance obeys $R < L_{\rm nec}$.

To get more information on the structure of pearl-necklaces the form factor is considered. In Fig.4.38 the spherically averaged structure factors are shown; for $u_0 = 0.016$ (a) and $u_0 = 0.03$ (b). In both figures, solid lines represent the structure before the transition (globule) while dashed lines give the structure after the transition (pearl-necklace). Firstly, let us consider the globular structures, corresponding to $\mu = 2.175$ in Fig. 4.38(a) and $\mu = 2.7585$ in Fig. 4.38(a). Both curves show a pronounced peak at $q \approx 3.1$ that is related to a globule size $R_{\rm globule} \approx 2.0$. Note that directly calculated from simulations one obtains $R \approx 2.1$. The pronounced oscillations at large q indicate that the globule has sharp boundaries and does not fluctuate strongly. Let us consider the structure factor of the dumbbell case at $u_0 = 0.016$ (dashed line in Fig. 4.38(a)). The shoulder seen at $q \approx 0.75$ gives bead-to-bead distance. Thus one obtains $l = 8.37$ (see Eqn. 2.103). This length can be identified as the distance between the beads' centers of mass. Using the data given in Table 4.3 one obtains

$$l_{\rm str} + 2\left(\frac{d_{\rm bead}}{2}\right) = 4.87 + 3.36 = 8.23,$$

which is found in a fair agreement with the shape of the form factor. The second shoulder seen at $q \approx 3.65$ is related to bead size. $d_{\rm bead} = 4\pi/q \approx 3.44$ which is in a good agreement with Table 4.3. Due to the strong fluctuations of the number of pearls the pearl-necklace form factor seen in Fig. 4.38(b) (dashed line) shows only one broad (smeared) shoulder. Therefore from the structure factor one cannot deduce anything specific for the pearl-necklace structure

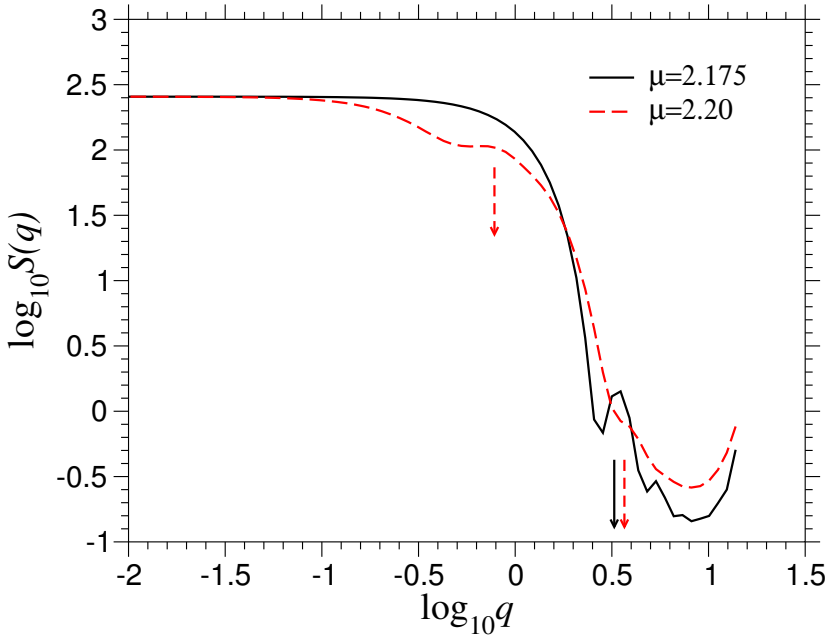

(a)

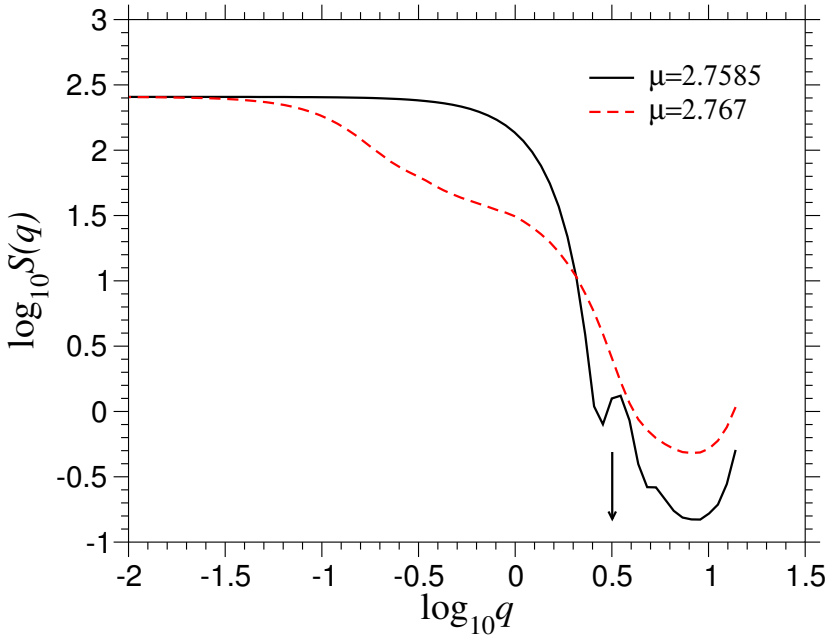

(b)

Figure 4.38: Single chain structure factors plotted for globules (black solid line) and pearl-necklaces (red dashed line) at (a) $u_0 = 0.016$ (dashed arrows point the shoulder corresponding to string length and the peak corresponding to bead size) and (b) $u_0 = 0.03$ (solid arrow denotes peak position that gives globule size).

in this case. Note that this is also a typical problem in scattering experiments on pearl-necklace structures.

One may also sample the density distribution function $\rho(r)$ of monomers around the center of mass of the chain. Fig. 4.39(a) shows the monomer density distribution function at $u_0 = 0.016$ for $\mu = 2.175$ and $\mu = 2.20$, while Fig. 4.39(b) displays the monomer density distribution function at $u_0 = 0.03$ for $\mu = 2.7585$ and $\mu = 2.76$. The narrow peaks seen at $\mu = 2.175, u_0 = 0.016$ and $\mu = 2.175, u_0 = 0.03$ correspond to the globular structures. However, for $u_0 = 0.016$ and $\mu = 2.20$ (Fig. 4.39(a)) the peak becomes broader and its location is shifted away from the center of mass, corresponding to the formation of a dumbbell. At $u_0 = 0.03$ and $\mu = 2.76$ (Fig. 4.39(b)) the distribution function exhibits two broad peaks. The existence of two peaks corresponds to a chain which has has four pearls. The distance between the peaks (about 6.9) is related to the string length (directly measured 6.11, see Table 4.3).

4.2.3 Influence of additional salt

In this section effects of additional salt are discussed for annealed PELs in poor solvent. Considering chains of length $N = 256$ at $\lambda_B = 1.0$, $\tau = 0.19$ one studies the behavior in a rather poor solvent. Adding low molecular salt ions to the solution the screening length of the electrostatic interaction $\lambda_D = (8\pi\lambda_B c_s)^{-1/2}$, with c_s being the concentration of a (monovalent) salt, will be reduced. In this way, one has a simple tool to vary the range of interaction. For very large salt concentration, i.e., at very short screening length $\lambda_D < b$ the interaction can be completely suppressed and the PEL chain becomes like a neutral one. In Fig. 4.40 the degree of charging is plotted as a function of the rescaled screening length for different chemical potential.

The corresponding behavior of the normalized m.s. end-to-end distance is shown in Fig. 4.41. In Fig. 4.42 one finds typical snapshots which illustrate the chain structure in the different regions. In the snapshots charged monomers are represented by red color and uncharged ones by yellow color.

Although solvent quality τ, coupling strength u and chemical potential μ are fixed, obviously there is another way to switch the configuration of the PEL chain between a highly charged stretched state and a weakly charged globule by tuning λ_D. In contrast to quenched PELs this is not a continuous crossover, but a discontinuous transition. At $\lambda_D < b$ the Coulomb interaction is almost fully screened, i.e., at any finite μ the chain will be completely charged. Nevertheless it forms a globule like neutral chains in a poor solvent. With growing λ_D the chain becomes continuously stretched. However, there appears a certain screening length λ_D^* where the penalty in interaction energy becomes larger than the penalty upon neutralizing almost all the charges which is $N_c \times \mu$. At those points the chain undergoes a discontinuous transition back into a globule which is now only weakly charged in contrast to the globule at small λ_D. Obviously, the transition point λ_D^* depends on the chemical potential. The transition points λ_D^* for various chemical potentials are given in Table 4.6. For larger μ, there appears an interesting feature: increasing λ_D the PEL chain exhibits non-monotonic stretching. Beyond a maximum stretching at a certain screening length the chain becomes

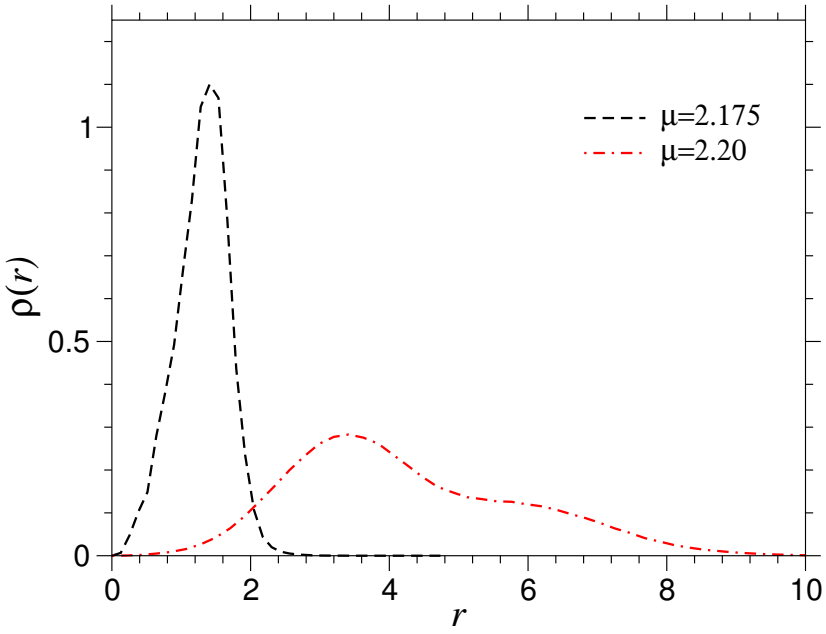

(a)

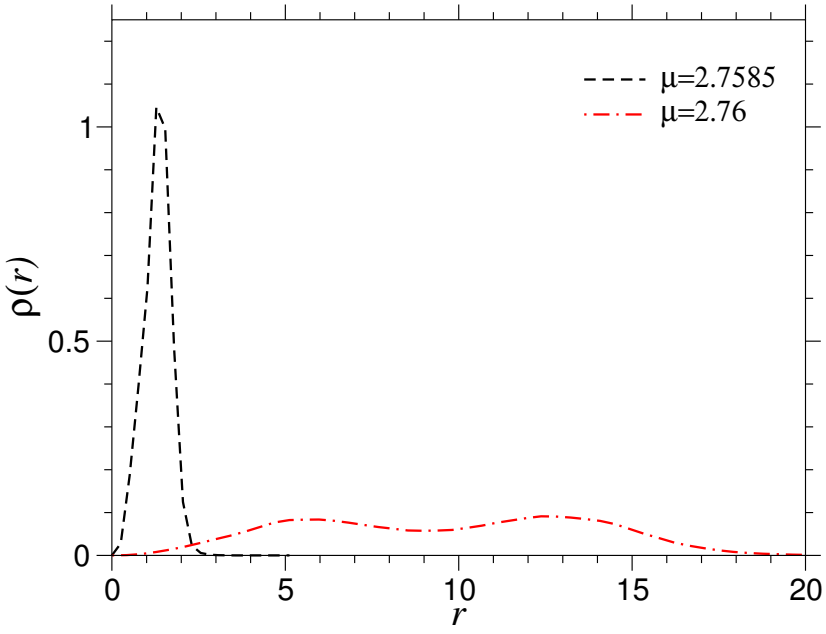

(b)

Figure 4.39: Density distribution function of monomers around the center of mass of chain ($N = 256$) at (a) $u_0 = 0.016$ and (b) $u_0 = 0.03$.

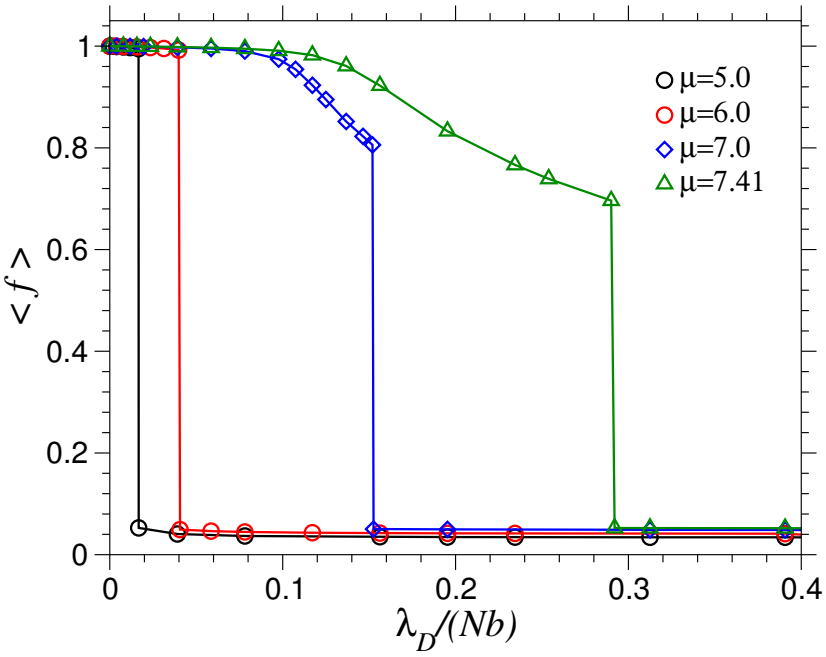

Figure 4.40: Degree of charging versus screening length at different charge chemical potentials ($N = 256$, $u_0 = 1$, $\tau = 0.19$).

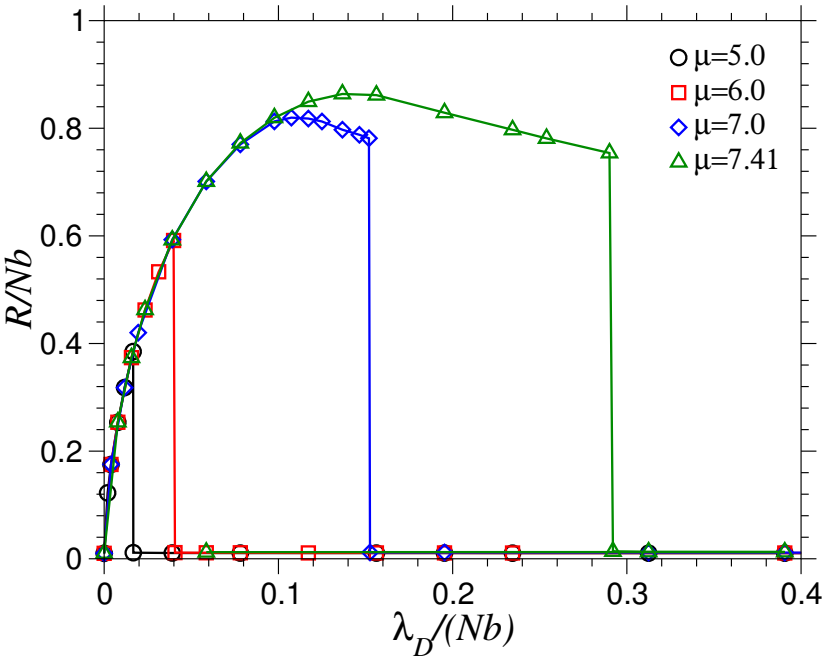

Figure 4.41: Normalized end-to-end distance versus screening length at different charge chemical potentials ($N = 256$, $u_0 = 1$, $\tau = 0.19$).

again more and more wiggled before finally undergoing the transition into a weakly charged globule. This behavior is due to a partial neutralization of monomer charges with increasing

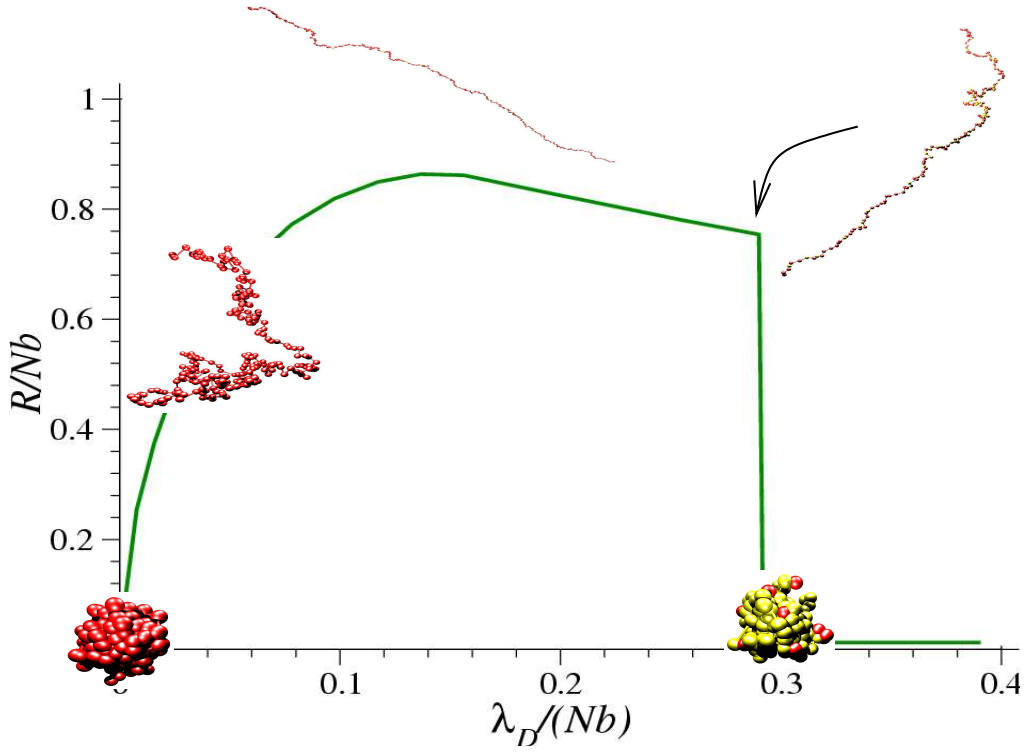

Figure 4.42: Snapshots taken from the chain $N = 256$ and with $\mu = 7.41$ for various values of screening length ($\tau = 0.19$).

μ	λ_D^*
5.0	4.27
6.0	10.03
7.0	38.98
7.41	74.50

Table 4.6: Transition point λ_D^* at different chemical potentials ($N = 256$, $\tau = 0.19$).

λ_D (see Fig. 4.40 at $\mu \geq 7.0$), which corresponds to a growing distance between neighboring charges.

At solvent quality $\tau = 0.19$, the maximal chemical potential at which there occurs a sharp transition is found 7.41. For larger chemical potentials, one cannot observe any sharp transition and the chain remains in an extended state. To enlarge the range of μ where a coil-to-globule transition occurs at large λ_D one has to reduce solvent quality and to go to larger τ.

The spherically averaged structure factors are given in Fig. 4.43. In this figure, the structure factor is plotted for different chemical potentials at the specific Debye lengths just before the transition. One curve shows the behavior after the transition which is quite the same for all chemical potentials as long as $\lambda_D > \lambda_D^*(\mu)$. At screening lengths $\lambda_D < \lambda_D^*$ for

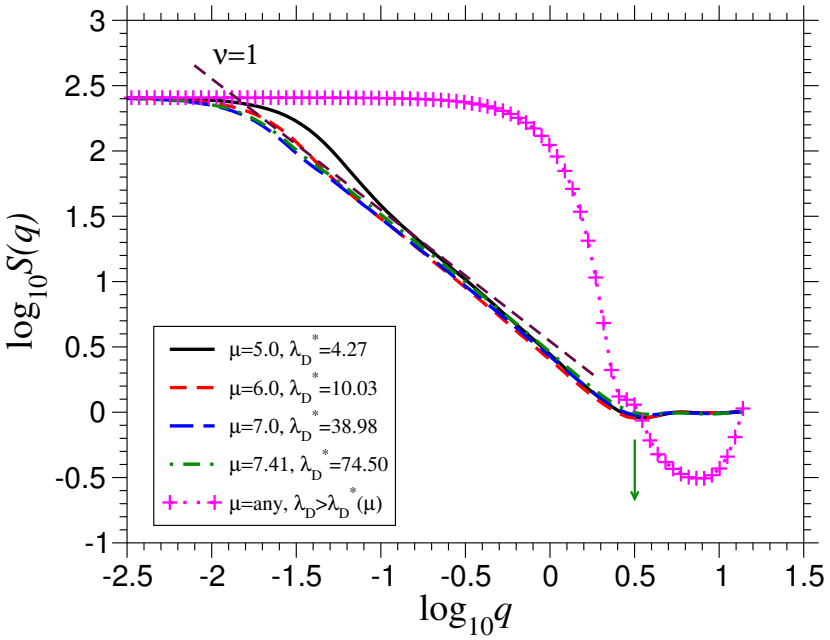

Figure 4.43: Structure factors of the PEL chain at different μ, ($N = 256$, $\tau = 0.19$). The cases at $\lambda_D = \lambda_D^*(\mu)$ show the behavior just before the transition and the case shown with plus symbol is the behavior above the transition. Note that for $\lambda_D > \lambda_D^*$ all curves map almost perfectly each other.

all chemical potentials the PEL chain is found to be highly stretched, $S \propto q^{-1}$. At screening lengths $\lambda_D > \lambda_D^*$ the chain is in a collapsed state. The peak at $\log_{10} q \approx 0.50$ gives the globule size $R \approx 2.0$.

Fig. 4.44 displays the spherically averaged structure factors at varying λ_D for chemical potential $\mu = 7.41$. This plot is quite illustrative to see the effect of added salt. The chain expands with increasing screening length. At $\lambda_D = 4$, i.e., $\lambda_D/b \approx 3.7$, the chain is swollen with $\nu \approx 0.6$. At $\lambda_D = 35$, i.e. $\lambda_D/Nb \approx 0.14$ the chain is highly stretched with $\nu \approx 1$. At $\lambda_D > \lambda_D^* \approx 74.5$ the chain collapses back into a weakly charged globule. For stretched, highly charged chains just before the transition back to a globule the local charge distribution along the chain is shown in Fig. 4.45. The contour distance in the plot, s, is measured in the units of b_0 from the middle of the chain;

$$-N/2 \leq s \leq N/2. \tag{4.5}$$

Very similarly to annealed PELs in good solvent there appears a charge accumulation at chain ends. The width of that region is given by the Debye length [34, 59].

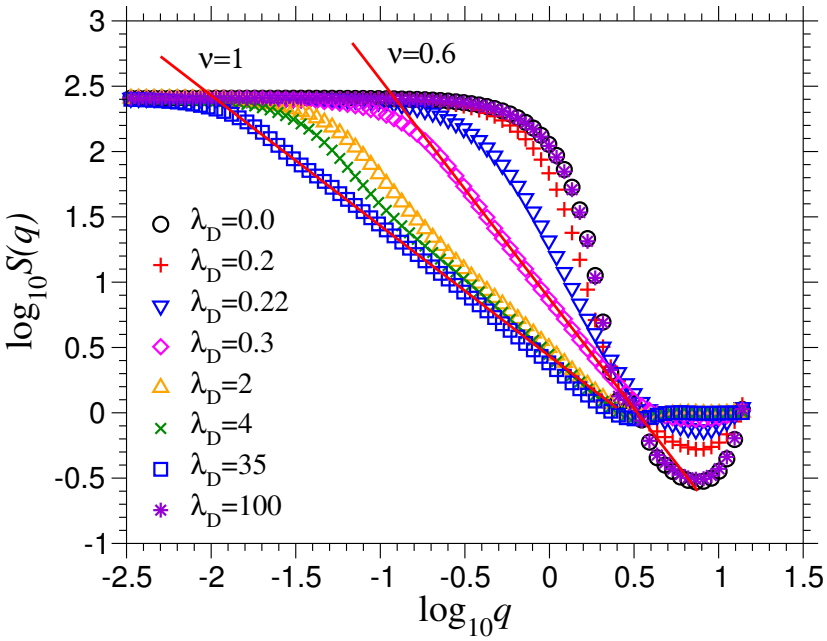

Figure 4.44: Structure factors of the PEL chain at varying λ_D for $\mu = 7.41$. The straight lines show certain scaling behavior.

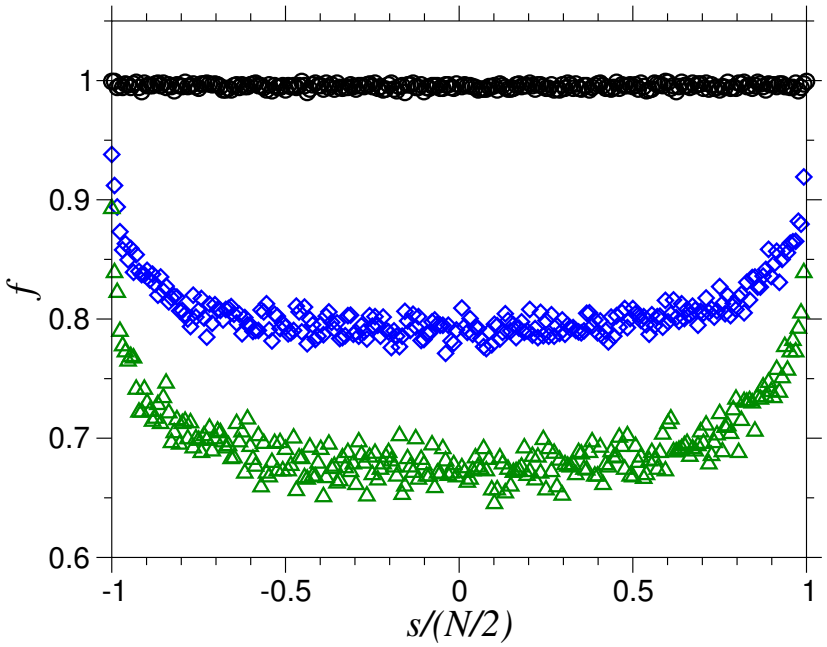

Figure 4.45: Degree of dissociation in the stretched state as a function of the position along the chain ($N = 256$), (1) circles (black): $\mu = 5.0; \lambda_D = 4.27; < f >= 0.995$, (2) diamonds (blue): $\mu = 7.0; \lambda_D = 38.98; < f >= 0.806$ and (3) triangle-up (green): $\mu = 7.41; \lambda_D = 74.87; < f >= 0.696$.

Chapter 5

Conclusions

Polyelectrolytes (PELs) are polymer chains containing a certain amount of ionizable monomers. When such polymers are dissolved in a polar solvent like water, the ion pairs dissociate and the polymer becomes charged. While the one type of charges is localized on the chain, the corresponding oppositely charged counterions are scattered in the solution [1]. PELs are present everywhere in our daily life. On the one hand biopolymers, including DNA and proteins, are PELs, on the other hand, many artificial water soluble polymers are charged. Generally speaking, the understanding of PELs is relatively poor compared to neutral polymer systems. In the case of PELs in a poor solvent, the complexity arises from the competition between repulsive long-ranged electrostatic interaction and local attractive volume interaction. Annealed PELs are even more complex due to the additional degree of freedom in charge distribution. So far simulation studies on PELs in a poor solvent were mainly focused on quenched PELs.

The theory predicts that the behavior of annealed PELs in poor solvents close to the Θ point $\tau < \tau^*$ is quite different than that at rather poor solvents $\tau > \tau^*$, where the characteristic distance from the Θ point is given by $\tau^* \simeq N^{-1/5}u^{-3/5}$.

In this work, extensive semi-grand canonical Monte Carlo simulations have been carried out to check the theoretical predictions in the different regions. A problem of interest is the influence of additional salt. This question has been studied by simulations with varying screening length λ_{D}.

In the case of rather poor solvents, the charge chemical potential is a non-monotonic function of the degree of charging f. The theory predicts that an annealed PEL undergoes a first-order phase transition in that case [36]. For the first time the simulation results reported here have given direct evidence that an annealed PEL indeed undergoes a first-order phase transition when the chemical potential (solution pH) reaches a certain value. The discontinuous transition occurs between a weakly charged compact globular structure and a strongly charged stretched configuration. The order of the transition has been determined using the histogram method of Lee and Kosterlitz [87]. At the transition point, the free energy has pronounced double minima corresponding to two coexisting phases. One minimum corresponds to a weakly charged globular structure and the other one to a strongly charged stretched configuration. The double minima structure provides direct evidence for the first order nature of the transition in agreement with theoretical predictions. In addition, finite size effects have been studied. For smaller chains, the transition seems to be continuous, but

for longer chains the transition is really discontinuous. Hence, it could be shown that former simulation studies [86] where the authors claimed to see a continuous transition were strongly affected by finite size effects [85].

Close to Θ point ($\tau < \tau^*$) the entropic term is dominating the chemical potential μ which remains then a monotonically growing function of f. In that case theory predicts no phase transition but a deformation of the globule. Later it was understood (to be precise, for quenched PELs) that the globule would become unstable with respect to the formation of pearl-necklaces [29]. Thus, it is expected that such inhomogeneous structures are stable at $\tau < \tau^*$. One may come close to the Θ point via two different routes: one is directly to reduce the scaled temperature τ. The second one is to enlarge the value of τ^*, by decreasing the coupling parameter. In this study the second way has been chosen. The results show that pearl-necklaces exist in annealed PELs indeed. The pearl-necklace structures have been quantitatively studied: with increasing coupling parameter, the number of pearls increases while the number of monomers per bead and the size of one bead decrease. These features are in a good agreement with theoretical predictions made for quenched PELs. But the observations for string length and string mass do not agree with theoretical predictions. One has to note that, for the chain lengths used in this study the strings are rather short objects. Obviously, asymptotic relations cannot be applied for them as done by theory. In multi-pearl structures, the fluctuations between states with different pearl numbers are large. This is due to the relatively small energy difference between these structures.

Qualitatively the charge distribution along pearl-necklace structures agrees with theoretical predictions [59], i.e. pearls are slightly less charged as strings.

Besides the agreement with theoretical prediction, the observation of pearl-necklace structures in annealed PELs is confirmed by recent experiments: poly(vinylamine) (PVA) exhibits a coil/globule-to-pearl-necklace transition by changing the pH [89].

Furthermore, as predicted by theory [46], the simulation results have shown that an annealed PEL displays a sharp transition from a highly charged stretched state to weakly charged globule at a critical salt concentration. An annealed PEL forms a fully charged compact structure at strong screening. With increasing screening length the chains start to swell. At a certain screening length, chain size and degree of charging are at maximum. For larger screening lengths, the size of chain and degree of charging are reduced before the chain undergoes a sharp transition into a globular state. The screening length depends on the chemical potential.

Although the present study could supply new insight into the behavior of annealed PELs and some features could be shown for the first time there remain open questions for further work:

(i) The behavior close to the Θ point should be studied by tuning the solvent quality directly towards the Θ point, i.e., by reducing τ absolutely. Enlarging τ^* by reducing coupling strength induces other effects due to the weak interaction. The study by decreasing τ itself may bring additional insight which might be directly related to experimental studies.

(ii) Investigating the influence of additional salt a non-monotonic stretching with growing

λ_D was obtained before the chain undergoes a coil-to-globule transition. To enlarge the region where this interesting behavior occurs one has to reduce the solvent quality, i.e., one has to enlarge τ.

(iii) Since in any real system one cannot omit the effects of counterions studies including counterions would be highly interesting. In the case of quenched PELs the role of the counterion entropy and its effect to the stability of the various structures is an intensively discussed question.

Appendix A

Cluster search algorithm

The specific structure quantities of pearl-necklace structures are studied by using a cluster search algorithm. Cluster search is important in many research areas, for example in picture analysis and percolation systems [99]. In such an algorithm, the question whether a group of monomers forms a cluster is often connected to a distance criterion, e.g. monomers with a distance smaller than a critical value belong to the same cluster. For a polymer one has to take into account chain connectivity. This implies that a pure distance criterion is not sufficient. Therefore, additionally one requires that there is a certain number of bonds between a pair of monomers along the chain contour [88, 100]. The resulting algorithm is iterative and contains the following steps:

1. At the beginning every monomer is considered to be a cluster of size 1 (cluster size: number of monomers belonging to a cluster).

2. Two clusters $C1$ and $C2$ are merged if they contain a pair of monomers ij with $i \in C1$, $j \in C2$ and $r_{ij} < r_c$. Along the chain monomers i and j have to have a distance larger than n_c bonds: $\mid i - j \mid > n_c$.

3. Step 2 is repeated over all clusters as long as one finds clusters that have to be merged.

4. Elimination of loops: clusters which lie completely or partially within another cluster are merged.

5. Definition of pearls: all clusters with a size larger than or equal to p_c are pearls. Pearls directly connected along the chain are merged.

6. Definition of strings: all clusters with a size smaller than p_c are strings. Strings directly connected along the chain are merged.

7. Elimination of dangling ends: strings at chain ends are merged to the end pearls.

Thus the algorithm has in principle three free parameters: r_c, n_c and p_c. The used empirical parameter set in this work is $\{r_c = 1.8, n_c = 10, p_c = 20\}$. Small changes of the three parameters do not have a significant effect on the final result. The parameter set is different than those in ref. [100], mainly due to the different bond potential and σ value.

Bibliography

[1] J. L. Barrat and J. F. Joanny. *Advances in Chemical Physics* **94**, 1 (1996).

[2] Ed. M. Hara, *Polyelectrolytes*. Marcel Dekker, New York (1993).

[3] K. S. Schmitz, *Macroions in solution and colloidal suspension (1st edition)*. VCH Publishers, New York (1993).

[4] S. Förster and M. Schmidt. *Advances in Polymer Science* **120**, 51 (1995).

[5] In: *Electrostatic Effects in Soft Matter and Biophysics*, edited by C. Holm, P. Kékicheff, and R. Podgornik, volume 46 of *NATO Science Series*. Kluwer Academic Publishers Dordrecht NL (2001).

[6] A.Katchalsky and P.Spitnik. *J. Polym. Sci.* **2**, 432 (1947).

[7] P. G. de Gennes, *Scaling Concepts in Polymer Physics, 2nd edn.* Cornell University Press, Ithaca (1985).

[8] H. Dautzenberg, W. Jaeger, J. Kötz, C. Seidel B. Philipp, and D. Stscherbina, *Polyelectrolytes Formation: Characterization and Application*. Hanser Publishers (1994).

[9] C. Morris, *Dictionary of Science and Technology*. Academic Press, San Diego, CA. (1992).

[10] A. Y. Grosberg and A. R. Khokhlov, *Statistical Physics of Macromolecules*. American Institute of Physics, New York (1994).

[11] M. Doi and S.F. Edwards, *The Theory of Polymer Dynamics*. Clarendon Press, Oxford (1986).

[12] M. Doi, *Introduction to Polymer Physics*. Clarendon Press, Oxford (1996).

[13] S.W. Lovesey and W. Marshall, *Theory of Thermal Neutron Scattering*. Oxford University Press (1971).

[14] R. Pecora, ed., *Dynamic Light Scattering*. Plenum Press, New York (1985).

[15] O. Kratky and G. Porod. *Rec. Trav. Chim.* **68**, 1106 (1949).

[16] W. Kuhn. *Kolloid Z.* **76**, 746 (1936).

[17] P. J. Flory. *J. Chem. Phys.* **17**, 303 (1949).

[18] P.J. Flory, *Principles of Polymer Chemistry*. Cornell Univ. Press, Ithaca (1953).

[19] M. J. Stephen. *Phys. Lett.* **53A**, 363 (1975).

[20] P. G. de Gennes. *J. Physique* **36**, L55 (1975).

[21] P. G. de Gennes. *J. Physique* **39**, L299 (1978).

[22] L. E. Reichl, *Modern Course in Statistical Physics*. Univ. of Texas Press, Austin (1980).

[23] J.P. Cotton. *J. Physique Lett.* **41**, L231 (1980).

[24] Y. Miyaki, Y. Einaga, and H. Fujita. *Macromolecules* **11**, 1180 (1978).

[25] M. Fukuda, M. Fukutomi, and T. Hashimoto. *J. Polym. Sci.* **12**, 87 (1974).

[26] A. Yamamoto, M. Fujii, G. Tanaka, and H. Yamakawa. *Polymer J.* **2**, 799 (1971).

[27] J. C. Le Guillou and J. Zinn-Justin. *Phys. Rev. Lett.* **39**, 95 (1977).

[28] L. A. Feigin and D. I. Svergun, *Structure Analysis by Small-angle X-ray and Neutron Scattering*. Plenum Press, New York (1987).

[29] A. V. Dobrynin, M. Rubinstein, and S. P. Obukhov. *Macromolecules* **29**, 2974 (1996).

[30] G.S. Manning. *J. Chem. Phys.* **51**, 924 (1969).

[31] M. Schmidt. *Macromolecules* **24**, 5361 (1991).

[32] D. Bratko and K.Dawson. *J. Chem. Phys.* **99**, 5732 (1993).

[33] B.Y. Ha and D. Thirumalai. *Macromolecules* **28**, 577 (1995).

[34] T. Zito and C. Seidel. *Eur. Phys. J. E.* **8**, 339 (2002).

[35] I. Borukhov, D. Andelman, and H. Orland. *Eur. Phys. J. B.* **5**, 869 (1998).

[36] E. Raphael and J. F. Joanny. *Europhys. Lett.* **13**, 623 (1990).

[37] P. Debye and E. Hückel. *Phys. Z.* **24**, 185 (1923).

[38] N. Z. Bjerrum. *Electrochem.* **24**, 321 (1918).

[39] T. Odijk. *J. Polym. Sci.* **15**, 477 (1977).

[40] T. Odijk and C. A. Houwaart. *J. Polym. Sci. Polym. Phys. Ed.* **16**, 627 (1978).

[41] J. Skolnick and M. Fixman. *Macromolecules* **10**, 944 (1977).

[42] A. V. Dobrynin, R. H. Colby, and M. Rubinstein. *Macromolecules* **28**, 1859 (1995).

[43] P.-G. de Gennes, P. Pincus, R. M. Velasco, and F. J. Brochard. *J. Phys. (Paris)* **37**, 1461 (1976).

[44] A. R. Khokhlov and K. A. Khachaturian. *Polymer* **23**, 1742 (1982).

[45] A. R. Khokhlov. *J. Phys. A* **13**, 979 (1980).

[46] P. G. Higgs and E. Raphael. *J. Phys. I* **1**, 1 (1991).

[47] P. G. Higgs and H.J. Orland. *J. Chem. Phys.* **95**, 4506 (1991).

[48] L. Rayleigh. *Philos. Mag.* **18**, 14 (1882).

[49] G. Taylor. *Proc. R. Soc. London Ser. A* **280**, 383 (1964).

[50] Y. Kantor and M. Kardar. *Europhys. Lett.* **27**, 643 (1994).

[51] Y. Kantor and M. Kardar. *Phys. Rev. E* **51**, 1299 (1995).

[52] A. V. Dobrynin and M. Rubinstein. *Macromolecules* **34**, 1964 (2001).

[53] M. Deserno. *Eur. Phys. J. E* **6**, 163 (2001).

[54] P. van der Schoot. *Langmuir* **13**, 4926 (1997).

[55] G. J. Fleer, M. A. Cohen Stuart, J. M. H. M. Scheutjens, T. Cosgrove, and B. Vincent, *Polymers at Interfaces*. Chapman & Hall, London, Glasgow, New York, Tokyo, Melbourne, Madras (1993).

[56] J.T.G. Overbeek. *Bull. Soc. Chim.* **57**, 252 (1948).

[57] R. R. Netz. *J. Phys.: Condens Matter* **15**, 239 (2003).

[58] Y. Burak and R. R. Netz. *J. Phys. Chem. B (in press)* (2004).

[59] M. Castelnovo, P. Sens, and J.-F. Joanny. *Eur. Phys. J. E* **1**, 115 (2000).

[60] J-P. Hansen and I.R. McDonald, *Theory of simple liquids*. Academic Press, New-York (1986).

[61] I. Borukhov, *Polyelectrolytes, Polyampholytes and Electrolytes in Solution and near Surfaces*. Ph.D. Thesis, Tel Aviv University (2000).

[62] M. J. Stevens and S. J. Plimpton. *Euro. Phys. J. B* **2**, 341 (1998).

[63] J. F. Joanny and L. Leibler. *J. Phys.(France)* **51**, 547 (1990).

[64] N. Metropolis and S. Ulam. *J. Amer. Statistical Assoc.* **44**, 335 (1949).

[65] K. Binder and D. W. Heermann, *Monte Carlo simulation in statistical physics*. Springer-Verlag, Berlin Heidelberg New York London Paris Tokyo (1988).

[66] N. Metropolis, A. W. Rosenbluth, M.N. Rosenbluth, A. H. Teller, and E. Teller. *J. Chem. Phys.* **21**, 1087 (1953).

[67] In: *Monte Carlo Methods in Statistical Physics 2nd ed.*, edited by K. Binder, volume 7 of *Topics Curr. Phys.* Springer, Berlin, Heidelberg (1986).

[68] H. Müller-Krumbhaar and K. Binder. *J. Stat. Phys.* **8**, 1 (1973).

[69] A. Baumgartner. *J. Chem. Phys.* **72**, 871 (1980).

[70] A. V. Lyulin, B. Dünweg, O. V. Borisov, and A. A. Darinskii. *Macromolecules* **32**, 3264 (1999).

[71] P. Chodanowski and S. Stoll. *J. Chem. Phys.* **111**, 6060 (1999).

[72] M. P. Allen and D. J. Tildesley, *Computer simulation of liquids*. Clarendon Press, Oxford (1987).

[73] R. Friedberg and J.A. Cameron. *J. Chem. Phys.* **52**, 6049 (1970).

[74] A. Milchev, W. Paul, and K. Binder. *J. Chem. Phys.* **99**, 2592 (1993).

[75] K. Kremer, Computer Simulation of Polymers. In: *in* Computer Simulation in Chemical Physics, edited by M.P. Allen and D.J. Tildesley, volume 397 of *NATO Advanced Science Institutes Series, Series C: Mathematical and Physical Sciences*, pages 397–459. Kluwer Academic Publishers, Dordrecht, Netherlands (1993).

[76] K. Kremer and G. S. Grest. *J. Chem. Phys.* **92**, 5057 (1990).

[77] M. Mandel, *Encyclopedia of Polymer Science and Engineering*, volume 11. J. Wiley, New York (1988).

[78] X. Auvray, R. Anthore, C. Petipas, J. Huguet, and M. Vert. *J. Physique (France)* **47**, 893 (1986).

[79] I. Borukhov, D. Andelman, R. Borrega, M. Cloitre, L. Leibler, and H. Orland. *J. Phys. Chem. B* **104**, 11027 (2000).

[80] E. V. Anufrieva, T. M. Birshtein, T. N. Nekrasova, O. B. Ptitsyn, and T. V. Sheveleva. *J. Polym. Sci.* **C16**, 3519 (1968).

[81] P. Dubin and U. P. Strauss. *J. Phys. Chem.* **77**, 1427 (1973).

[82] R. A. Marcus. *J. Phys. Chem.* **58**, 621 (1954).

[83] S. Lifson. *J. Chem. Phys.* **26**, 727 (1957).

[84] T. L. Hill. *J. Polym. Sci.* **23**, 549 (1957).

[85] S. Uyaver and C. Seidel. *Europhys. Lett.* **64(4)**, 536 (2003).

[86] A. P. Sassi, S. Beltrán, H. H. Hooper, H. W. Blanch, and J. Prausnitz. *J. Chem. Phys.* **97**, 8767 (1992).

[87] J. Lee and J. M. Kosterlitz. *Phys. Rev. Lett.* **65**, 137 (1990).

[88] H.J. Limbach and C. Holm. *J. Phys. Chem. B* **107**, 8041 (2003).

[89] L. J. Kirwan, G. Papastavrou, and Michal Borkovec. *Nano Letters* **4 (1)**, 149 (2004).

[90] A. Katchalsky, J. Mazur, and P. Spitnik. *J. Polym. Sci.* **23**, 513 (1957).

[91] D. Baigl, M. Sferrazza, and C. E. Williams. *Europhys. Lett.* **62 (1)**, 110 (2003).

[92] S.G. Starodoubtsev and K. Yoshikawa. *J. Chem. Phys.* **100**, 19702 (1996).

[93] K. Yoshikawa, Y. Yoshikawa, Y. Koyama, and T. Kanbe. *J. Am. Chem. Soc.* **119**, 6473 (1997).

[94] M. Ueda and K. Yoshikawa. *Phys. Rev. Lett.* **77**, 2133 (1996).

[95] Y. Yoshikawa, Y. S. Velichko, and Kenichi Yoshikawa. *Eur. J. biochem.* **268**, 2593 (2001).

[96] T. A. Waigh, R. Ober, and C. E. Williams. *Macromolecules* **34**, 1973 (2001).

[97] S. Minko, A. Kiriy, G. Gorodyska, and M. Stamm. *J. Am. Chem. Soc.* **124**, 3218 (2002).

[98] A. Kiriy, G. Gorodyska, S. Minko, W. Jaeger, P. Stepànek, and M. Stamm. *J. Am. Chem. Soc.* **124**, 13454 (2002).

[99] D. Stauffer, *Introduction to Percolation Theory (1st ed.)*. Taylor and Franci, London Philadelphia (1985).

[100] H. J. Limbach, *Struktur und Eigenschaften von Polyelektrolyten im schlechten Lösungsmittel*. Ph.D. Thesis, Johannes Gutenberg University Mainz (2001).

List of Figures